Copyright Warning & Restrictions

The copyright law of the United States (Title 17, United States Code) governs the making of photocopies or other reproductions of copyrighted material.

Under certain conditions specified in the law, libraries and archives are authorized to furnish a photocopy or other reproduction. One of these specified conditions is that the photocopy or reproduction is not to be "used for any purpose other than private study, scholarship, or research." If a, user makes a request for, or later uses, a photocopy or reproduction for purposes in excess of "fair use" that user may be liable for copyright infringement,

This institution reserves the right to refuse to accept a copying order if, in its judgment, fulfillment of the order would involve violation of copyright law.

Please Note: The author retains the copyright while the New Jersey Institute of Technology reserves the right to distribute this thesis or dissertation

Printing note: If you do not wish to print this page, then select "Pages from: first page # to: last page #" on the print dialog screen

ABSTRACT

TEMPORAL AND SPATIAL EFFECTS OF SHOCK OVERPRESSURE ON BLOOD-BRAIN BARRIER PERMEABILITY IN BLAST-INDUCED TRAUMATIC BRAIN INJURY

by
Matthew Joseph Kuriakose

Exposure to shock waves is the leading cause of traumatic brain injury (TBI) in military personnel and blast-induced TBI (bTBI) is considered the signature wound in recent conflicts in Iraq and Afghanistan. Many researchers attempt to replicate field-relevant shock waves in laboratory settings through the use of gas-driven shock tubes in order to investigate the generation and propagation of shock waves and also explore possible mechanisms of bTBI. Among several injury mechanisms of bTBI, damage to the blood-brain barrier (BBB) has been identified as a potential candidate and has been the focus of several clinical and experimental investigations aimed to establish injury baselines and discover timelines for therapeutic intervention for neurotrauma. It is hypothesized that BBB permeability in blast increases with increasing overpressure and varies differentially in different brain regions as a function of time post-injury. In order to test this hypothesis, the blast injury model is characterized and effects of an end reflector plate studied, prior to using this injury model in the study of BBB permeability post-blast injury. BBB breakdown is studied across the frontal cortex, striatum, somatosensory barrel field cortex, thalamus, hippocampus, and cerebellum at fifteen minutes, four, and twenty-four hours at blast overpressures of 35, 70, 130, and 180kPa. Finally, effects of oxidative stress on BBB permeability are delineated at four hours for 180kPa blast exposure, as well as the introduction of a potential treatment for nicotinamide adenine dinucleotide phosphate oxidase (NOX)-mediated BBB damage following blast injury.

End effector studies are conducted with the use of four different end plate configurations (0.625, two, four inches, and an open end). Use of end reflector plate allows for precise control over the intensity of reflected waves penetrating into the shock tube and, at a calculated optimized distance, can eliminate secondary waves from the test section, confirmed by pressure sensor recordings. Numerical simulations combined with experimental data offer detailed insight into spatiotemporal dynamics of shock waves and wave attenuation via internal pressure expansion. Diffusion of the driver gas inside of the shock tube is responsible for velocity increase of reflected shock waves.

Blood-brain barrier permeability is primarily assessed by extravasation of sodium fluorescein and Evans blue into brain parenchyma. Maximum extravasation of tracers (and hence BBB permeability) occurs in the frontal cortex at four hours following injury and increases with increasing blast overpressure. Abundance of tight junction proteins occludin and claudin-5 is also measured at different time-points after injury. Significant extravasation is observed immediately after blast across several brain regions, suggesting a shockwave-induced mechanical disruption of the BBB even at mild overpressures. Results also indicate the presence of s100-β in the blood serum as well as monocyte infiltration to the brain parenchyma, further validating increased BBB permeability. Within 24 hours, extravasation of sodium fluorescein and Evans blue returns close to control values across all brain regions studied.

NOX is shown to be upregulated in vascular endothelial cells, resulting in an increase in superoxide production four hours post-blast. The use of apocynin, a selective NOX inhibitor, is shown to ameliorate production of superoxide at this time and significantly reduce MMP activity, tight junction breakdown, and BBB extravasation.

TEMPORAL AND SPATIAL EFFECTS OF SHOCK OVERPRESSURE ON BLOOD-BRAIN BARRIER PERMEABILITY IN BLAST-INDUCED TRAUMATIC BRAIN INJURY

by
Matthew Joseph Kuriakose

A Dissertation
Submitted to the Faculty of
New Jersey Institute of Technology
and Rutgers University Biomedical and Health Sciences – Newark
in Partial Fulfillment of the Requirements for the Degree of
Doctor of Philosophy in Biomedical Engineering

Department of Biomedical Engineering

August 2018

APPROVAL PAGE

TEMPORAL AND SPATIAL EFFECTS OF SHOCK OVERPRESSURE ON BLOOD-BRAIN BARRIER PERMEABILITY IN BLAST-INDUCED TRAUMATIC BRAIN INJURY

Matthew Joseph Kuriakose

Dr. Namas Chandra, Dissertation Advisor — Date
Distinguished Professor of Biomedical Engineering, NJIT

Dr. Bryan J. Pfister, Committee Member — Date
Professor of Biomedical Engineering, NJIT

Dr. James Haorah, Committee Member — Date
Associate Professor of Biomedical Engineering, NJIT

Dr. Kakulavarapu V. Rama Rao, Committee Member — Date
Research Assistant Professor of Biomedical Engineering, NJIT

Dr. Vijayalakshmi Santhakumar, Committee Member — Date
Associate Professor of Pharmacology, Physiology, and Neuroscience
Rutgers New Jersey Medical School

Dr. Pranela Rameshwar, Committee Member — Date
Professor of Medicine, Rutgers New Jersey Medical School

BIOGRAPHICAL SKETCH

Author: Matthew Joseph Kuriakose

Degree: Doctor of Philosophy

Date: August 2018

Undergraduate and Graduate Education:

- Doctor of Philosophy in Biomedical Engineering,
  New Jersey Institute of Technology, Newark, NJ, 2018

- Bachelor of Science in Biomedical Engineering,
  New Jersey Institute of Technology, Newark, NJ, 2013

Major: Biomedical Engineering

Presentations and Publications:

Kuriakose, M., Kakulavarapu, V., Younger, D. & Chandra, N. Temporal and spatial effects of blast overpressure on blood-brain barrier permeability in traumatic brain injury. *Nature Scientific Reports*. 2018.

Kakulavarapu, V., Iring, S., Younger, D., Kuriakose, M., Skotak, M., Alay, E., Pfister, B. & Chandra, N. A single primary blast-induced traumatic brain injury in rodent model causes cell-type dependent increase in NADPH oxidase isoforms in vulnerable brain regions. *Journal of Neurotrauma*. 2018.

Kakulavarapu, V., Younger, D., Kuriakose, M. & Chandra, N. Single primary blast-induced traumatic brain injury in rodent model causes cell-type dependent increase in NADPH oxidase isoforms in vulnerable brain regions. *Society for Neuroscience Annual Meeting*. Washington, DC, Nov. 2017.

Kuriakose, M. & Chandra, N. Temporal and spatial considerations of blood-brain barrier dysfunction following blast-induced traumatic brain injury. *Northeast Bioengineering Conference*. Newark, NJ, Apr. 2017.

Kuriakose, M., Skotak, M., Misisitia, A., Kahali, S., Sundaramurthy, A. & Chandra, N. Tailoring the blast exposure conditions in the shock tube for generating pure, primary shock waves: the end plate facilitates elimination of secondary loading of the specimen. *Plos One*. 2016.

Kuriakose, M., Alay, E., Skotak, M. & Chandra, N. Comparing direct v indirect mechanisms of injury in blast injury animal model. *Military Operational Medicine Research Program In-Progress Review*, Fredrick, MD, Jul. 2016.

Kuriakose, M. & Chandra, N. Experimental investigation of cavitation as a mechanism of primary blast-induced traumatic brain injury. *National Neurotrauma Symposium*. Lexington, KY, Jun. 2016.

Kuriakose, M. & Chandra, N. Fundamental understanding of the mechanism of cavitation in blast-induced traumatic brain injury. *Computational Cellular Biology of Blast and Casualty Care Review Meeting*. Arlington, TX, Feb. 2016.

This humble work is dedicated to my family, especially Chris, Mom, and Dad.
To each of my teachers and all of my friends.
And, most of all, to a loving God who placed these wonderful people in my life.

ACKNOWLEDGMENT

I would like to give my sincere appreciation to my advisor, Dr. Namas Chandra. I will always be grateful to you for taking a chance on me, a student you barely knew, and inviting me to pursue this meaningful work with you. Our time together wasn't always easy and as trying and frustrating as this journey was, at times, for me, I can only imagine it was doubly so for you. Please know I'm deeply grateful for your patience. Needless to say, your advice and guidance, both within and outside the realms of research, were critical in my completion of this Ph.D. program and dissertation.

I would also like to thank the members of my dissertation committee. Dr. Kakulavarapu Rama Rao, thank you for teaching me the tenets of wet lab work, for helping me stay focused when discouragement threatened to derail my progress and for all of the friendly conversations and taco treks. I never would have made it this far without you, Rama. Dr. Viji Santhakumar, your wise counsel and honest feedback gave me confidence during a time when faith was in short supply. Your energy and friendship truly helped me navigate some of the most difficult times of the program, Viji, and for that I will always be grateful. Dr. Bryan Pfister, I've always appreciated your sincerity and belief in me. Both the confidence you placed in me from my undergrad till now (I hope) and your support of me and my work will always be valued. I'll know I've really wrapped up here when I no longer see you in the gym in the morning. Dr. James Haorah, as much as I've relied on your technical expertise, I am abundantly more grateful for your friendship. Thanks for taking the time to learn my story and encourage my progress, James. Dr. Pranela Rameshwar, thank you for your honesty and transparency throughout

the dissertation progress. I've always valued your willingness to meet and offer whatever was needed, whether encouragement, counsel, or scientific input. Especially grateful for your consistent support towards the end of the program.

My completion of this dissertation is as much of a testament to my colleagues as it is to my dedication. Many thanks to Dr. Maciej Skotak, who was the first person who taught me how to do research at this level and still remains a treasured source of objective, unbiased, and usually uncomfortable advice. To both Dr. Molly Townsend and Dr. Madhu Murugan: you brought a breath of fresh air to our research group and helped take some of the focus off me, for which I'll be forever grateful. Molly, your conversations have offered me perspective that I never knew I was lacking; thanks for that. I'm excited to see where to the road takes you. Madhu, your willingness to candidly share the stories from your doctoral program and the consideration to go-to-bat for me is something I've always appreciated; we're lucky to have you. To Eren, your brotherhood will always be cherished. I've never had any doubt that I could find support and a primal, Turkish roar from your corner. My flawless fantasy football advice seems like a poor trade for your humble wisdom and steadfast support…but I suppose a deal's a deal. Stephanie and Arun, thank you for taking care of me during the early and late stages of my biochemistry work, respectively. Your willingness to learn and to teach was always helpful and especially considerate as you attempted to manage all of the experiments on this side of the lab. Manny, when I needed someone to talk me out of walking away from the program, it seemed like you were always there. Your encouragement was necessary for my completion and although I often didn't agree with your NBA opinions or basketball bravado, they never failed to bring a smile to my face.

To all the PhD students who overlapped with my tenure here–Danny, Sudeepto, Jose, Abdus, Aravind, Aswati, Mat, Alex, Millie, Jessica, Yiming, and Ning Ning-please know how much I valued working alongside you. My life was made infinitely more enjoyable knowing that I didn't traverse this journey alone. For those waiting to graduate, know that it'll come quicker than you know. I'd love the chance to celebrate with each of you when that time comes. You've earned it.

To the Masters and Bachelors students–Anthony, Jon, Brian, Katherine, Debanjan, Yoni, Madison, Jeff, Melissa, John, Chris, Smit, Sunny–thank you for allowing me to teach you and for bringing a much-needed sense of light-heartedness to our group. I pray that I made your time in our lab at least a little more enjoyable.

To Pam, Chang, Courtney, and Luipa, we made it together. Your friendship consistently pushed me to keep my eyes fixed on the brighter days ahead and now, as I stand on the doorstep, I look forward to celebrating with you. It may be difficult now to appreciate the journey to this point, but when you get the chance to do so, I sincerely pray I was as much of a warm, guiding presence for you as you all were for me.

To the family who has tirelessly and unceasingly offered me an abundant serving from their treasury of love; know that I give all of this to you. To Mom & Dad; your boy finally did it. I hope I can make you proud and that we may have many more smiles and celebrations in the future. Our relationship is so profoundly marked by love and I can so clearly see your caring fingerprints all over this chapter of my life. Deeply and eternally indebted to you both. To Chris…you're my elder brother, my mentor, my best and longest friend. My words fall hopelessly short of capturing just how much you mean, and will always mean, to me. I love you with every fiber of my being and know that, even

when I'm now known as Dr. Matthew Kuriakose, I'll still consider myself, first and foremost, Chris's younger brother and forever smile at the thought. Much love, bro; we made it.

For any good that you may see in me, let it be known that it is nothing more than a merciful gift from my Lord and Savior Jesus Christ. My hope, joy, and purpose is forever tied to Him and I pray that through this dissertation and all future aspirations and accomplishments I may bring glory to the Name above all names.

†

TABLE OF CONTENTS

TABLE OF CONTENTS
(Continued)

Chapter **Page**

TABLE OF CONTENTS
(Continued)

Chapter **Page**

LIST OF FIGURES

LIST OF FIGURES
(Continued)

LIST OF FIGURES
(Continued)

Figure **Page**

CHAPTER 1

INTRODUCTION

Over the past two decades, there has been a drastic increase in the number of blast-induced traumatic brain injuries (bTBI) sustained by both military and civilian populations, largely due to the increased use of improvised explosive devices (IEDs) in acts of terrorism and warfare domestically and abroad[1-3]. While blunt force traumatic brain injury represents the most well-known and well-studied TBI modality, investigation of blast-induced neurotrauma, an injury often unaccompanied by external indications, continue to puzzle clinicians and medical professionals. As the number of relevant experimental investigations continues to increase, researchers draw ever closer to uncovering details regarding mechanical and biochemical injury sequelae and the promise of preventative and therapeutic interventions that follow.

Exposure to shock waves is identified as the leading cause of traumatic brain injury (TBI) in military personnel[4,5]. The injuries associated with explosive detonation are classified into four different categories based on their etiology: 1) primary, caused by pure shock waves, 2) secondary, resulting from penetration of fragmentation (shrapnel) and other projectiles into the brain parenchyma, 3) tertiary, originating from impact with other objects, and 4) quaternary, caused by exposure to heat and toxic gases[6-8]. It appears mixed type of injuries are expected near the epicenter of a blast. Traveling over long-distances, the shock wave could be the sole source of injuries far from the explosion, making primary blast TBI (bTBI) particularly onerous[9]. Researchers have been attempting to replicate field-relevant shock waves in laboratory settings through the use

of shock tubes in order to investigate the generation and propagation of shock waves and possible mechanisms of bTBI, also referred to as blast induced neurotrauma (BINT)[10,11]. Increased focus on bTBI has resulted in intensified research efforts and a number of groups have opted to use compressed-gas driven shock tubes to study the etiology of blast injury[12-17]. All categories of blast injuries can occur in the field[18-20], and it is challenging to isolate cases of pure primary blast injuries among military personnel. In order to study biological effects of shock waves in the laboratory, it is crucial that these generated experimental wave forms are free of any artifacts. To date, there is only a limited understanding of conditions affecting shock wave propagation inside of the shock tube, what crucial differences exist between testing inside versus outside of the shock tube, and how the end-effects affect the shock wave profile and propagation[21,22].

Since their inception in 1899[23], shock tubes have been widely used in a variety of research areas for studying phenomena which require extremely high temperatures and heating rates or occurring at extremely fast but controllable rates: high temperature chemical kinetics[24,25], molecular spectroscopy[26], and to simulate interaction of plasma with Earth's magnetosphere[27], just to name a few prominent examples. However, in the biomedical field, shock tubes found application as research tools relatively recently, with just a few existing peer-reviewed reports published pre-2010[28-31]. Typically, shock tubes share major design features, which utilize three essential components: driver (breech), driven (which includes the test section) and the end-reflector. The subtle differences in the design and operation of the tube have significant impacts on the resulting pressure history measured inside of the tube: volume of the breech, breech-to-test section diameter ratio, circle-to-square transition and length of the driven section. It is generally accepted

that the shock wave closely resembling the Friedlander waveform (Figure 2.1) should be used for any experiments aiming at replicating field blast conditions[32,33]. This waveform consists of a sharp, almost instantaneous rise in pressure (shock front) followed by exponentially decaying pressure[34]. It is critical to accurately characterize the amount of loading sustained by subjects (it is of particular importance for studies which use animal models) and to tailor specific pressure profiles via optimization of shock tube configuration. To the best of the author's knowledge, systematic experimental characterization of conditions inside of the shock tube received only limited attention[35,36], in spite of vast theoretical and empirical evidence regarding the fate of the shock wave traveling on the outside of the shock tube[37,38].

Despite the increase in studies related to bTBI in recent years, there is only a limited understanding of how blast waves interact with the brain and cause injury, which has precluded the establishment of comprehensive diagnostic criteria for bTBI and potential therapeutic strategies. A recent survey reported that more than 30 phase III clinical trials aimed at targeting TBI have failed[39-42]. Identifying how blast-induced neurotrauma displays a temporal and spatial evolution of neuropathology in various regions of the brain is critical for the identification of injury mechanisms and the development of preventative measures and treatments for bTBI patients. Among many mechanisms of injury, damage to the blood-brain barrier (BBB) has been identified as a potential candidate and has been a focus of several clinical and experimental investigations aimed to establish injury baselines and discover timelines for therapeutic interventions for neurotrauma[43,44].

The blood-brain barrier is a highly, selectively-permeable membrane that separates the brain from the circulatory system. The BBB is dynamically modulated by cellular interactions between endothelial cells and the tight junctions that join them, as well as pericytes, and astrocytes that support the endothelial capillaries[45-51]. Many neurological disorders including stroke[52-55], Alzheimer's disease[56,57], Parkinson's disease[49,58], HIV-1 encephalitis[51,59], epilepsy[60,61], and multiple sclerosis[62-64] display impaired BBB permeability. BBB disruption is also one of the most frequently investigated mechanisms of injury in blunt TBI and has been commonly used as an assay to determine the degree and extent of injury[65-69]. Several groups have reported abnormal opening of BBB in closed cortical injuries[70-72], weight drop models[73,74], and blast models[69,75-80]. Reported results are derived from different probing methodologies, with different injury models, at different injury intensities, in different spatial regions of the brain. Limited number of studies has implicated increased BBB permeability in the pathology of blast-induced traumatic brain injury but, to the author's knowledge, no such investigation has resolved the temporal and spatial resolution of BBB changes in bTBI, especially as a function of increasing biomechanical blast loadings. It is important to note that not all blast models impart the same type of injury on experimental animal and, for this reason, authors compared the results of this work only to models that feature pure, primary blast injury void of secondary and tertiary effects[21,81].

In addition to increased BBB permeability, the role of oxidative stress has been implicated in multiple modes of TBI [82,83] and is mainly induced by reactive oxidative species (ROS). These include, but are not limited to, superoxide ($O2\cdot-$), hydroxyl radical ($HO\cdot$), and hydrogen peroxide (H_2O_2) [84,85]. While a basal level of ROS is to be expected

due to normal reactions of oxidative phosphorylation, redox-reactions, and mechanisms of the electron transport chain, an excess amount, as seen after injury, can be harmful. NADPH oxidase (NOX) is a multi-subunit enzyme that catalyzes the formation of superoxide radicals, from present molecular oxygen. As shown in previous studies, including work from this group, NOX is upregulated following blast injury[65,86] and various isoforms are expressed in a slew of neurological cell types including neurons, vascular endothelial cells, astrocytes, and microglia.

Oxidative stress has also been linked to the breakdown of the blood-brain barrier (BBB). In work previously published by this group, increased permeability of the BBB was most significantly seen four hours post-blast across the cerebral hemisphere, with most pronounced injury seen in the frontal cortex. Damage to the BBB was shown through extravasation of tracers Evans blue and sodium fluorescein, the dislodging of tight junction proteins, and leakage of blood-borne cells into the brain parenchyma and vice versa. While increased permeability was seen immediately (fifteen minutes) following injury, extravasation persisted and increased four hours later. While immediate opening of the BBB is likely caused by the mechanical forces of the primary blast wave, the authors hypothesize that the continued increase in permeability is at least partially due to the role of secondary injury mechanisms like oxidative stress.

Several groups have attempted to establish a connection between these two secondary injury mechanisms, most usually through the role of matrix metalloproteinases. MMPs are endopeptidases that degrade the ECM of various cell types. While tightly controlled in normal, "uninjured" conditions by MMP inhibitors and tissue inhibitors of MMPs, uncontrolled activation has been observed due to oxidative

stress[47,87-90]. This in-turn degrades the brain endothelium and substantially increases the permeability of the BBB. The role of MMPs in BBB degradation has been well investigated[47,91-95].

This work attempts to test the hypothesis that, in a well-characterized, artifact-free shock tube, a rodent model will experience an increase in blood-brain barrier permeability under shock loading and that permeability is further increased by concurrent oxidative stress. This is tested via the completion of three specific aims: 1) Characterization and validation of the blast injury model, which includes the detailed investigation on shock wave propagation and pressure transmission within the shock tube, 2) Use of the above injury model to study the temporal and spatial effects of blast overpressure on blood-brain barrier permeability following blast-induced traumatic brain injury, and 3) Examination of the role of oxidative stress in BBB breakdown following injury, with a closer look at a potential preventative intervention for blast-induced neurotrauma.

CHAPTER 2

SHOCK TUBE CHARACTERIZATION: EFFECT OF END REFLECTOR PLATE

2.1 Background and Significance

Exposure to shock waves is identified as the leading cause of Traumatic Brain Injury (TBI) in military personnel[4,5]. The injuries associated with explosive detonation are classified into four different categories based on their etiology: 1) primary, caused by pure shock waves, 2) secondary, resulting from penetration of fragmentation (shrapnel) and other projectiles into the brain parenchyma, 3) tertiary, originating from impact with other objects, and 4) quaternary, caused by exposure to heat and toxic gases[6-8]. It appears mixed type of injuries are expected near the epicenter of a blast, while shock wave is far reaching, compared to the other TBI risk factors associated with explosive blast. Traveling over long-distances, the shock wave could thus be the sole source of injuries far from the explosion, making primary blast TBI (bTBI) particularly onerous[9]. Researchers have been attempting to replicate field-relevant shock waves in laboratory settings through the use of shock tubes in order to investigate the generation and propagation of shock waves and possible mechanisms of bTBI, also referred to as blast induced neurotrauma (BINT)[10,11]. Increased focus on bTBI has resulted in intensified research efforts and a number of groups have opted to use compressed-gas driven shock tubes to study the etiology of blast injury[12-17]. All categories of blast injuries can occur in the field[18-20], and while it is challenging to isolate cases of pure primary blast injuries among military personnel, in order to study biological effects of shock waves in the

laboratory, it is crucial that these generated experimental wave forms are free of any artifacts. To date, there is only a limited understanding of conditions affecting shock wave propagation inside of the shock tube, what crucial differences exist between testing inside versus outside of the shock tube, and how the end-effects affect the shock wave profile and propagation[21,22].

Since their inception in 1899[23], shock tubes have been widely used in a variety of research areas for studying phenomena which require extremely high temperatures and heating rates or occurring at extremely fast but controllable rates: high temperature chemical kinetics[24,25], molecular spectroscopy[26], and to simulate interaction of plasma with Earth's magnetosphere[27], just to name a few prominent examples. However, in the biomedical field, shock tubes found application as research tools relatively recently, with just a few existing peer-reviewed reports published pre-2010[28-31]. Typically, shock tubes share major design features, which utilize three essential components: driver (breech), driven (which includes the test section) and the end-reflector. However, the subtle differences in the design and operation of the tube have significant impacts on the resulting pressure history measured inside of the tube: volume of the breech, breech-to-test section diameter ratio, circle-to-square transition and length of the driven section[96]. It is generally accepted that the shock wave closely resembling the Friedlander waveform (Figure 2.1) should be used for any experiments aiming at replicating field blast conditions[32,33]. This waveform consists of a sharp, almost instantaneous rise in pressure (shock front) followed by exponentially decaying pressure (blast wind)[34]. It is critical to accurately characterize the amount of loading sustained by subjects (it is of particular importance for studies which use animal models) and to tailor specific pressure profiles

via optimization of shock tube configuration. To the best of the author's knowledge, systematic experimental characterization of conditions inside of the shock tube received only limited attention[35,36], in spite of vast theoretical and empirical evidence regarding the fate of the shock wave traveling on the outside of the shock tube[37,38].

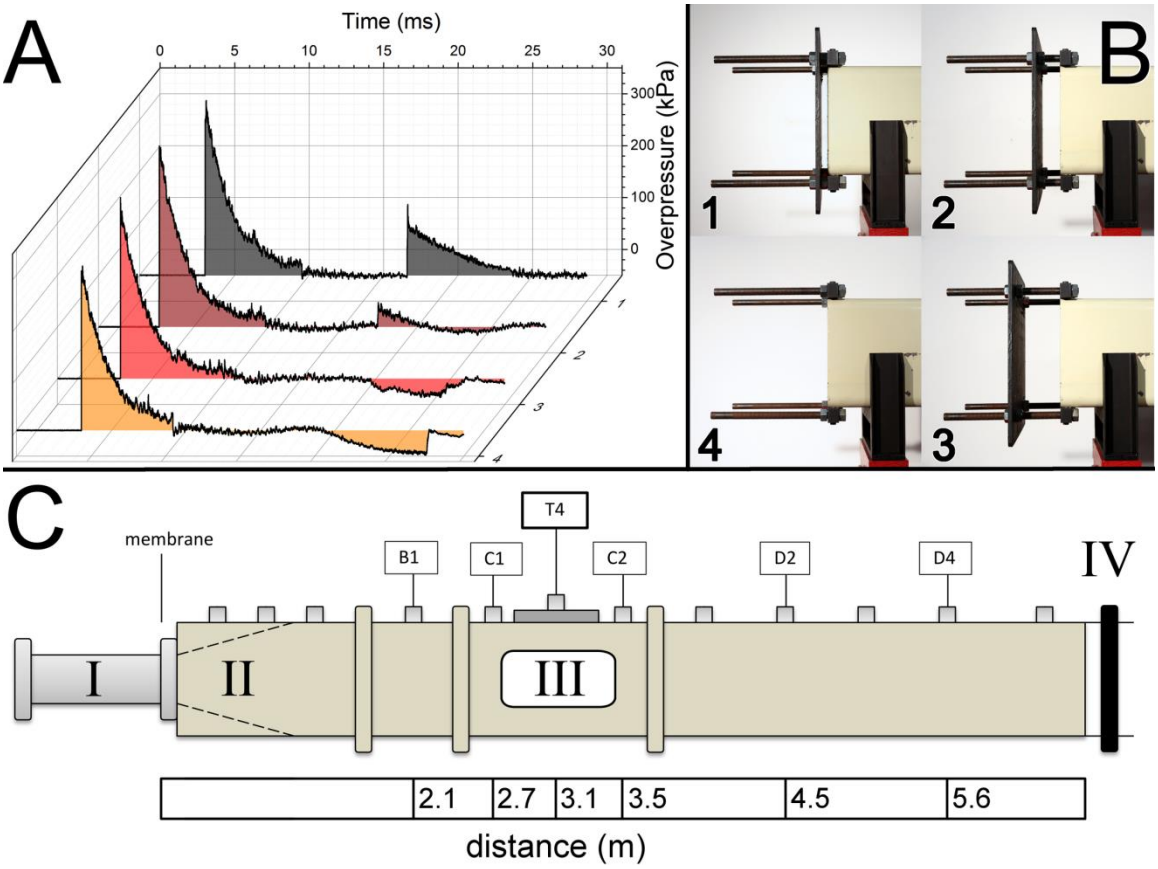

Figure 2.1 The representative incident shock wave profiles generated using helium as a driver gas and Mylar membrane (thickness of 1.016 mm), with accompanying secondary reflected shock and underpressure waves are presented (A). The profile of the secondary wave depends on the gap between the end plate reflector and the exit of the shock tube (B): 1. 0.625-inch, 2. 2-inch, 3. 4-inch, and 4. open end. (C) Schematics of the 9-inch square cross section shock tube indicating the breech (I), transition (II), test section (III) and end plate (IV). Distribution of pressure sensor locations is also illustrated. Typically sensors B1, C1, T4, C2, D2, and D4 were used in experiments to track the shock wave profile evolution along the entire length of the shock tube. The scale bar indicates the distance of specific sensor from the breech, i.e., Mylar membranes installation port.

In this work, the characteristics of the propagating shock wave (peak overpressure, duration, impulse and velocity) and secondary waves were followed by measuring the pressure-time profiles at six sensors distributed along the tube. Results of this work demonstrate conditions inside of the shock tube can be controlled and secondary waves eliminated by careful adjustment of the end plate reflector gap; thus the specimen is exposed only to a single shock wave with well-defined characteristics.

2.2 Materials and Methods

2.2.1 The Shock Tube

The shock tube housed at the Shock Wave Testing facility at the Center for Injury Biomechanics, Materials and Medicine ($CIBM^3$) at the New Jersey Institute of Technology has a 9" square cross section and a modular design with the following characteristics: 1) adjustable volume breech, 2) variable length transition section, 3) the 6 meter long test section, equipped with bullet-proof glass windows for high speed video observation of the specimen during the shock wave exposure, and 4) the reflector end-plate (Figure 2.1). In this study, the compressed helium was filled into the fixed volume breech, separated from the main body of the shock tube with Mylar membranes of three thicknesses (*vide infra*). The pressure inside the breech was continuously monitored using a WIKA A-10 sensor (0-340 atm range) and the burst pressure was recorded for all the tests.

2.2.2 Overpressure Measurement

Incident blast overpressure waves and secondary waves were measured using a series of pressure sensors distributed along the shock tube (Figure 2.1C). A custom made LabView program running on in-house built data acquisition system based on National Instruments PXI-6133 S Series multifunction DAQ modules and PXIe-1082 PCI Express chassis was used for this purpose. Pressure sensors used in these experiments were PCB Piezotronics (Depew, NY) model 134A24. All data were recorded at 1.0 MHz sampling frequency and the typical acquisition time was 200 milliseconds.

2.2.3 Experimental Design

This study was designed as two factor experimental design, 4 x 3. Two experimental variables investigated in this study are: 1) the distance between the reflector plate and the end of the shock tube (four levels) and 2) shock wave intensity (three levels). The distance between the reflector plate and the end of the shock tube was adjusted as shown in Figure 2.1B. Four different gap lengths were used: 1) 0.625", 2) 2" and 3) 4", and 4) open end. The incident blast overpressure was controlled by adjusting the thickness of Mylar membranes sandwiched between the breech and expansion section. The thickness was adjusted by stacking individual membranes with thickness of 0.01 inches (0.254 mm). In this study three membrane thicknesses (0.02, 0.04, and 0.06 inches, denoted as two, four or six membranes, respectively) were used. All tests were performed using single fixed breech volume of 6.5×10^{-3} m^3, and were repeated six times for each combination of experimental covariates. Additional tests were also performed with a fully closed shock tube (in triplicates for all three membrane thicknesses) to establish boundary conditions for reflected wave intensities and velocities.

2.2.4 Numerical Simulations

The propagation of blast waves are modeled in the shock tube environment. The air inside the shock tube through which the blast wave propagates is modeled using Eulerian elements. The size of the Eulerian domain corresponds to the physical dimensions of the shock tube used in the experiments (cross-section: 229 x 229 mm). The heterogeneous meshing of the shock tube was adopted, with fine mesh near the end and coarse mesh elsewhere, in order to decrease total number of elements in the model without sacrificing accuracy

The finite element (FE) model is solved using the nonlinear transient dynamic procedure with the Euler-Lagrangian coupling method (Abaqus 6.10). In this procedure, the governing partial differential equations for the conservation of mass, momentum, and energy, along with the material constitutive equations and corresponding equations defining the initial and boundary conditions are solved simultaneously. The Eulerian framework allows the modeling of highly dynamic events (e.g., shock) which would otherwise induce heavy mesh distortion. An enhanced immersed boundary method was used to provide the coupling between the Eulerian and the Lagrangian domains.

2.2.5 Comparison with Field Blast Waves

Comparison of experimental data (overpressure profile recorded by sensor at T4 location) with idealized field blast profiles were performed using ConWep 2.1.0.8[97]. The blast wave profiles were simulated as hemispherical ground explosion which were generated by TNT charge with weight in the range 10-2000 kg in the standoff distance range of 2-25 m. Only these profiles falling within range of both BOP and impulse of experimental data were used.

2.2.6 Statistical Analysis

Data from experiments preformed at different experimental conditions (end plate gap) were pooled together in three subsets according to blast intensity (membrane thickness). Data was checked for normality using Ryan-Joiner test (similar to Shapiro-Wilk) in Mintab 17.0. Then multiple comparison two-tailed t-test was performed with Bonferroni correction and $p < 0.003$ was considered statistically significant. Power analysis was performed with GPower 3.1.9.2 software. All data are presented as mean and standard deviation.

2.3 Results

2.3.1 Blast Overpressure and Burst Pressure

Peak blast overpressures (BOP) for different membrane thicknesses and back plate conditions are presented in Figure 2.2. BOP increased with membrane thickness and shows a direct correlation with the burst pressure (the maximum pressure measured in the breech at the time of membrane rupture). The variations between the measured BOP in experiments where the same membrane thicknesses were used are relatively small for all four back plate conditions, as evidenced by narrow standard deviation values (Figures 2.2A-C). The blast overpressure is found to be a linear function of the burst pressure. The variations of the maximum burst pressure can be attributed to sample-to-sample differences in Mylar membrane mechanical properties, typical for this class of commercially available materials [98]. The variation in burst pressure increases with Mylar

membrane thickness (i.e., number of membranes), as evidenced by increasing standard deviation.

The general observed trend is that the peak BOP decreases as the shock wave travels down the tube, and the end plate configuration has no effect on the peak BOP, with an exception of peak overpressures recorded at sensor locations C1 and T4, for which differences are not statistically significant ($p > 0.05$, Figure 2.2D).

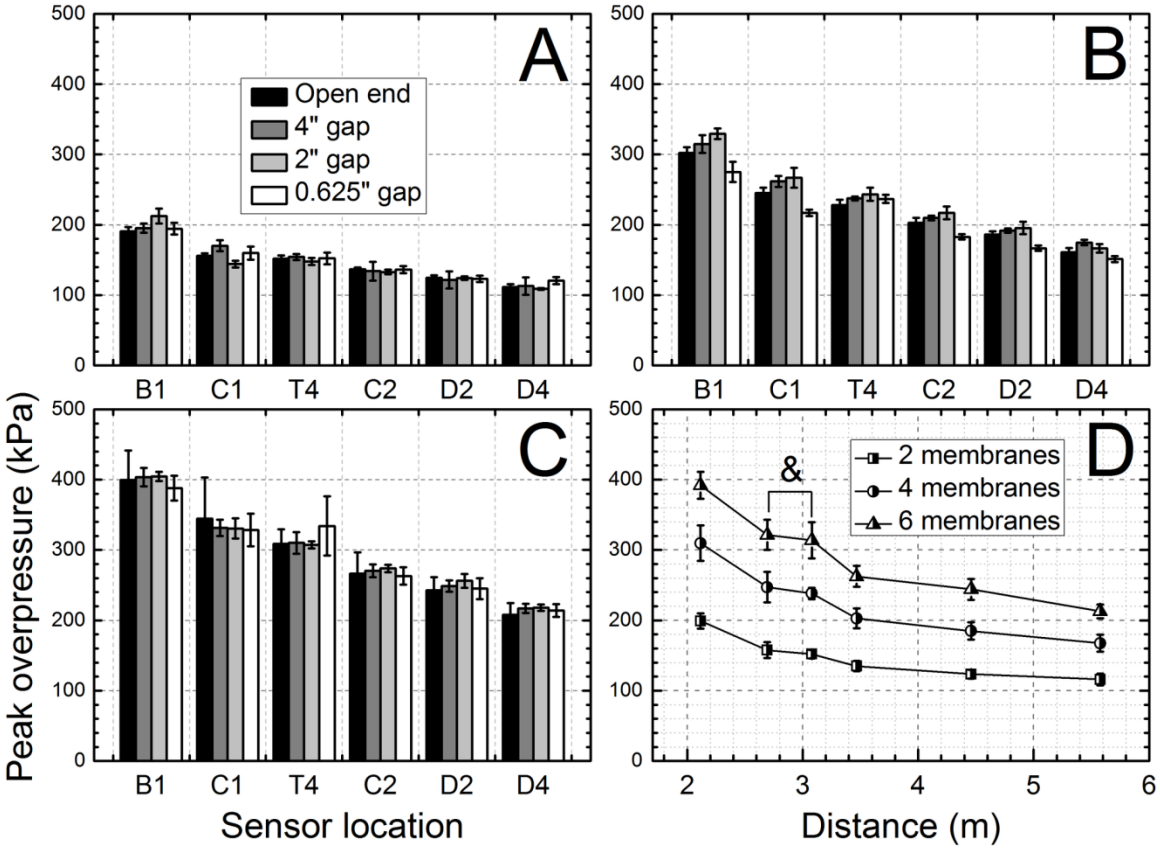

Figure 2.2 Peak overpressure inside of the shock tube as a function of sensor location and membrane thickness: (A) 0.02", (B) 0.04", and (C) 0.06". Peak overpressure values averaged among experiments performed using the same Mylar membrane thickness: (D) differences of average BOPs for sensors C1 and T4 are not statistically significant (marked with ampersand &, $p > 0.05$) in respective test groups.

2.3.2 Incident Shock Wave Velocities

The calculated values of the velocity of the shock front, traveling in the shock tube are presented in Figure 2.3. Velocities were calculated using the distance between sensors and the arrival times of the shock front at sensor locations. The shockwave velocities increase with the thickness of the Mylar membrane, but just as in the case of peak BOPs there appears to be virtually no difference between the shock velocities for varying back plate conditions. For all three Mylar membrane thicknesses used in these experiments the general observed trend is that the shock wave velocity decreases with the distance travelled in the shock tube: 540 to 500 m/s (deceleration: -16.4 $m \cdot s^{-2}$, Figure 2.3A), 630 to 570 m/s (-22.9 $m \cdot s^{-2}$, Figure 2.3B) and 680 to 620 m/s (-23.3 $m \cdot s^{-2}$, Figure 2.3C), for the membrane thickness of 0.02, 0.04 and 0.06 inches, respectively. It is also clear that the shock wave velocity variation is higher the closer the measurement location is to the breech. The pooled data for all measurements show narrow standard deviations for the velocities for all sensor locations after the test section sensor T4 (C2, D2 and D4). The velocities remain unchanged until shock wave reaches sensor D2 ($p < 0.005$, power: >0.95 with respect to velocities at T4 and C2) for all three tested membrane thicknesses (Figure 2.3D).

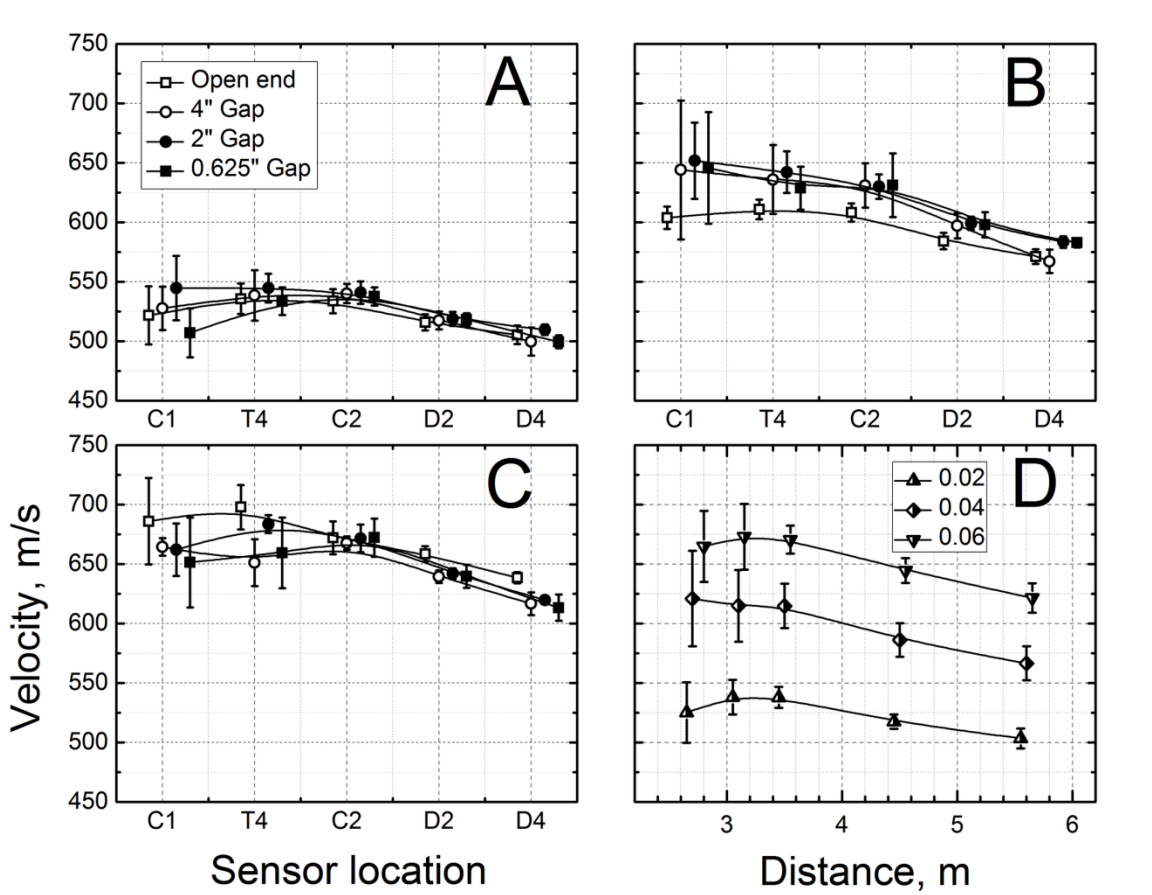

Figure 2.3 Calculated shock waves velocities at different sensor locations as a function of BOPs generated using Mylar membranes with thicknesses of: (A) 0.02", (B) 0.04", and (C) 0.06". Shock wave velocities were averaged for all experiments performed using the same Mylar membrane thickness (D). Individual data points were horizontally shifted for clarity of presentation. The B1 sensor was used as a reference for all calculations.

2.3.3 Impulse

The integrals of the shock wave overpressures versus time (impulse) generated using three different membrane thicknesses are depicted in Figure 2.4 using graphical methods. In general, the impulse values increase with increased number of Mylar membranes (burst pressure) used (Figures 2.4A-C). Within the same group the impulse variation along the length of the shock tube is relatively small, except for the C1 and D4 sensors. The most important differences are observed near the end of the shock tube, where the

impulse is significantly higher for 0.625” end gap, when are compared to other end plate configurations (Figures 2.4A-C).

The results of analysis of all pooled data revealed (Figure 2.4D) that differences between impulse values recorded at the C1 and T4 locations are statistically significant ($p < 0.003$, power: >0.95) when compared to other sensor locations. Similarly to BOP measurements the standard deviations tend to increase with increasing burst pressure (number of Mylar membranes used). Experimental overpressure profiles recorded in the test section (T4 sensor location) match field explosion BOPs and impulses retrieved simulated using TNT charge weight of 19.8, 34.2 and 66.0 kg at standoff distance of 7.0-7.6 m for two, four and six membranes, respectively.

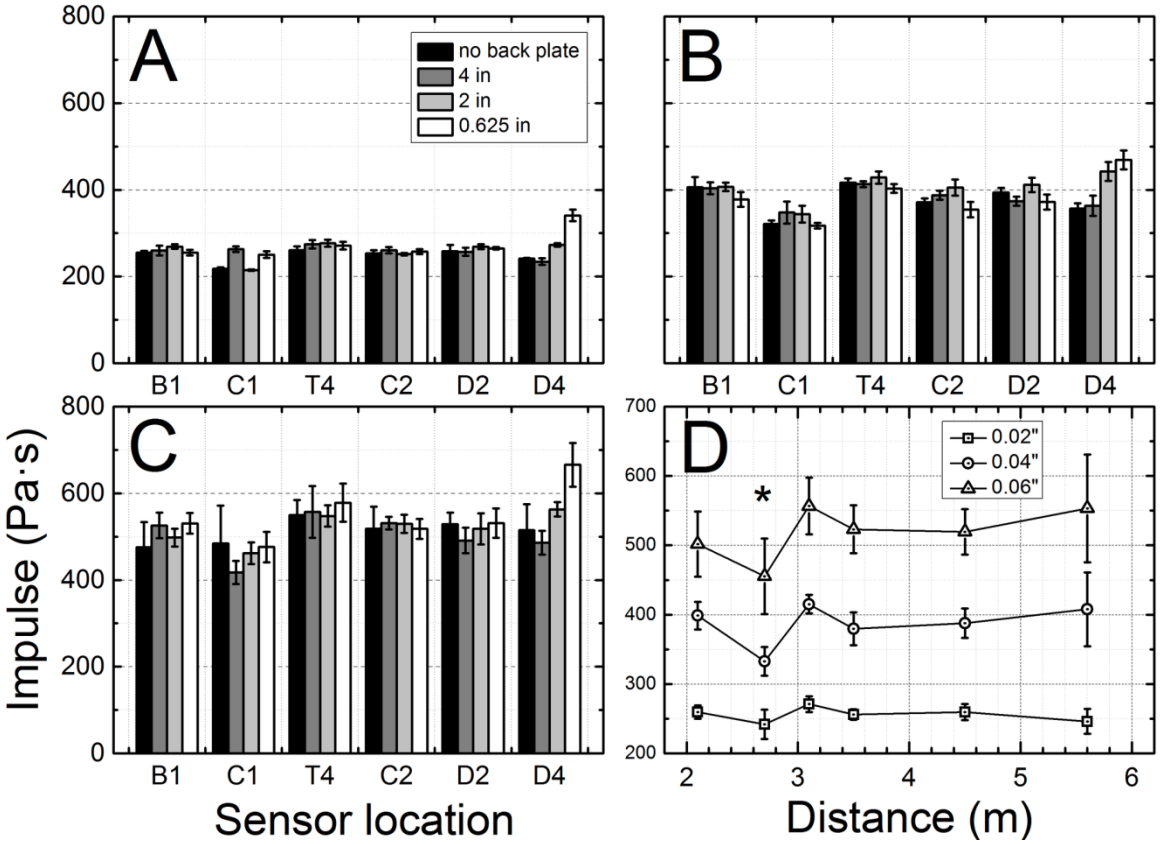

Figure 2.4 Positive phase impulse measured for the shock waves traveling inside of the shock tube as a function of sensor location and membrane thickness: (A) 0.02", (B) 0.04:, and (C) 0.06". The average impulse of shock waves recorded for three respective Mylar membrane thicknesses used as a function of sensor location along the shock tube (D). Asterisk indicates impulse value recorded by the C1 sensor, which shows statistically significant difference in respective data sets ($p < 0.003$, power: > 0.95).

2.3.4 Quantification of Secondary Positive and Underpressure Waves

The significance of the reflection waves and under-pressure waves on the loading of the test subject (in the test section at the T4 sensor location) is illustrated in Figure 2.5. When the end is fully open, the under-pressure wave that was generated had a minimum peak within 35% to 45% of the intensity of the original shock wave (peak blast overpressure) in the test section (as measured at T4 location). This means that the test subject (i.e., animal model) is being loaded with the original shock wave, and then shortly thereafter also by under-pressure wave, coming from the opposite direction. Implementing a back

plate four inches away from the mouth of the shock tube decreases the under-pressure ratio to about 20% in the test section. Bringing the plate two inches closer completely eliminates the observed under-pressure waves, but causes a secondary reflected shock wave to travel back into the shock tube. In this configuration, the test subject is exposed to the original shock wave plus the additional reflection wave, with intensity of merely 10-15% of the original shock front, coming from the opposite direction. When the plate-to-shock tube gap is further decreased to 0.625 inches, the peak overpressure of incident to reflected shock wave ratio in the test section increases to 30-40% of the original shock front BOP. Velocities of reflected underpressure (open end and 4" gap) and overpressure waves (2" and 0.625" gap) are presented in Figure 2.6. The underpressure waves generated under all test configurations propagate inside of the shock tube with subsonic velocities (Figures 2.6A and B), while overpressure reflected waves retain supersonic but somewhat diminished velocities (Figures 2.6C and D).

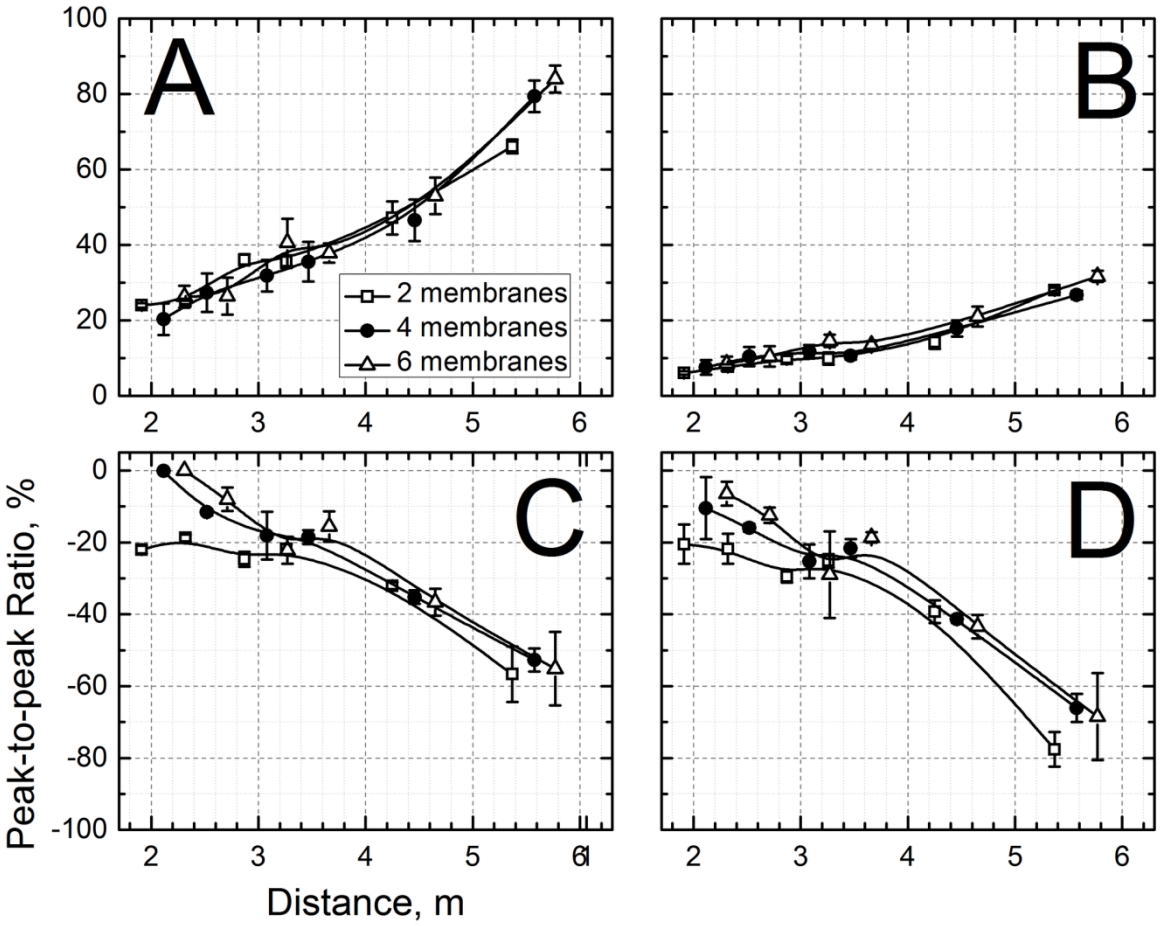

Figure 2.5 The ratios of peak overpressure between incident and reflected shock wave measured at different locations inside of the shock tube as a function of sensor distance from the breech and blast intensity: (A) 0.625" gap, (B) 2" gap between end of the shock tube and reflector plate. The ratios between incident peak overpressure and the lowest level of measured reflected underpressure for blasts generated when the gap between the end of the shock tube and reflector plate was 4" (C) and with open end (D). The data points were horizontally shifted for clarity of presentation.

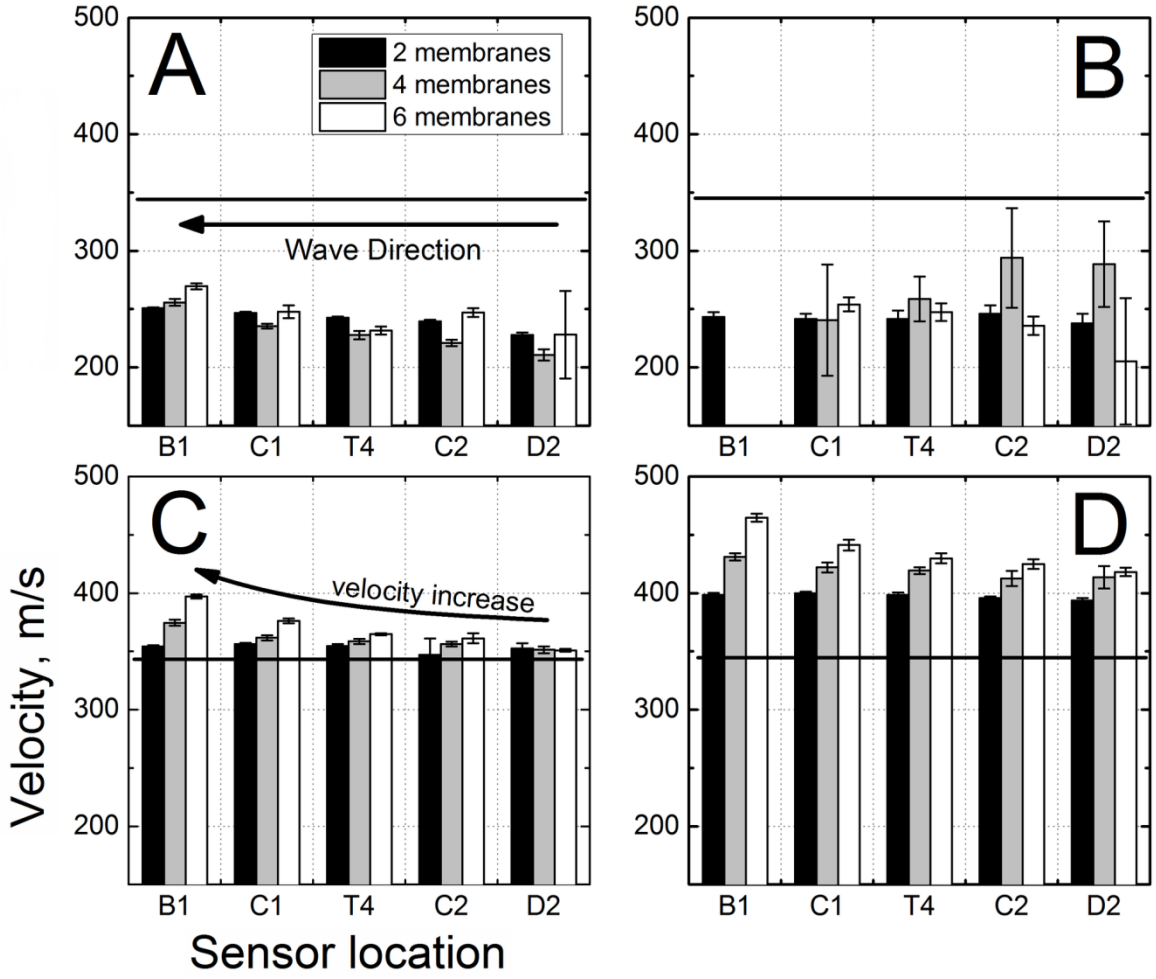

Figure 2.6 Velocities of reflected underpressure (A, B) and overpressure (C, D) waves generated with: (A) open end, (B) 4" gap, (C) 2" gap, and (D) 0.625" gap. The straight arrow indicates the direction of reflected waves' propagation. The horizontal lines indicate the speed of sound in air. The velocity of reflected waves increases with the distance from the end of the shock tube, which is caused by increased helium (driver gas) concentration closer to the breech. The D4 sensor was used as reference.

2.3.5 Optimization of End Plate Gap

This work demonstrates control of the loading conditions inside of the shock tube can be easily achieved by the optimization of the end plate gap distance. The exposure of the specimen can be limited to a single shock wave without additional secondary over- or underpressure waves by optimization of the end plate gap distance. For this purpose, authors ran a series of tests generating shock waves with three different magnitudes. The

shock tube end plate was set in the reflected shock wave regime (0.625" and 2" gap). Three linear functions were generated for both configurations (Figure 2.7A) and it turned out all these functions converge in a single point at 2.8 inches. The optimized end plate gap was then used to verify predictions and as can be seen in Figures 2.7B-D there are no secondary artifacts in the test section as measured by sensor located at T4.

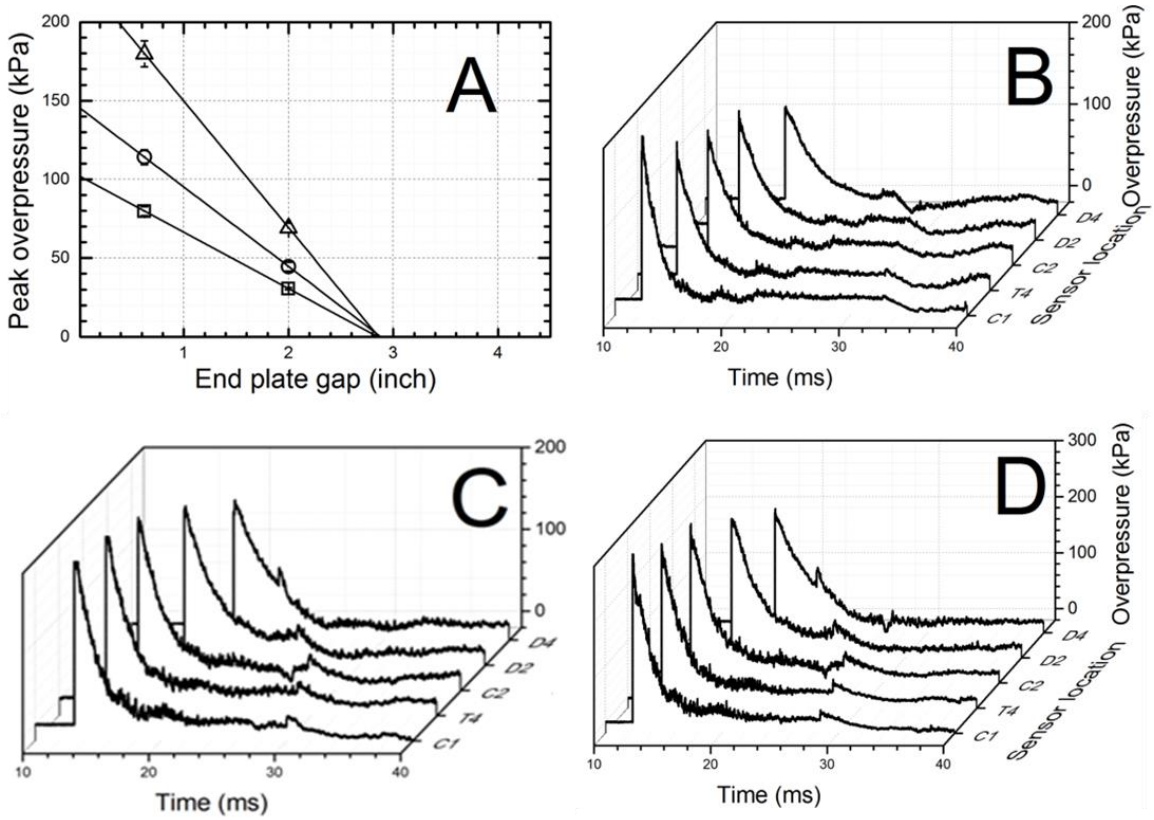

Figure 2.7 The optimization of the end plate to the shock tube gap distance. (A) Reflected peak overpressure values measured at the D4 location for three different membrane thicknesses (0.02, 0.04 and 0.06 inch) and two different end plate gap sized (0.625 and 2.0 inches) were used to identify the optimal gap size, i.e. the point on the plot where all linear functions converge (x_0 = 2.85 inch). Overpressure profiles recorded using optimized end plate position at three different blast intensities generated using: (B) 0.02", (C) 0.04", and (D) 0.06".

2.3.6 Numerical Simulations of Shock Wave Propagation

Numerical simulations of the shock wave propagating in the tube were also performed (Figure 2.8). The data recorded by the T4 sensor was used as the input for all three membrane thicknesses used in the experimental design. A representative example of results is presented in Figure 2.8B for pressure history of a shock wave generated using Mylar membrane with thickness of 0.020" and 2 inch end plate gap. Overall, the results between simulations and experiments agree well. It would appear all characteristic features (peak overpressure, duration, and velocity) are replicated with good accuracy and fidelity for incident as well as for secondary waves.

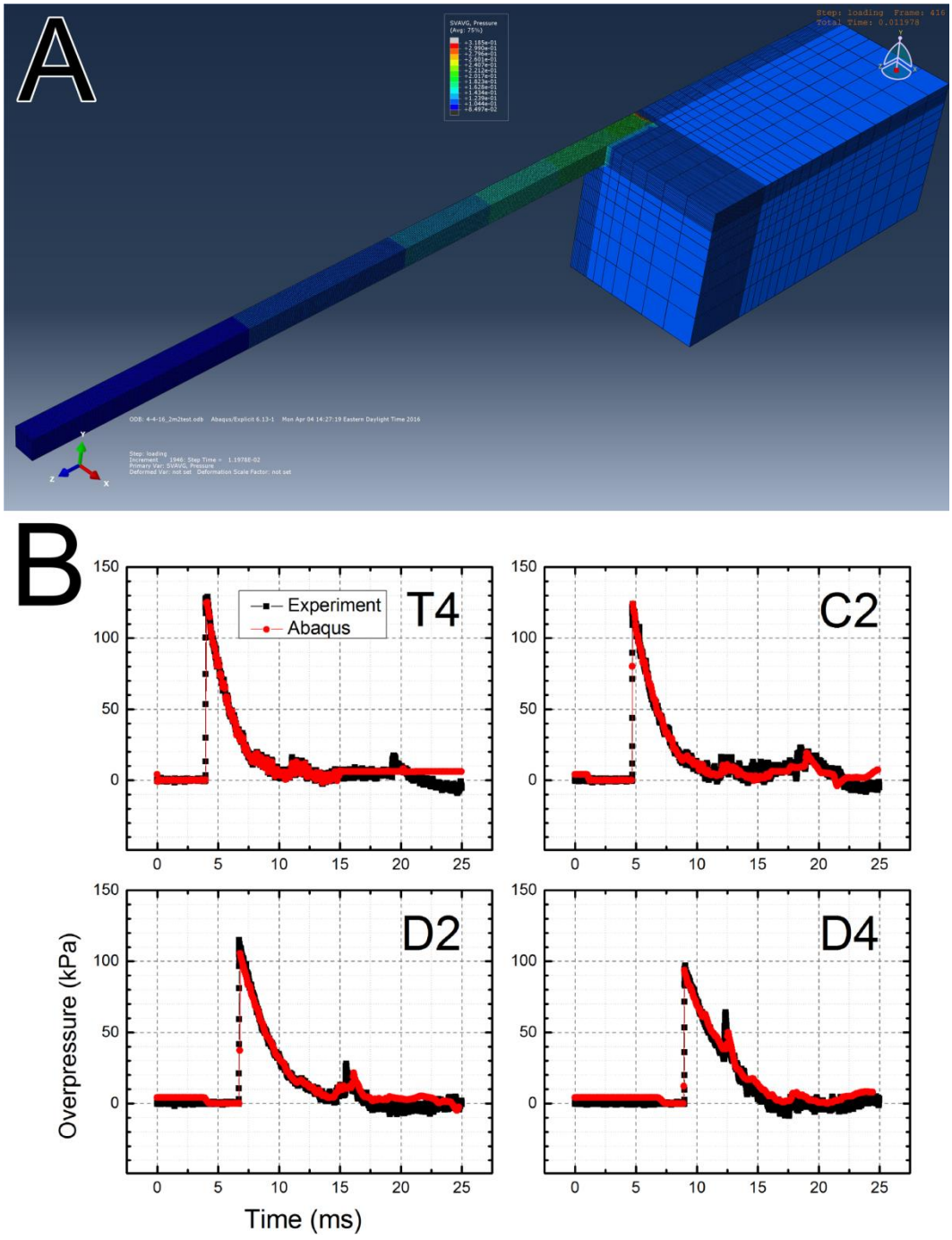

Figure 2.8 Numerical simulations: (A) isometric view of the full scale model of the 9 inch square cross section shock tube, (B) comparison of pressure traces recorded experimentally and obtained as results of numerical simulations with Abacus software for shock wave generated using 0.020" thick Mylar membrane and 2 inches end plate gap. Input feed for simulations was composed using initial 15 ms of the incident overpressure recorded by T4 sensor and 10 ms of baseline signal. This was done to eliminate secondary loading waveform from input data, which leads to erroneous calculations.

2.3.7 Experimental x-t Diagram

In order to establish boundary conditions for the x-t diagram measurements of shock wave propagation in the shock tube, secondary waves with 0.625" endplate distance were taken. This configuration results in generation of the maximum reflected pressures in the shock tube and three replicates per each of three membrane thicknesses were taken. The other extreme case is fully open end which results in the underpressure secondary wave, and comparison between these two cases (fully closed reflected waves and the fully open underpressure waves) is presented in Figure 2.9.

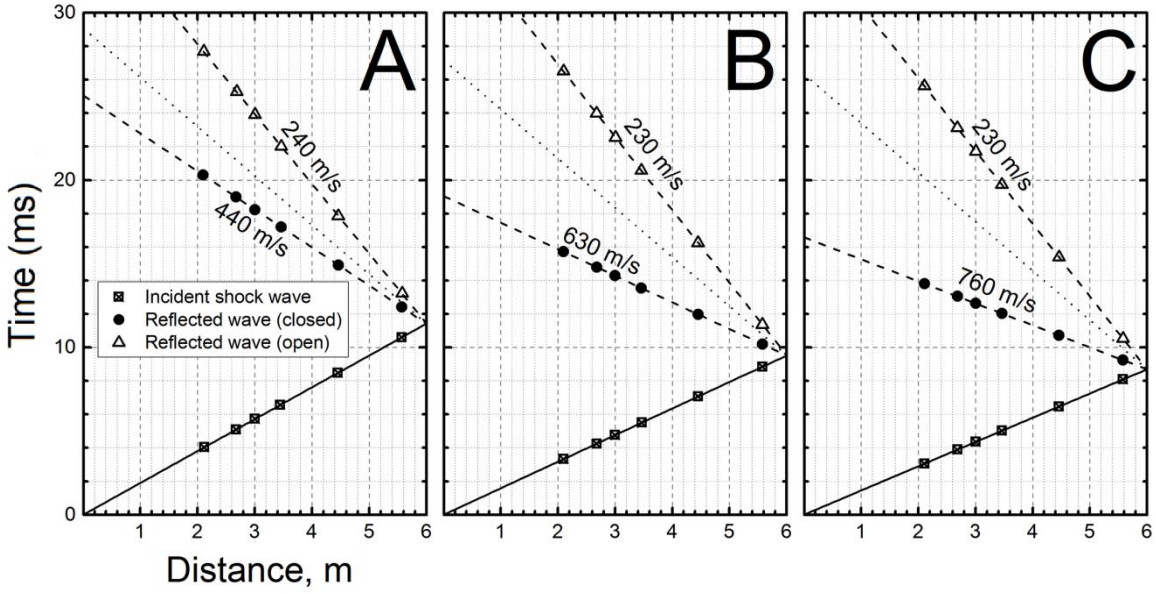

Figure 2.9 The distance-time (x-t) diagrams for incident and reflected waves based on experimental arrival times obtained at membrane thicknesses of: (A) 0.02, (B) 0.04, and (C) 0.06 inches, respectively. The traces representing reflected waves are from experiments when the tube was fully closed and the underpressure waves observed when no endplate was present. Speed of sound for reflected wave domain is marked as dotted line.

2.4 Discussion

Compressed-gas driven shock tubes remain the most widely used and convenient method to generate controlled characteristics shock waves in laboratory setting[16,99]. In spite of the popularity of this test device, the development of the blast wave along the length of the tube is not well understood, and clarification is required regarding the nature of loading conditions (presence of reflection and under-pressure waves) inside the shock tube. Earlier work from this group has clearly shown that in order to simulate primary blast conditions, the specimen have to be placed well inside the shock tube[22,100]. But even at this new location, compressive or expansive pressure waves can still affect the loading condition of the specimen. If these secondary waves are not properly extinguished they can be introduced after the original shock wave, and thus result in additional, potentially unwanted biomechanical load sustained by the test subject. The mitigation of secondary loading is thus of paramount importance for studying the effects of shock waves, especially for delineation of elementary mechanisms of bTBI. In this chapter, the use of an end-reflector plate to modify the reflection and under-pressure waves that reenter the shock tube and resulting loading conditions was investigated and described.

The incident pressure measured in the shock tube decreases as the shock wave propagates towards the exit (Figure 2.2), independent of the test configuration used. However, there are no statistically significant differences in BOPs measured by C1 and T4 sensors ($p > 0.05$, marked with ampersand). This indicates the dynamics of shock wave generation: the expanding driver gas impact is decreasing until it reaches minimum at C1, since the volume expansion exceeds B1 sensor position (calculated using ideal gas conditions), thus the BOP registered by C1 sensor remains virtually constant between C1

and T4 sensors, which is then followed by BOP decay further downstream (C2, D2 and D4 sensors, Figure 2.2D). The calculated average velocities of shock waves generated using three different membrane thicknesses, are in line with these observations (Figure 2.3), i.e. the decrease in BOP is accompanied by respective decrease in shock wave velocity. The impulse measurements reveal more detailed picture of the dynamics of the system (Figure 2.4). While the impulse is diminishing in the driver gas affected region (B1 to C1) the impulse of 'free' shock wave is increasing (C1 to T1) and thus fully developed shock wave is present at T4 location (Figure 2.4D). Further downstream the impulse is not changing its value, but considering the BOP is steadily decreasing with accompanying decreased velocity it indicates the dissipation of energy of the shock wave. There are currently a number of competing theories which explain the decay of shock waves. The decay of spherical and cylindrical shock waves (3D and 2D waves encountered in the field conditions) is caused by purely geometrical factor as the intensity of the shock wave decreases with as an inverse of the square radius (distance) from the epicenter ($1/r^2$, for shock waves separated from the source) or following linear relationship ($1/r$), respectively[101]. However, these two are not applicable to unidimensional waves generated in the shock tube. The viscous effects near the shock tube walls (wall friction, growth of the boundary layer) were proposed as explanation of observed attenuation of the shock wave intensity in the tube[102,103]. These effects are considered more important for shock tubes with relatively small diameters ranging from 0.3 to 3.8 cm[102], while in this case the diameter is much larger (9 in, or 22.86 cm) and thus these effects are less likely to be responsible for observed attenuation. The dusty medium was proposed as responsible for decay of the shock waves propagating in the

shock tube[35,36]. In the present case, this effect is negligible, since no appreciable sized particles were purposely introduced into the environment and typically the number of dust particles in the air is insufficient to be solely responsible for the intensity decay. The hypothesis suggesting the rarefaction wave following the incident shock wave was also proposed as a mechanism of shock wave dissipation[100,104], but in the experimental data generated here, this type of waves were never observed. However, in this model used for numerical simulations the agreement between experimental data and theory is excellent (Figure 2.8). This model doesn't include any of postulated mechanisms of shock wave attenuation discussed in this paragraph. Thus, it appears simple expansion of the pressure contained within the shock wave is solely responsible for observed attenuation.

The values of impulses at the D4 sensor location for both short gap (0.625" and 2", Figure 2.4) end plate configurations are obscured by presence of secondary shock waves, which overlap with a primary wave (Figure 2.8B). This illustrates the loading experienced by the specimen in that location, i.e. the loading is never a single primary shock wave, but a sum of primary and secondary loading. The nature of secondary loading will depend on the end configuration and it will be: 1) additional reflected shock wave with intensity dependent on end plate gap, or 2) underpressure wave (for sufficiently large gap and open end). Independent of the nature of the secondary loading the conditions experienced by the specimen mounted in the location are more complex than those encountered in any other location in the shock tube. The specimen receives almost double the loading of the original shock wave (for tests conducted with 0.625 and 2 inch gap) or mixed mode loading of incident over- and secondary under pressure waves (for four inches gap and open end configuration).

The gap size between the reflector plate and the end of the shock tube governs the type of generated secondary wave, i.e., when it is below critical distance reflected overpressure waves are generated, however when the gap size is larger than the critical size, the under-pressure waves are created (Figures 2.1A, 2.5 and 2.6). The nature of the generated waves dictates their propagation speed: the under-pressure waves generated during experimentation don't exceed the speed of sound (Mach number = 1.0, marked as horizontal lines in plots presented in Figure 2.6), which is in agreement with existing knowledge[105]. The reflected waves for the shortest end-plate gap travelled faster than the speed of sound, but were slower than the original shock front (Figures 2.3, 2.6 and 2.9). Moreover, an increase in velocity with the time of propagation for all reflected positive pressure shock waves was observed. This phenomenon is caused by increased concentration of the driver gas (helium) in the part of the shock tube closer to the breech (sound speed in helium is 1007 m/s, while it is 343 m/s in air at 20 °C) shortly after the membrane burst. Also, it should be noted that these reflected over- and under-pressure waves travel in the opposite direction of the original shock wave.

The calculated velocities of the underpressure and reflected shock waves illustrate the impact of the driver gas has on the dynamics of the shock wave propagation. As the compressed helium ruptures the membrane, the original shock wave travels into the body of the shock tube, and the driver gas is diffusing towards the test section. The reflected wave traveling towards the breech is propagating in the mixture of air and helium, and hence reflected shock wave velocity gradually increases. This effect is more pronounced for shots with six membranes (0.06" thickness), because higher helium pressure is necessary to cause membrane rupture (average burst pressure was 250, 490 and 730 psi,

for membrane thickness of 0.02, 0.04 and 0.06 inch, respectively). The velocity of reflection waves is decreased compared to the original shock front, because of energy loss after the reflection (and the portion of the blast that escapes through openings at the mouth of the tube).

The reflection and under-pressure ratios shown in Figure 2.6 demonstrate the effect of positioning an end-reflector plate at the end of the shock tube and potential additional loading that a test subject may sustain due to plate positioning or its absence. In order to minimize the loading caused by secondary waves reentering the shock tube, the end-reflector position has to be optimized to find the position where the action of over- or underpressure waves traveling back inside of the shock tube is minimized or completely eliminated. This can be achieved by running a series of calibration experiments at different incident shock wave intensities and end plate gap distances. However, this knowledge must be coupled with proper positioning of the specimen far away from the end of the shock tube to eliminate any possibility of end effects on the tests specimen.

In this chapter, means to eliminate unwanted secondary artifacts in order to obtain pure shock wave waveform in the test section of the shock tube were systematically evaluated. It is of particular importance for the study of effects of shocks on biological systems, with particular emphasis on the brain. Application of reflector end plate positioned within optimized perimeter resulted in elimination of virtually all secondary positive and negative pressure waves. Results indicate the end of the shock tube is less favorable location to test specimen due to complexity of loading conditions. Incident shock wave exiting shock tube results in formation of underpressure waves, while

reflected pressure waves are created when the end is fully closed or the reflector plate is at relatively short distance from the muzzle. Numerical simulations were used to corroborate the findings and combined with analysis of experimental data these results indicate shock wave decompression as plausible decay mechanism. The tests done in this study should serve as a strong starting point for researchers attempting to ensure accurate loading of test subjects in a compressed-gas driven shock tubes.

CHAPTER 3

TEMPORAL AND SPATIAL EFFECTS OF BLAST OVERPRESSURE ON BLOOD-BRAIN BARRIER PERMEABILITY FOLLOWING TRAUMATIC BRAIN INJURY

3.1 Background and Significance

Blast-induced traumatic brain injuries (bTBIs) are the signature wounds in military and civilian populations due to the increased use of improvised explosive devices and asymmetric warfare in military conflicts and acts of terrorism, domestically and overseas[1-3]. Despite the increase in studies related to bTBI in recent years, there is only a limited understanding of how blast waves interact with the brain and cause injury, which has precluded the establishment of comprehensive diagnostic criteria for bTBI and the potential of therapeutic strategies. A recent survey reported that more than 30 phase III clinical trials aimed at targeting TBI have failed[39-42]. Understanding how blast-induced neurotrauma displays a temporal and spatial evolution of neuropathology in various regions of the brain is critical for the identification of injury mechanisms and the development of preventative measures and treatments for bTBI patients. Among many mechanisms of injury, damage to the BBB has been identified as a potential candidate and has been the focus of several clinical and experimental investigations aimed to establish injury baselines and to determine the timelines for therapeutic interventions for neurotrauma[43,44].

The blood-brain barrier (BBB) is a highly, selectively-permeable membrane that separates the brain from the circulatory system. The BBB is dynamically modulated by cellular interactions between endothelial cells, the tight junctions that join them,

pericytes, and astrocytes that support the endothelial capillaries[45-51]. Many neurological disorders including stroke[52-55], Alzheimer's disease[56,57], Parkinson's disease[49,58], HIV-1 encephalitis[51,59], epilepsy[60,61], and multiple sclerosis[62-64] display impaired BBB permeability. BBB disruption is also one of the most frequently investigated mechanisms of injury in blunt TBI and has been commonly used to evaluate the degree and extent of injury[65-69]. Several groups have reported abnormal opening of the BBB in closed cortical injuries[70-72], weight drop models[73,74], and blast models[69,75-80]. Reported results are derived from different probing methodologies, with different injury models, at different injury intensities, in different spatial regions of the brain. A limited number of studies has implicated increased BBB permeability in the pathology of blast-induced traumatic brain injury but, to the author's knowledge, no such investigation has resolved the temporal and spatial resolution of BBB changes in bTBI, especially as a function of increasing biomechanical blast loadings. While a number of groups have assessed the BBB permeability following blast[77,106-109], it is important to note that not all blast models impart the same type of injury on experimental animals and, for this reason, authors compared the results of this work only to models that feature pure, primary blast injury void of secondary and tertiary effects[21,81].

In this study, rats were exposed to a range of shock waves in a field-validated shock tube and permeability of the BBB was assayed by extravasation of Evans blue (which binds to albumin, a 66kDa protein abundant in blood) and sodium fluorescein (a 376Da molecule) in the frontal cortex, striatum, somatosensory barrel-field cortex, hippocampus, thalamus, and cerebellum. Rats were exposed to sub-mild (35kPa), mild (70kPa), mild-moderate (130kPa), and moderate (180kPa) blast overpressures; these

classifications were based on a 24-hour survival dose-response of rodent models based on this group's previous results (see Figure 2 of reference 57). Also, the Department of Defense (DOD) Instruction 6490.11 dated September 18, 2012 has established policies, responsibilities and procedures for mTBI occurring in the battlefield. When service members are involved in a potential concussive event, they are separated for medical observations and mandatory rest period. DOD defines potential concussive events as the presence of service members within 50m of a blast or exposure to more than a single blast in a year[1]. Based on theoretical analysis, the peak blast overpressure of 180kPa can occur at a distance of about 10m for 100kg TNT explosive. The same blast will produce 130kPa BOP in about 12m, 70kPa in a distance of 16m and 35kPa in a distance of 23m[97]. These field blast loadings were achieved using operating characteristics like membrane thickness, transition length, driver gas, driver volume, and end plates[96]. Additionally, three different time-points post-injury (15min, 4hr, and 24hr) were chosen in order to develop a temporal profile of BBB opening and to identify the extent of barrier breach.

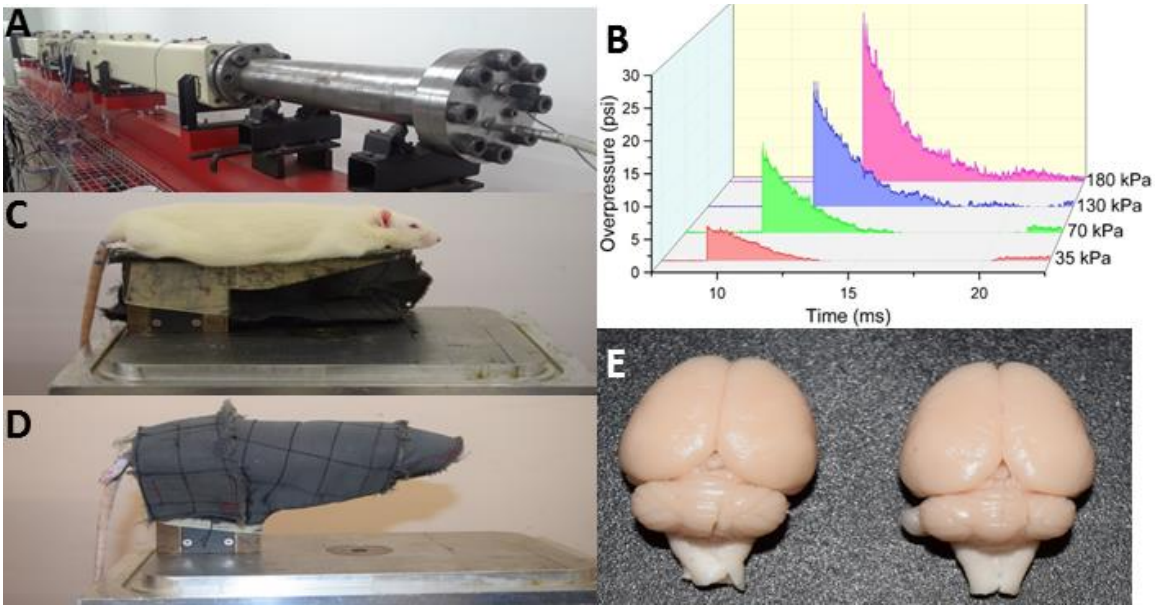

Figure 3.1 The shock tube housed in the blast lab in the center for injury biomechanics, materials, and medicine at NJIT. (A) The 9-inch, square cross-section, 6 meters long shock tube instrumented with pressure sensors along the top of the shock tube. (B) Representative pressure-time profiles acquired from pressure sensors in the shock tube at the four overpressures used in this chapter. (C) Rat holder mounted in the test section of the shock tube, with rat placed in the prone position (top) and (D) tightly wrapped in a harness to minimize head and body motion during blast. (E) Control (left) and injured (right) brains following perfusion-fixation. All blood in the neurovasculature has been washed away, as seen from the white appearance of the brains, confirming that all tracers measured has leaked from the vessels into the brain parenchyma.

3.2 Materials and Methods

3.2.1 Animal Preparation

A total of 88 adult, 10-week old male Sprague Dawley rats (Charles River Laboratories) weighing between 300-350 g were used throughout this study, in accordance with protocols approved by Rutgers University Institutional Animal Care and Use Committee (IACUC). Animals were housed at 22° C with free access to food and water in a 12 hour dark-light cycle. Animals were divided among sham and injured groups for four different blast overpressures and three different time-points post-injury. All methods used

throughout the study were performed in accordance with protocols, guidelines, and regulations approved by Rutgers University IACUC.

3.2.2 Exposure to Blast and Tracer Injections

Rats were exposed to a single shock wave at the Center for Injury Biomechanics, Materials, and Medicine (New Jersey Institute of Technology) in the modular, field-validated shock tube described in previous publications[86,96,110,111]. Based on preliminary findings, an obvious difference was observed between sham and blast groups, where an n=4 was sufficient to achieve a power value of 0.9 (α=0.05 and combined SD of 0.819) based on power analysis. An n=1-2 was added in case of mortality or inadequate perfusion. Continuing the study, an n=5-6 was maintained for all blast groups (for 70 and 130kPa groups, only three animals were used, but statistical significance was achieved). Prior to blast exposure, animals were anesthetized with 5% isoflurane, released in a chamber containing 95% air and 5% CO_2, until unresponsive to noxious stimulation. At this point the rats were mounted and immobilized on a custom rat-holder in the test section of the shock tube. Sham animals were anesthetized and received noise exposure, but kept outside of the shock tube, away from the shock wave. Exposed animals were subjected to a single blast of 35, 70, 130, or 180 kPa peak overpressure and euthanized via transcardial perfusion-fixation at prescribed time-points (15 mins, 4hrs, 24hrs). Tracers were injected two hours prior to euthanasia (animals in the 15 min group received injections prior to blast exposure). Sodium fluorescein was administered via the lateral tail vein (376 Da, 20% dissolved in phosphate-buffered saline [PBS], .02g/mL, 0.7mL delivered), under isoflurane anesthesia at the same time Evans blue was (69 kDa when bound to albumin, 2% solution dissolved in PBS, .002g/ml, 0.7mL delivered). Two hours

were given as to give sufficient time for the tracers to circulate the body multiple times and perfuse even deeper neurovasculature across all experimental groups. Other groups have used both these dyes to assess BBB permeability up to four hours following tracer administration[69,112]. Half-life of EB in circulation was confirmed to be over four hours, while the same is true for NaF half-life[113-115], instilling confidence that allowing two hours for circulation and extravasation for these tracers is adequate.

As a quality control measure, high-speed video was monitored and recorded with a Photron FASTCAM Mini UX100 operating at a framerate of 5000fps to capture any substantial head/body movement during blast, in order to exclude the effects of secondary/tertiary injury from this study. Approximately two seconds of video footage were recorded per exposure and then saved via PFV (Photron FASTCAM Viewer) 3.3.5 software. Incident overpressure at the location of the animals in the test section of the shock tube was recorded at 1.0MHz sampling frequency by a custom LabView program running on in-house built data acquisition system based on National Instruments PXI-6133 32 MS Memory S Series Multifunction DAQ Modules and PXIe-1082 PXI Express Chassis. PCB Piezotronics (Depew, NY) model 134A24 pressure sensors were used in all experiments.

3.2.3 Tissue Preparation, Absorption Spectrophotometry, Ex-Vivo Imaging and Analysis

Rats were perfusion-fixed two hours following tracer administration. Prior to perfusion, blood serum was extracted from the left ventricle (approximately 3ml volume). Rats were transcardially perfused with phosphate buffered saline (PBS) and brains fixed with 4% paraformaldehyde (PFA). Brains were then liberated from cranial vaults, immersed in 4% PFA for an additional 48 hours and cryoprotected through immersion in 30% sucrose.

Appearance of brains can be seen in Figure 3.1E, all color from the brain was removed indicating a complete saline perfusion. Brains were then dissected into 100 micron sections using Rat Brain vibratome (Kent Scientific Corp.) and mounted on glass slides. Regions of interest included the frontal cortex, striatum, somatosensory barrel-field cortex, hippocampus, thalamus, and cerebellum. Each animal offered 30 sections across five regions that were analyzed. Slides contained between two to three sections, resulting in over 200 slides scanned throughout this study. Slides containing different brain regions were digitized (10x magnification) using Leica Aperio Versa 200 digital pathology grade slide scanner. Fluorescent intensities were quantified after excitation at 488nm (sodium fluorescein), 50ms exposure, and 594nm (Evans blue), 125ms exposure, using AreaQuant software specifically designed for this imaging application (Leica Biosystems) and expressed as average fluorescence intensity/unit area. This imaging technique allows for visualization of micro-structural details and digital scanning affords the ability to image large brain regions with no loss of resolution. In order to quantify fluorescence intensities, regions of interest were manually outlined in different brain section. For each channel (green 488nm and red 594nm), a minimum intensity threshold value was selected to exclude any background fluorescence from calculation. The AreaQuant algorithm then determines if the intensity value of each pixel enclosed in the outlined region exceeds the minimum intensity threshold and outputs the total area of positive stain for each brain regions, the average intensity in each channel, and the expression profile of the tracers.

As a means to validate the results of fluorescent image quantitation, absorption spectrophotometry was conducted on homogenized frontal cortices extracted from control and acutely injured rats (n=5, 180kPa). Rats were sacrificed via saline perfusion

(no fixation) and brains were extracted, sectioned, and frozen in dry ice. Absorption was measured and standard curve generated from seven gradient dilutions of Evans Blue. Experimental samples were plotted against the curve (R^2 = 0.998) using SpectraMax i3 (Molecular Devices) microplate reader and SoftMax Pro 6.5 software. Output concentration was converted into micrograms per mg of brain tissue.

3.2.4 ELISA

As a means to alternatively evidence BBB disruption, tight junction protein changes were examined in the cerebral hemisphere by using ELISA. Following perfusion with PBS, brains were excised from the skull and cerebrum was homogenized in CellLytic-M (Sigma) using sonicator with probe amplitude set to 45% on ice. Samples were then centrifuged at 14,000g at 4°C. The protein concentration in the samples was estimated bicinochoninic acid (BCA) method (Thermo Scientific, Rockford, IL). Subsequently, samples were diluted in PBS and loaded onto ELISA plate (LSBio, Seattle, WA). Serum samples were also loaded onto same plate for tight junction protein quantification and separate serum ELISAs were run for s100-β. Plates were read in microplate reader (Spectra Max i3, Molecular Devices) at wavelength of 450nm. Steps of ELISA were conducted in accordance with manufacturer instructions and samples plotted against a standard curve made up of eight samples (R^2 = 0.995, 0.999 for occludin and claudin-5, respectively) using SoftMax Pro 6.5 software.

3.2.5 Immunofluorescence

In order to further prove blood-to-brain leakage following blast injury, double-immunofluorescence studies for RECA-1 and CCL2 were conducted in the frontal cortex, four hours post-injury (n = 3) as a means to detect infiltration of monocytes into the brain

parenchyma. Following transcardial perfusion-fixation, cryoprotection in sucrose, and tissue sectioning (20μm thick sections for immunohistochemistry), sections were mounted in glass slides and washed with 10mM PBS, fixed in ice-cold methanol (100%) solution for ten minutes at –20 °C. The tissue sections were blocked with 10% donkey serum at room temperature for 1 hour in PBS containing 0.03% Triton X-100. Fixed tissues were incubated overnight at 4 °C with respective primary antibodies to RECA-1 (Mouse monoclonal, Abcam, 1:50) and CCL2 (Rabbit polyclonal, Abcam, 1:50). Double immunofluorescence was performed using Alexafluor 594 for RECA-1 and Alexafluor 488 for CCL2. Slides containing different brain regions were digitized (20x magnification) using Leica Aperio Versa 200 fluorescent microscope and slide scanner.

3.2.6 Statistical Analysis

Data are presented as mean + standard error of the mean. Statistical significance was determined using one-way analysis of variance (ANOVA) to compare mean fluorescence intensities of different brain regions for sodium fluorescein and Evans blue with a Tukey pairwise test done to determine differences between individual time-point and overpressure groups. Statistical comparisons were also made for each blast overpressure and each time-point post injury. Normalcy and population variance homogeneity were assessed with Shapiro-Wilk and Levene's tests respectively. Differences between means were assessed and probability levels of $p < 0.05$ were considered statistically significant. Minitab 17 Statistical Software was used for all analyses and Origin 2017 was used for generation of bar plots. Bar plots presented are in semi-log scale in order to capture magnitudinal differences between groups. Fluorescent images were taken using Aperio Versa software and analysis and export done via ImageScope software (LEICA Corp.).

3.3 Results

3.3.1 Primary Blast Induces Breakdown of the Blood-Brain Barrier

The blast injury model developed at NJIT, capable of reproducing field-relevant blast overpressures and previously characterized[86,111,116,117] was used throughout this study (Figures 3.1A and 3.1B). All test animals were mounted in the custom-made rat holder and placed in the test section of the shock tube (Figures 3.1C). Rats were immobilized with the head restrained in order to ensure no confounding head movements and possible acceleration/deceleration that can be artifacts of this study (Figures 3.1C and 3.1D). Rats (n=6) were exposed to a single blast exposure of varying overpressures (see above) and subjected to transcardial perfusion (with phosphate buffered saline)-fixation (with 4% paraformaldehyde) within 15 min from exposure of animals to blast loading. The extent of extravasation of both sodium fluorescein and Evans blue was evaluated in all selected regions of the brain (Figures 3.2 and 3.3). These quantitative results support the assertion that blast-induced BBB opening allows for extravasation of molecules of 69kDa or smaller immediately following injury and, given an increase in molecular mass, extravasation of tracers was less widespread.

The fluorescence detection method of extravasation was also validated with absorption spectrophotometry for Evans blue. Animals (n=5) exposed to 180kPa shock wave showed an average of 45.6% increase in the tissue content of EB than control animals wherein the precise concentration of EB present in tissue was derived from a standard curve made of seven different EB dilutions (Figure 3.2I).

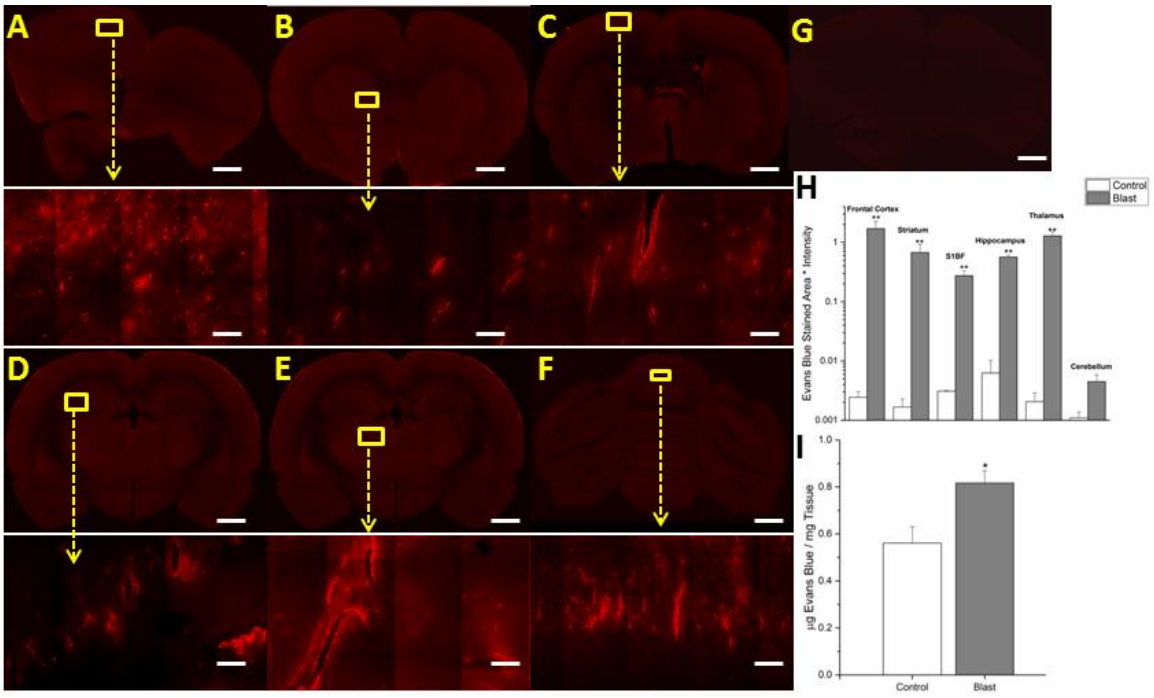

Figure 3.2 Fluorescent images of Evans blue extravasation. Images show whole coronal sections as well as zoomed-in 40x images in representative regions in the (A) frontal cortex, (B) striatum, (C) somatosensory barrel-field cortex, (D) hippocampus, (E) thalamus, and (F) cerebellum, 15 minutes following 180kPa blast exposure. Control images were dramatically enhanced, yet still show limited visibility, due to the absence of extravasated dye. Frontal cortex was taken as a representative control image (G). Quantitation of extravasation is shown using a semilog plot in order to capture magnitudinal differences (H). Absorption spectrophotometry results of Evans blue in control and injured rats (n=5) (I). [*] indicates a difference in intensity compared with control with a statistical significance of $p < 0.05$, [**] indicates $p < 0.01$. Scale bars equal 1mm in coronal sections and 50µm in 40x images.

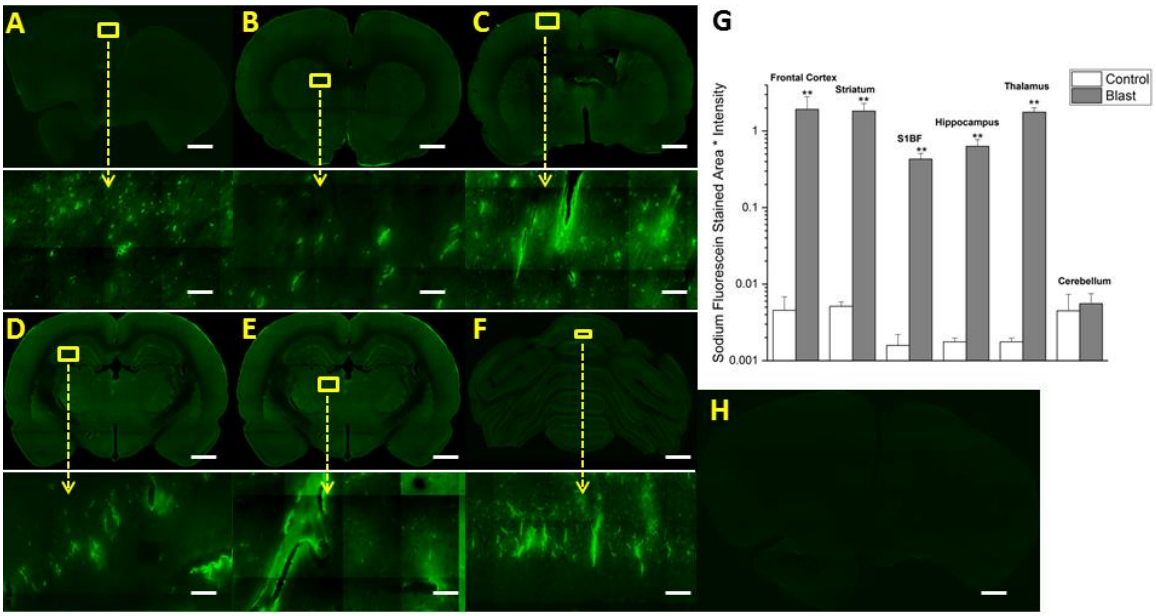

Figure 3.3 Fluorescent images of sodium fluorescein extravasation. Images show whole coronal sections as well as zoomed-in 40x images in representative regions in the (A) frontal cortex, (B) striatum, (C) somatosensory barrel-field cortex, (D) hippocampus, (E) thalamus, and (F) cerebellum, 15 minutes following 180kPa blast exposure. Quantitation of extravasation is shown using a semilog plot in order to capture magnitudinal differences (G). Control images were dramatically enhanced, yet still show limited visibility, due to the absence of extravasated dye. Frontal cortex was taken as a representative control image (G). [**] indicates $p < 0.01$. Scale bars equal 1mm in coronal sections and 50μm in 40x images.

3.3.2 Different Brain Regions Express Different Degrees of BBB Permeability Following Moderate Blast Injury

After exposing animals to moderate blast (180kPa), differential damage was observed in six different regions immediately following trauma (~15 min). In almost every region studied, statistically significant differences ($p < 0.01$), as determined by ANOVA followed by Tukey test, in the levels of both extravasated dyes was observed, highlighting the diffuse nature of bTBI (Figures 2-3). The quantitative values of the fluorescence intensities of EB (as measured by intensity * stained area) between control and blast injury groups in different brain regions are as follows: frontal cortex (control 0.002432, blast 1.699085, 700-fold, $p = 0.006$), striatum (control 0.001674, blast

0.675456, 400-fold, p = 0.001), somatosensory-barrel field cortex (control 0.003094, blast 0.274115, 90-fold, p = 0.009), hippocampus (control 0.006258, blast 0.564796, 90-fold, p = 0.001), thalamus (control 0.002056, blast 1.282525, 600-fold, p = 0.002) and cerebellum (control 0.001102, blast 0.00448, 4-fold, p > 0.05); and for sodium fluorescein: frontal cortex (control 0.004555, blast 1.91963, 400-fold, p = 0.008), striatum (control 0.005134, blast 1.822249, 300-fold, p = 0.008), somatosensory barrel-field cortex (control 0.001584, blast 0.429447, 250-fold, p = 0.009), hippocampus (control 0.00794, blast 0.630788, 80-fold, p = 0.009), thalamus (control 0.003556, blast 1.767197, 500-fold, p = 0.004) and cerebellum (control 0.004479, blast 0.055629, 30-fold, p > 0.05). The most robust changes occurred in the frontal cortex, striatum, and thalamus for both tracers while minimal to no statistically significant extravasation was observed in the cerebellum, which aligns well with results from previous investigations[69,118]. In every other region analyzed, there is at least a tenfold difference in the amount of extravasated dyes compared to controls in the acute time period.

3.3.3 Blood-Brain Barrier Permeability Varies as a Function of Time Following Moderate Blast Injury

In order to determine the time-course for blood-brain barrier permeability following blast, groups of (n=4-6) rats were sacrificed at specified times post-injury (15 min, 4 hours, 24 hours). While the amount of extravasation was significant for both sodium fluorescein and Evans blue immediately after blast, there was an even greater increase in tracer penetration four hours following the blast exposure (Figures 3.4 and 3.5). Increases over controls were as follows for Evans blue at four and 24 hours, respectively (four hour blast values followed by fold-increase and 24 hour blast values followed by fold increase): frontal cortex (3.270751, 1300-fold, 0.005012, 2-fold), striatum (1.681731, 1000-fold,

0.006758, 4-fold), somatosensory barrel-field cortex (0.427674, 150-fold, 0.005808, 1-fold), hippocampus (0.781473, 120-fold, 0.00166, < 1-fold), and thalamus (2.080952, 1000-fold, 0.005169, 2-fold) and for sodium fluorescein: frontal cortex (3.365124, 700-fold, 0.014903, 3-fold), striatum (1.966033, 400-fold, 0.00229, < 1-fold), somatosensory barrel-field cortex (0.596185, 400-fold, 0.003732, 2-fold), hippocampus (0.885597, 100-fold, 0.006966, < 1-fold), and thalamus (2.223883, 600-fold, 0.014472, 4-fold). Interestingly, 24 hours post-injury, the extravasation of EB and NaF returned back to that of control levels (Figures 3.4 and 3.5) suggesting possible resealing occurring at or before 24 hours.

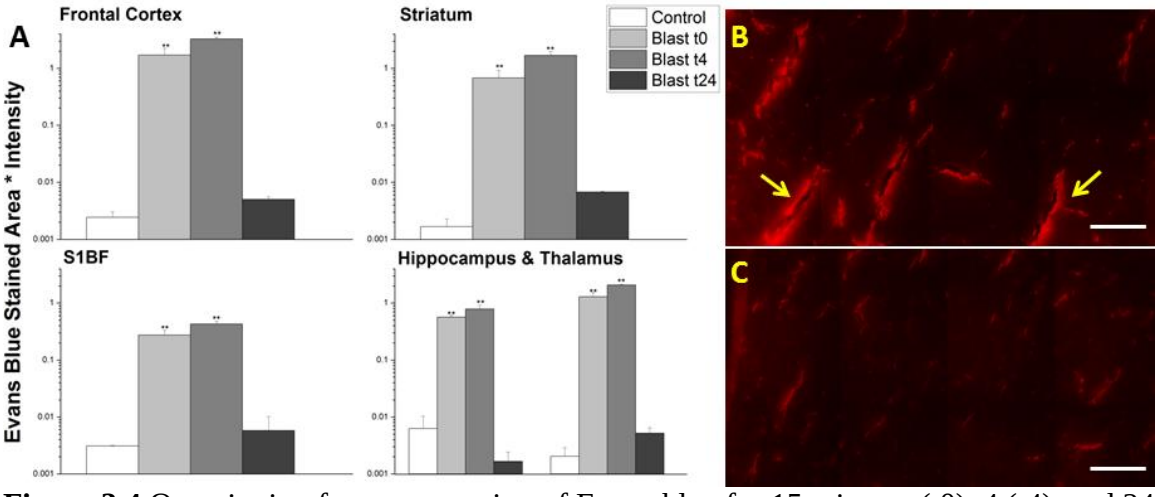

Figure 3.4 Quantitation for extravasation of Evans blue for 15 minutes (t0), 4 (t4), and 24 (t24) hours post-180kPa blast exposure in frontal cortex, striatum, somatosensory barrel-field cortex, hippocampus, and thalamus using a semilog plot in order to capture magnitudinal difference between 4 (B) and 24hrs (C). Arrows indicate areas of leakage from the vessels, which are more pronounced in four hours than any other time point studied in this investigation. [**] indicates a difference in intensity compared with control with a statistical significance of $p < 0.01$. Scale bar equals 100μm.

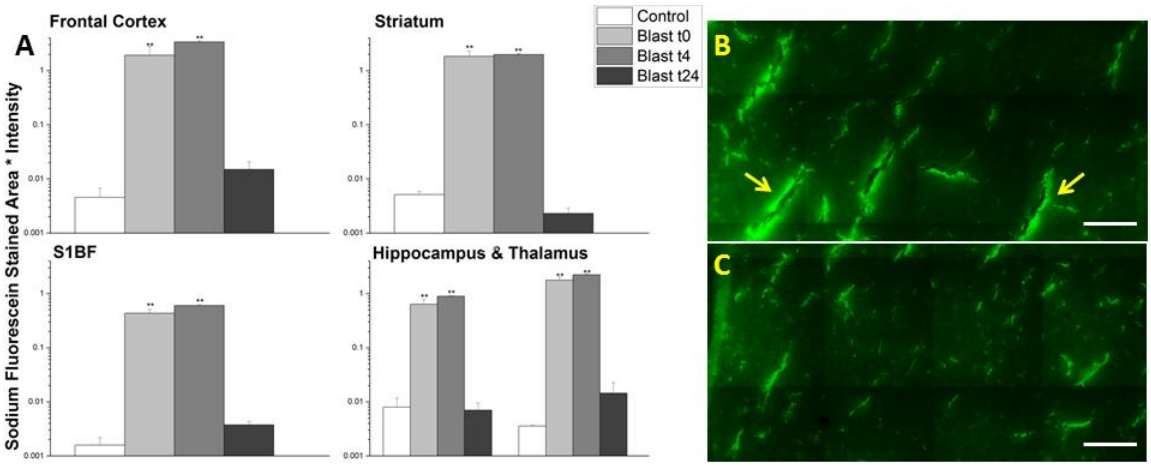

Figure 3.5 Quantitation for extravasation of Evans blue for 15 minutes (t0), 4 (t4), and 24 (t24) hours post-180kPa blast exposure in frontal cortex, striatum, somatosensory barrel-field cortex, hippocampus, and thalamus using a semilog plot in order to capture magnitudinal difference between 4 (B) and 24hrs (C). Arrows indicate areas of leakage from the vessels, which are more pronounced in four hours than any other time point studied in this investigation. [**] indicates a difference in intensity compared with control with a statistical significance of $p < 0.01$. Scale bar equals 100μm.

As an alternate means to investigate BBB disruption as well as to examine possible mechanisms of BBB permeability change following blast, levels of tight junction proteins (TJPs) occludin and claudin-5 were determined in lysates from cerebral hemispheres by quantitative ELISAs. Statistically significant reductions in tight junction protein abundance were observed at this time point, which serves as further evidence of the compromised BBB (Figure 3.6). Noteworthy that such reduction in TJPs in brain lysates is accompanied by a concomitant increase in their levels in serum samples obtained from the same animals that are used for evaluation of brain levels of tight junction proteins. These data not only strongly suggest that shockwave propagated from blast is able to dislodge TJPs from the cerebral vasculature but also that these proteins translocate to blood.

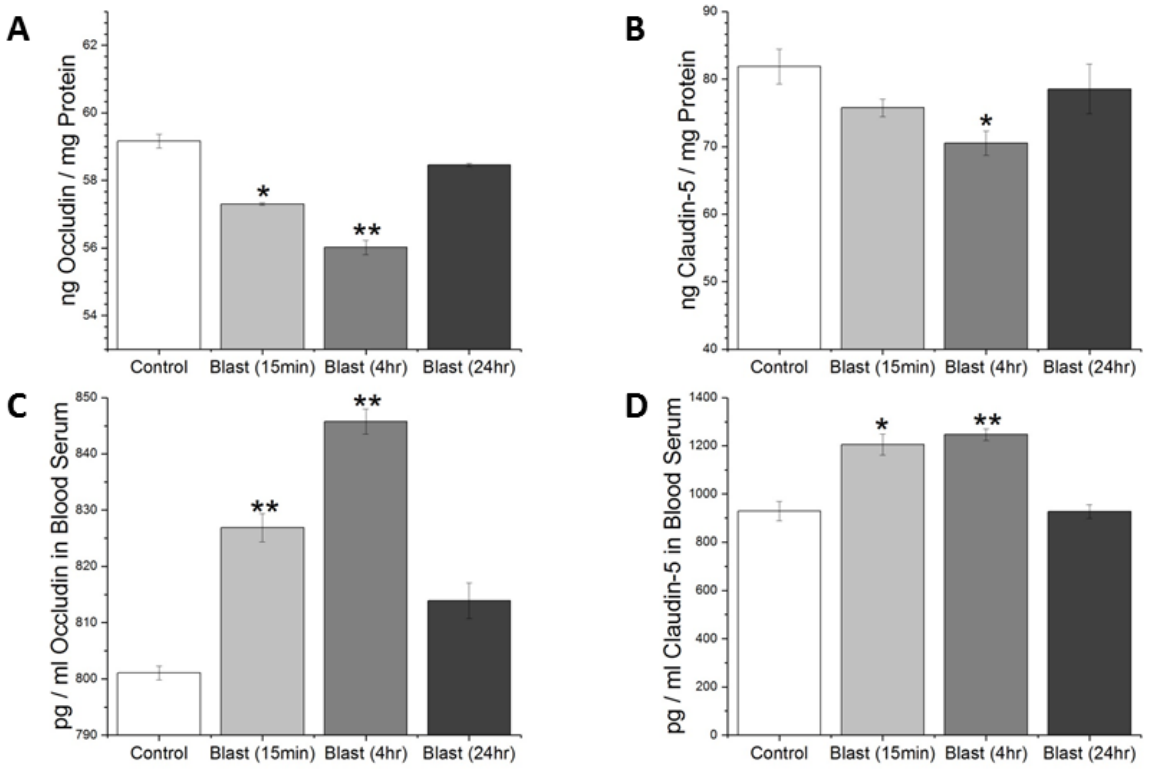

Figure 3.6 Concentrations of tight junction proteins occludin and claudin-5, respectively in brain (A and B) and blood serum (C and D). Assay conducted for blast (180kPa BOP) samples fifteen minutes, four, and twenty four hours post-exposure and compared with controls. [*] indicates a difference in intensity compared with control with a statistical significance of $p < 0.05$, [**] indicates $p < 0.01$.

3.3.4 The Extent of BBB Permeability Displays a Tendency to Increase as a Function of Blast Overpressure

In order to determine the effects of blast overpressure on BBB permeability, groups of (n=3) rats were exposed to mild shockwaves of 35, 70 and 130kPa BOPs and sacrificed immediately after blast. While no measurable extravasation was induced at 35kPa, there is clear evidence of leakage starting at 70kPa (Figures. 3.7 and 3.8) and extravasation quantitation for both tracers showed a tendency to increase with increasing overpressure. The fluorescence intensity increases over controls and were as follows for Evans blue at 35, 70 and 130kPa, respectively as determined by post-ANOVA Tukey test: frontal cortex (0.014762, 6-fold, 0.826735, 340-fold, 0.898087, 370-fold), striatum (0.00983,

5-fold, 0.118309, 70-fold, 0.355441, 200-fold), somatosensory barrel-field cortex (0.0036, 1-fold, 0.101135, 30-fold, 0.215851, 70-fold), hippocampus (0.0.007685, 1-fold, 0.15515, 25-fold, 0.15437, 25-fold), and thalamus (0.003252, 2-fold, 0.380609, 180-fold, 0.773843, 380-fold) and for sodium fluorescein: frontal cortex (0.030414, 7-fold, 1.146571, 250-fold, 1.91895, 260-fold), striatum (0.012241, 2-fold, 0.201411, 40-fold, 0.545131, 100-fold), somatosensory barrel-field cortex (0.003914, 2-fold, 0.132123, 80-fold, 0.256239, 160-fold), hippocampus(0.013312, 1-fold, 0.172132, 20-fold, 0.205551, 25-fold), and thalamus (0.00404, 1-fold, 0.181371, 50-fold, 0.302787, 85-fold).

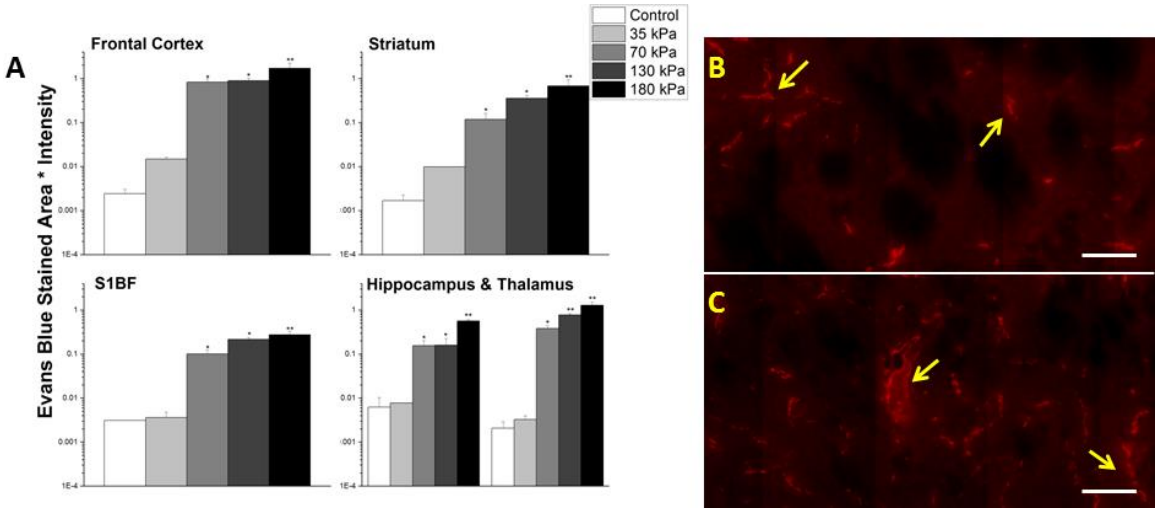

Figure 3.7 Quantitation of extravasation of Evans blue for 35, 70, 130, and 180kPa blast overpressures, 15 minutes post-exposure in frontal cortex, striatum, somatosensory barrel cortex, hippocampus, and thalamus using a semilog plot in order to capture magnitudinal differences **(A)**. The striatum was chosen for illustrative purposes and to qualitatively depict the differences between 70 **(B)** and 130kPa **(C)**. Leaks appear longer and more intense with increasing overpressure in the same brain regions. [*] indicates a difference in intensity compared with control with a statistical significance of $p < 0.05$, [**] indicates $p < 0.01$. Scale bar equals 100μm.

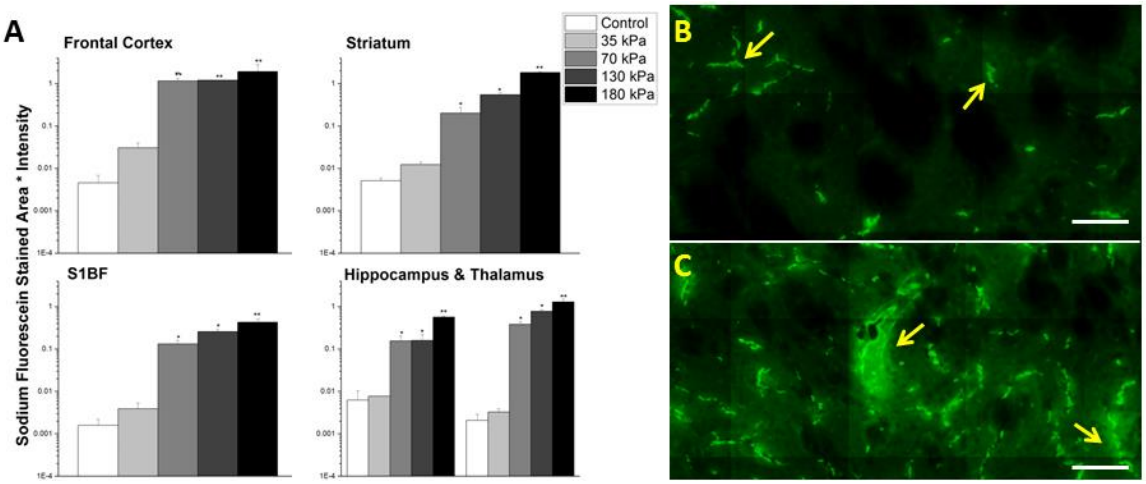

Figure 3.8 Quantitation of extravasation of sodium fluorescein for 35, 70, 130, and 180kPa blast overpressures, 15 minutes post-exposure in frontal cortex, striatum, somatosensory barrel cortex, hippocampus, and thalamus using a semilog plot in order to capture magnitudinal differences **(A)**. The striatum was chosen for illustrative purposes and to qualitatively depict the differences between 70 **(B)** and 130kPa **(C)**. Leaks appear longer and more intense with increasing overpressure in the same brain regions. [*] indicates a difference in intensity compared with control with a statistical significance of $p < 0.05$, [**] indicates $p < 0.01$. Scale bar equals 100μm.

3.3.5 Additional Evidence of Leakage into and out of Brain Following Blast Injury

In order to more strongly display the presence of brain-specific proteins in circulation following blast injury, an ELISA was conducted for s100-β at 4 and 24 hours post-moderate blast (180kPa) in serum samples ($n = 3$, Figure 3.9). At four hours post-injury, concentration of s100-β rose from 399 pg/ml to 594 pg/ml, a statistically significant increase of 48.8% ($p = 0.037$). However, after 24 hours, the protein levels in serum fall to 27 pg/ml, an increase of only 7% from control values ($p > 0.05$).

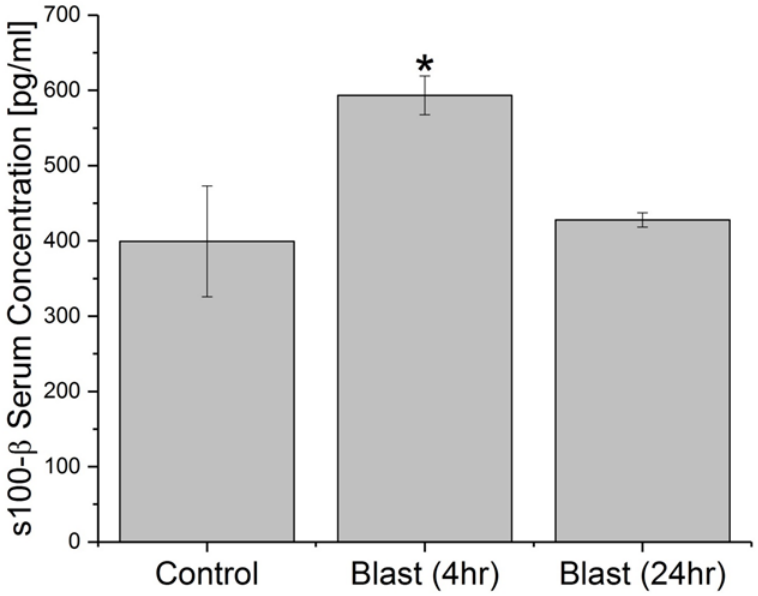

Figure 3.9 Concentration of s100-β in blood serum. Assay conducted for blast (180kPa BOP) samples four and twenty four hours post-exposure and compared with controls. [*] indicates a difference in intensity compared with control with a statistical significance of $p < 0.05$.

Similarly, as an alternative means to demonstrate the presence of blood-borne proteins in the brain parenchyma, an immunofluorescence stain was done for CCL2 (monocyte marker) and RECA-1 (endothelial cell marker) at four hours post-moderate blast in the frontal cortex (n = 3, Figure 3.10). Results indicate that, qualitatively, the presence of monocytes around blood vessels increased following blast compared to controls.

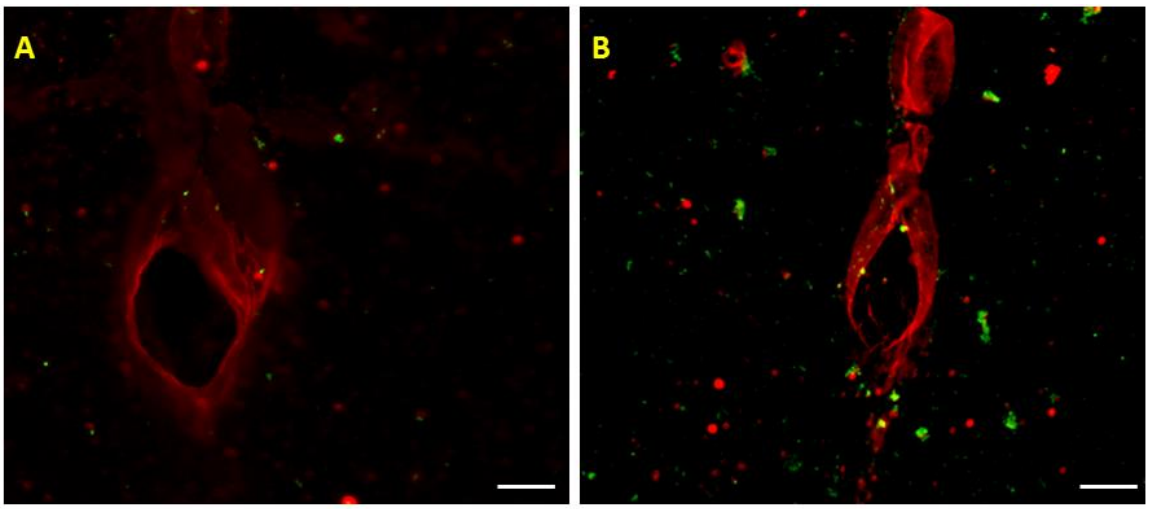

Figure 3.10 Immunofluorescence in frontal cortex for endothelial cell marker (RECA-1) and monocyte marker (CCL2) at four hours post-exposure for control (A) and moderate (180kPa BOP) blast (B). Scale bar equals 50μm.

3.4 Discussion

This work focused on establishing spatial and temporal relationships of the BBB permeability as a function of overpressure in blast-induced traumatic brain injury. Through the use of two tracers (Evans blue and sodium fluorescein) injected intravenously in the lateral tail vein of the rat, the degree of the BBB disruption following injury was functionally assayed. At the sub-mild overpressure (35kPa) very limited extravasation of dyes was observed. A breach in the BBB was first observed at a mild blast overpressure (70kPa) which revealed a significant increase in barrier permeability almost immediately after blast (~15min). In addition to extravasation of tracers (NaF and EB), absorption spectrophotometry was used to demonstrate the breakdown of the BBB by the presence of EB in brain parenchyma. The results of the absorption spectrophotometry offer interesting piece of corroboratory information; unlike gross blunt injuries, where there is a substantial amount of extravasated tracers recorded[119,120],

in this mild-moderate blast injury, a difference of only about 250 picograms of EB was observed between injured and control groups (Figure 3.2).

It is interesting to note that the extravasation of the tracers showed a significant increase as early as 15min following the blast, strongly supporting the hypothesis that direct biomechanical loading of the primary blast was able to disrupt the BBB (Figures 3.2 and 3.3). It is worthy to note that there is no physical impact of external objects as in CCI or weight drop models, nor a specific fluid pressure in subdural space as in fluid percussion model. However, while the degree of BBB disruption appears large when compared to controls (which was negligible), the physiological as well as neurological state of the animal were not altered based on visual observation of the animal's status including unaltered gait, righting and startle reflexes (data not shown). This strongly suggests that this injury can be classified as a subtle, tissue-level mechanical disruption of vasculature. Therefore, caution must be exercised when comparing these results with those from blunt injury models, where injury severity is greater and degree of extravasation is larger but the injury is highly local, mostly restricted to the site of external impact or fluid pressure[70,71,121]. As noted earlier, the degree of the BBB permeability increased further at four hours post-injury (Figures 3.4 and 3.5), which not only indicates the persistence of the BBB disruption but also indicates that, in addition to direct biomechanical loading (shock loads that lasts for a transient period of approximately 3 milliseconds), some secondary mechanisms may be activated post-injury and contribute to BBB disruption for hours after initial trauma.

While several secondary mechanisms have been implicated in the degradation of the BBB including oxidative stress[47,65,68,78], matrix metalloproteinase activity and

neuroinflammation[47,68,73,122], pericyte detachment[50,123-125], astrocytic end-feet swelling and detachment[126-129], among others, precise involvement of one or more of these mechanisms contributing to BBB disruption in bTBI remains to be determined. Previous studies have cited maximum degree of damage to the BBB following mild-moderate TBI (although not blast) occurring between 4-6 hours of injury[43,70,74]. The lack of a detailed time course of BBB disruption in blast injury is a primary motivation for this work and a greater understanding of the temporal nature of the evolution of pathology and contributions of precise mechanisms during the time-course of BBB disruption in blast-induced neurotrauma will aid in diagnostic and therapeutic discoveries[130].

The integrity of the tight junctions was also assessed in the current study immediately following moderate blast, four, and twenty-four hours post injury. Tight junctions are water-tight seals that connect adjacent endothelial cells across the brain vasculature[46,47]. These complexes are comprised of several proteins that anchor the tight junction to the surface of endothelial cells and represent a strong mechanical junction that is the foundation of the BBB. Several groups have studied the integrity of the tight junctions as a means to assess the state of the BBB[65,79,86,131,132]. In the present study, the abundance of tight junction proteins (occludin and claudin-5) was evaluated quantitatively via ELISA (Figure 3.6A and 3.6B). In the acute phase of injury (~15 mins), a reduction in tight junction protein abundance was observed in both occludin ($p = 0.012$) and claudin-5 ($p > 0.05$). Although the reduction in claudin-5 was not statistically significant, it displays a strong tendency to decrease. These results strongly support the tenet that a direct mechanical loading may be able to break and dislodge tight junction complexes and cause subsequent reduction in integrity of the BBB, which may have

manifested in the extravasation of the dyes. Further, at four hours post-blast, levels of occludin and claudin-5 were reduced ($p = 0.002$, $p = 0.035$, respectively) suggesting that, in addition to direct mechanical forces, secondary factors that are likely activated four hours post-injury also contribute to the reduction in TJPs. Such sustained decrease in these proteins may in part be responsible for greater compromise in BBB integrity four hours post-injury observed in the present study. While several factors have been implicated in the breakdown of tight junction proteins, oxidative stress and increased matrix metalloproteinase activity have been shown to contribute to the disruption of the BBB[47,65]. Moreover, restoration of the levels of occludin and claudin-5 observed in the present study within twenty-four hours post-blast corroborates the absence of extravasation seen at 24 hours post-blast.

While the reduction in the brain levels of tight junction proteins suggest a possibility of their dislodging by direct impact of the shockwaves, authors sought to examine the accountability of these proteins in the blood stream, since it is likely that once dislodged, these proteins may be translocated into blood stream. Therefore, the levels of these proteins in serum samples were estimated by quantitative ELISA. Interestingly, a close, inverse correlation on the levels of these proteins between brain homogenates and serum was observed (Figure 3.6C and 3.6D). Fifteen minutes post-injury, there was a significant increase in the amount of occludin ($p = 0.012$) and claudin-5 ($p = 0.011$) detected in the blood serum compared to controls. The amount of detected tight junction proteins further increased four hours post-injury ($p < .001$, $p = 0.002$) for occludin and claudin-5, respectively. These results not only corroborate the ELISA results in the brain tissue, but also give strong support to the assertion that the tight

junction proteins are being mechanically dislodged from the tight junction complexes and being taken up into circulation. Moreover, a complete recovery of these TJPs to the control levels in brain and blood 24 hours post-injury corroborates well with the absence of any extravasation of EB or NaF which together indicate the possibility of resealing of the BBB at this time point.

Several studies that report increased levels of astrocytic protein s100-β in the blood indicate the breakdown of the BBB[47,65,75,133-135]. The current study shows increased s100-β in serum from animals exposed to blast provides additional support to extravasation studies and together represent the involvement of astrocytic defects in the compromise of BBB following blast injury.

To demonstrate infiltration of any blood-borne cells entering the brain parenchyma, an immunofluorescence stain was performed to identify the presence of monocytes in the vicinity of vascular endothelial cells using CCL2 and RECA-1, respectively (n = 3, Figure 3.10). CCL2 is a monocyte chemoattractant protein which presents on blood monocytes and is integral in monocyte mobilization while RECA-1 is a common vascular endothelial marker[136-138]. The increased number of CCL2 staining in the frontal cortex near blood vessels indicates that monocytes are leaking from the blood into the brain parenchyma four hours post-injury. This supports the extravasation results for Evans blue and sodium fluorescein.

In the current study, differential degree of BBB permeability was observed spatially across different brain regions. Such differential blood-brain barrier permeability may, in part, be due to variations in the vascular architecture (density, size, orientation) in different brain regions. Cavaglia's group characterized the variation in neurocapillary

density in the adult rat hippocampus and cortical structures[139]. The hippocampal CA1 region revealed a significantly lower capillary density compared to CA3, but a much more extensive blood-brain barrier leakage. This may instinctively point to an inverse relationship between vascular density and BBB vulnerability; however Cavaglia's studies also showed that neocortical regions have a much higher vascular density compared to neighboring gray/white matter junctions. Since gray matter regions (frontal cortex, thalamus, etc.) have a higher vascular density than the white matter regions, the mechanical shock loading in the acute phase of injury in conjunction with the onset of secondary mechanisms during latter stages may damage the brain regions containing higher vascular densities more than others. Supporting this tenet, these results and many other studies reveal higher degree of BBB damage in the frontal cortex (Figures 3.2-3.5)[69,78,118,132]. In addition to vascular density (number of vessels, vessel length, etc.), it is also possible that vascular orientation and cellular architecture may also be, in tandem, responsible for the observed spatial variation of BBB permeability. From a purely biomechanical perspective, a combination of vascular architecture and, to some extent, perivascular attachment to astrocytes is one of the possible mechanisms to the observed response to the mechanical disruption of tight junctions.

While it is strongly assumed that the propagation of shock uniformly travels and loads the whole brain, absence of BBB damage in cerebellum is interesting. The lack of functional BBB damage in the cerebellar regions has been reported by several groups, but there is still uncertainty to its cause[69,118,140]. Several groups have shown vascular volume in the cerebellum to be higher than that in the cerebrum[141-143], but Holash et. al determined that this difference was due to the inclusion of pia vasculature[144]. Without

pial vessels (which have a BBB quite different from the parenchymal vessels in terms of tight junction distribution and astrocytic ensheathment[145]), the vascular volume of the cerebellum and cerebrum are comparable. Most extravasation studies use intravascular tracers, which do not discriminate between pial and intraparenchymal vessels in the cerebellum. The authors speculate that the lack of extravasation in the cerebellum based on these methods is due to the presence of the pial vessels, but more work needs to be done to validate this hypothesis (ie. isolating parenchymal vessels).

Further, in the current study, based on the high magnification images (Figures 3.2-3.5, 3.7-3.8) it is tempting to speculate that larger diameter blood vessels had greater leakage compared to smaller ones. Hypothetically, given a larger cross-sectional area, these vessels bear a greater brunt of the passing shock wave and hence are more damaged than their smaller counterparts. It is also possible that these larger vessels only appear to leak more because of a greater vascular volume: more vessel content, the more blood is able to leak out in the presence of a vascular rupture. In this case, vessels of all sizes would experience a similar mechanical load from the shock wave and show a similar pattern of leakage (with only differences in leakage volume, proportional to vessel size), which is consistent with the results of this study. When a shock/stress wave encounters a vasculature, the biomechanical forces will be proportional to the projected area and the difference in acoustic impedance between the different materials that make up the local tissue construct. The resistance to deformation will be proportional to the structural integrity of the vasculature vis-à-vis the surrounding cellular architecture. As different subregions of the brain have different architectures and biomechanical characteristics, the

forces, the deformation and hence the BBB leakage will be a function of the specific region under question even if the loading is identical.

After 24 hours following mild blast, a statistically significant decrease in extravasation was observed in all brain regions, which represents possible evidence of a resealing BBB in combination with the restoration of TJPs (Figures 3.4-3.6). A recent study also reported a reduction in BBB damage 24 hours after injury in mice exposed to moderate blast (100kPa)[146]. This, however, may not preclude continued presence of phenotypic changes of the TBI in brain structures since vascular leakage of various blood born substances into the parenchyma may trigger secondary events such as microglial activation leading to neuroinflammation.

At all time-points, in all regions, the total amount of extravasated sodium fluorescein tracer was greater than Evans blue, an intuitive result given the difference in size between these two tracers. One needs to be careful in interpreting the results in terms of fold increase since the baseline data for the smaller molecule, sodium fluorescein, was higher than the larger Evans blue. In no region was there a collection of sodium fluorescein in the absence of Evans blue; meaning that in the current work, there was an insignificant number of breaches in the BBB which could accommodate the 376Da sodium fluorescein but not the larger 69kDa Evans blue.

The present study showing a strong tendency of higher extravasation in animals exposed to 130kPa compared to 70kPa in the acute phase of the injury suggests the BBB permeability changes are directly proportional to increasing BOP, at least in the acute phase of the injury. Interesting that after four hours post-injury such magnitude of difference in the extravasation of EB and NaF as a function of BOP is absent. While the

reason for this is not known, the author speculates that differences in these injuries become more apparent after the acute phase of injury, and such significant changes may be masked once secondary mechanisms begin to occur (four hours), which may uniformly exacerbate injury conditions since, in the immediate phase of injury (~15min), all leakage of the BBB is attributed to the mechanical insult of the shock wave. Therefore, the resulting biomechanical injury may not be grossly different between mild and moderate overpressures at time interval (four hours) where secondary mechanisms begin to occur. Indeed, such differential changes in BBB permeability have also been reported in other investigations[86,117], which may superimpose the mechanical injury with the influences of secondary biochemical mechanisms (e.g., oxidative stress, neuroinflammation).

Our efforts to establish a sub-mild injury model of bTBI led to identifying 35kPa as a BOP that does not show any tracer extravasation. However, the BBB permeability changes are significant with a minimal BOP of 70kPa and increased further as a function of increasing BOPs (Figures 3.7 and 3.8). These results indicate that the mechanical loading sustained at 35kPa is insufficient to cause the significant damage to the BBB that was seen at 70kPa and higher overpressures. Therefore, 70kPa BOP offers a basal injury threshold for the BBB permeability changes to occur under primary blast loading. These studies together demonstrate that BBB permeability is a sensitive phenotypic marker for mTBI in the acute phase of the injury wherein a direct mechanical disruption is able to cause vascular rupture. Accordingly, alterations in the integrity of BBB may be considered a prognostic event to scale the injury severity (i.e., sub-mild to mild vs moderate TBI) as well as the extent of pathological outcomes in blast TBI.

In summary, this work addresses a clear gap in knowledge in the understanding of the BBB permeability in the pathophysiology of blast-induced traumatic brain injury. The results and conclusions presented herein should provide the baseline for future studies attempting to connect the BBB permeability and the pathophysiological progression of bTBI. However, while the authors maintain that these results are reproducible in age-matched rats exposed under the same loading conditions, it is important that the described experimental model is replicated as closely as possible in order to reproduce these results. For example, non-primary injuries will likely be observed if animals are located outside or near the end of the shock tube or if animals are not properly fixed and thus may reveal an altered injury profile.

.

CHAPTER 4

SPATIAL AND CELL-DEPENDENT INCREASE IN NADPH OXIDASE FOLLOWING BLAST-INDUCED NEUROTRAUMA

4.1 Background and Significance

Traumatic brain injury (TBI) resulting from different episodes of head trauma is one of the leading causes of morbidity and mortality in both military personnel and civilian populations. TBI causes approximately 1.5 million deaths and hospitalizations annually in the USA[147-149]. Blast-induced TBI (bTBI) is the most prevalent form of brain injury in soldiers in combat zones due to the widespread use of high explosives in the war zones and an increasing number of cases has also been reported in civilian populations the use of improvised explosive devices (IEDs) by insurgents[150,151].

Among many pathological factors associated with either primary mechanical injury or secondary biochemical cascades, oxidative stress has been shown to play a major role in various models of TBI[82,83]. The main inducers of oxidative stress are reactive oxygen species (ROS) which include superoxide (O2·−), hydroxyl radical (HO·), and hydrogen peroxide (H_2O_2)[84,85]. ROS are normally produced in several metabolic reactions, including redox-reactions (oxidation/reduction), oxidative phosphorylation and in a normal process of electron transport chain reactions. There are a number of enzymes that produce free radicals during their catalytic reactions, which include the NADPH oxidase family, cytochrome P450 (CYP450), cyclooxygenase (COX), lipoxygenase (LOX), and xanthine oxidase (XO).

The NADPH oxidase (NOX) is a multi-subunit enzyme that catalyzes the reduction of molecular oxygen and oxidation of NADPH to generate superoxide radicals ($O_2^{\bullet -}$). NOX comprises subunits that are both plasma membrane-bound (cytochrome b_{558}, comprised of $p22^{phox}$ and $gp91^{phox}$) and cytoplasmic ($p40^{phox}$, $p47^{phox}$, and $p67^{phox}$), which spans across the lipid bilayers[96,152]. A number of NOX isoforms were identified in the brain which include NOX1, NOX2, and NOX4, and their cellular distribution is highly dependent on the cell type[153]. Neurons express both NOX1 and NOX2, microglia are enriched with NOX2, while only small amounts of NOX isoforms were identified in astrocytes[154].

Extensive experimental evidence suggests NOX plays a significant role in the pathophysiology of various forms of TBI. NOX has been shown to be upregulated in a brain in controlled cortical impact model of trauma[153] and closed head injury models[155-157]. This group has previously reported increased protein expression of NOX1 in a rodent model of a single blast injury at different blast overpressure exposures[65,86]. While these studies establish a primary role of NOX1 in the pathophysiology of various forms of TBI, no studies have been performed to determine the spatial and temporal resolution of NOX family of enzymes in the brain and their role in the pathophysiology of bTBI. These results show that, in bTBI, a single blast overpressure exposure is capable of biomechanically loading the whole brain which may trigger a cascade of biochemical events consistent with regional vulnerabilities.

The present study therefore examined the spatial resolution of two isoforms of NOX (NOX1 and NOX2), and their cellular distribution and changes in rats exposed to moderate blast TBI. Levels of superoxide and formation of protein adducts of 4HNE

were also determined. Based on the evidence that blast overpressure waves travel through the whole brain, authors speculate that blast-induced NOX-related oxidative stress will be diffuse across the brain[158]. Moreover, that different neural cell types have differential susceptibility to the oxidative stress-inducing effect of the primary blast.

4.2 Materials and Methods

4.2.1 Animal Preparation

Adult, 10-week-old male Sprague-Dawley (Charles River Laboratories) rats weighing 320–360 g were used in all the studies. The animals were housed with free access to food and water in a 12-h dark-light cycle at 22°C. All procedures followed the guidelines established in the Guide for the Care and Use of Laboratory Animals and were approved by Rutgers University Institutional Animal Care and Use Committee (IACUC) before experiments. Rats were divided into two groups (sham controls and animals exposed to a moderate blast of 180 kPa). A total number of 24 rats were used in this study as follows: Immunoblotting (3 controls and 3 blast-injured); immunofluorescence studies (four controls and four blast-injured); superoxide production studies (5 controls and 5 blast-injured). For immunofluorescence studies, each brain tissue was processed to obtain several sections (>10) from frontal cortex, striatum, hippocampus, thalamus and cerebellum. Each of those sections was used for identification of NOX1 and NOX2 isoforms in neurons, astrocytes and microglia by double immunofluorescence analysis.

Similarly, for superoxide production, several sections from different brain regions of animals (5 control and 5 blast-injured) were used for regional analyses.

4.2.2 Blast Injury

Rats were exposed to a single blast wave at the Center of Injury Biomechanics, Materials and Medicine (New Jersey Institute of Technology, Newark) in the 9-inch square cross section shock tube as described previously[86,111,117]. The primary shock wave generated in this shock tube has been validated against the pressure-time profiles measured experimentally in the live-fire explosion experiments[96] and against theoretical pressure-time profiles associated with the detonation of C4 explosive (see ref.[111] for details). All rats were anesthetized with a mixture of ketamine (100mg/kg) and xylazine (10 mg/kg) at 10:1 ratio administered via intraperitoneal injection. Rats were subjected to a single exposure to 180±5 kPa peak overpressure (duration: 6.5±0.5 ms, impulse: 320±20 kPa·ms) and euthanized four hours post-TBI. All rats were mounted in the middle of the shock tube (2.8 meters from the breech, and 3 meters from the exit) in a prone position, i.e. were strapped securely to the aluminum plate using a cotton cloth wrapped around the body (see Figure 1B in reference [86]). The cloth provides no protection against the shock wave, but prevents any excessive head motion[117]. Sham control rats received anesthesia and noise exposure but without blast exposure, i.e., anesthetized animals were placed next to the shock tube, and then a single blast was fired.

As a quality control measure, high-speed video recording was monitored to capture any substantial head and body motion during the blast so as to exclude the impact of tertiary bTBI. Following blast injury, animals were monitored closely for any

signs of trauma-related distress (e.g., apnea). For immunoblot analysis, rats were anesthetized and transcardially perfused with phosphate buffered saline (PBS, pH 7.0) whereas for immunofluorescence studies, rats were first perfused with PBS followed by 4% paraformaldehyde; brains were then isolated and cryoprotected in 30% sucrose.

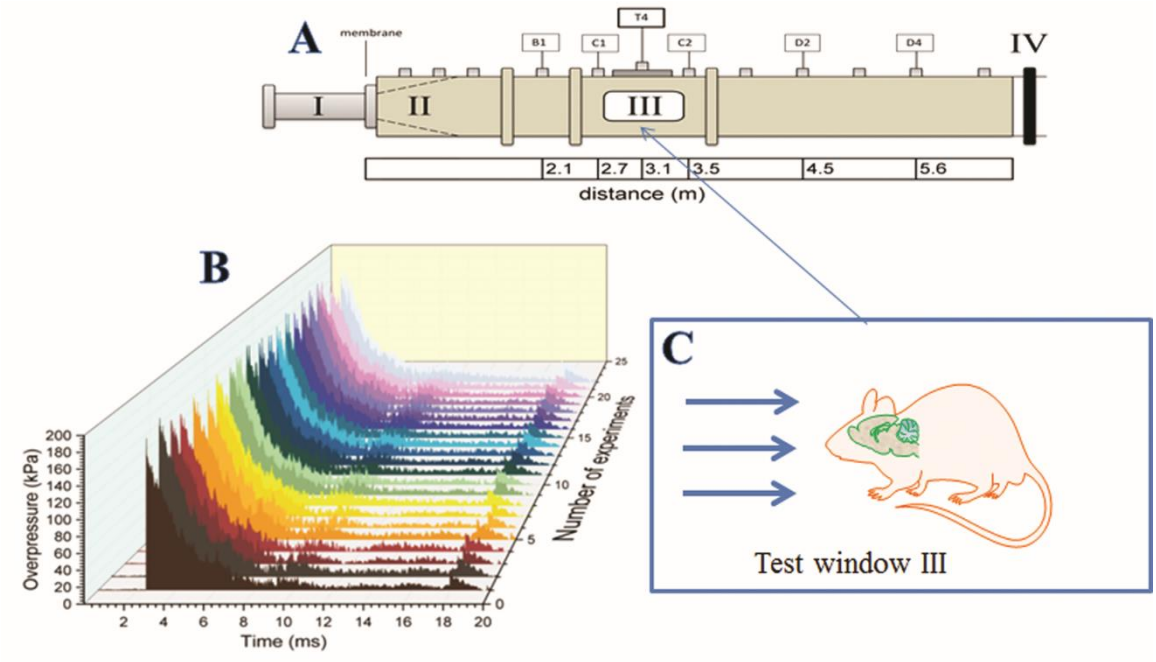

Figure 4.1 Schematic depiction of the shock tube. (A) Schematic of 9 in X 9 in square 30 feet long shock tube with section I-Breech with high pressure helium gas separated from section II by different thickness of mylar sheets that generate pure shock wave in section III where the specimens are located. Section IV is past the section and is a design requirement; the pressure-time cycle is identical to live fire tests with actual C-4 (or TNT equivalent) explosives at specified stand-off distance. (B) Composite of actual experimental profiles that generate 180kPa with only about 5kPa variation in peak pressure and less than a millisecond in duration. The front of the pressure rise indicates shock wave conditions. (C) Schematic of rodent model in prone facing the shock front. The shock travels in the rostral-caudal direction traversing pre-frontal cortex, striatum, hippocampus, thalamus, visual cortex and cerebellum within a period of a millisecond with minimal attenuation of pressure loading.

4.2.3 Western Blotting

Prior to evaluating spatial resolution of NOX1 and NOX2 protein changes in different brain regions by immunofluorescence, authors first examined their levels in cerebral

hemisphere and cerebellum by immunoblot. Following perfusion with PBS, brains were excised from the cranial vaults, the whole left hemisphere and cerebellum were separately homogenized in ice-cold conditions using CellLytic-M (Sigma) using sonicator with probe amplitude set to 45%. Samples were then centrifuged at 14,000× g at 4^0C. The protein concentration in the samples was estimated by bicinchoninic acid (BCA) method (Thermo Scientific, Rockford, IL). Subsequently, 10-20 μg of protein per lane was loaded into 4–15% SDS-PAGE gradient gels (Bio Rad). Proteins separated according to their molecular size were then transferred onto PVDF membranes using Turbo Protein Transfer instrument (Bio Rad Laboratories) using manufacturer's instructions. Membranes were blocked with 5% milk dissolved in Tris-Buffered saline containing 0.1% Tween-20 (TBS-T) and incubated overnight at 4^0C with NOX 1 antibody (Sigma-Aldrich) or NOX2 antibody (Novus Biologicals) or 4HNE (Abcam, Cambridge, MA) at a dilution of 1:1000. Bands were visualized using Western Pico Chemiluminescence Substrate (Thermo Scientific) on Chemi Doc Imaging System (Bio Rad Laboratories). For densitometric quantitation of western blots, images were digitized using a BioRad GS800 calibrated densitometer, and analyzed with BioRad Quantity One software.

4.2.4 Immunofluorescence and Microscopy

In order to evaluate the spatial changes of NOX1 and NOX2 proteins in different brain regions, as well as to identify cell-specific changes in discrete brain regions, double-immunofluorescence studies were performed of two isoforms of NOX with NeuN, GFAP and Iba1, markers of neurons, astrocytes and microglia respectively in frontal cortex, striatum, hippocampus, thalamus and cerebellum. Briefly, four hours post-injury, both

sham and TBI animals were transcardially perfused with PBS followed by 4% paraformaldehyde (PFA). After perfusion, the brains were removed from cranial vaults and incubated in 4% PFA for additional 48 h and cryoprotected by immersing in 30% sucrose. Brains were then dissected into 2 mm thick sections using rat brain slicer (Kent Scientific Corp.) and embedded in OCT (Optimal Cutting Temperature) media and quickly frozen in isopentane cooled to liquid nitrogen temperature. Frozen sections were stored at -80 °C until ready for sectioning. Brain sections (20 μm thick) were prepared from the frozen tissue blocks, using Leica CM3050 cryostat and immunofluorescence was performed. Briefly, tissue sections mounted on glass slides prepared from four individual animals in each group were washed with 10 mM phosphate buffered saline (PBS), fixed in ice-cold methanol (100%) solution for 10 minutes at -20 °C. The tissue sections were blocked with 10% donkey serum at room temperature for 1 hour in PBS containing 0.03% Triton X-100. Fixed tissues were incubated overnight at 4 °C with respective primary antibodies to NOX1, NOX2, GFAP, NeuN and Iba1. Double immunofluorescence was performed using donkey-antirabbit Alexafluor 594 for NOX1 or NOX2 and donkey-antimouse Alexafluor 488 for GFAP, donkey-antirabbit Alexafluor 488 for NeN and donkey-antigoat Alexafluor 488 for Iba1. The specificity of each antibody staining was validated by excluding each primary antibody (negative controls) and visualized for any non-specific fluorescence. However, the primary antibody specificity was not independently validated by blocking the binding to tissue with the corresponding antigen. Slides containing different brain regions were digitized (20x magnification) using Leica Aperio Versa 200 fluorescent microscope and slide scanner.

Fluorescence intensities in each region were quantitated using AreaQuant software (Leica Biosystems) and expressed as average fluorescence intensity/unit area.

4.2.5 Superoxide Production

Superoxide ($O_{2.}^-$) levels in different brain regions were measured using dihydroethidium (DHE) following the method of Kim et al[159]. Briefly, control and blast-induced animals (5 controls and 5 animals immediately following blast) were injected with 5mg/kg DHE (Molecular Probes, MA, dissolved in DMSO) intraperitoneally and four hours after blast, animals were transcardially perfused first with PBS followed by 4% PFA, brains excised and 50 µm thin sections of different brain regions were prepared using Leica VT 1000S vibratome and mounted. DHE immunofluorescence in each region was visualized by digitizing the images using Leica Aperio Versa 200 slide scanner. Fluorescent intensities in each region were quantitated using AreaQuant software (Leica Biosystems) and expressed as average fluorescence intensity/unit area.

4.2.6 Image Acquisition and Analysis

Slides with mounted coronal sections from the brain were imaged at 20x magnification using Leica Aperio Versa 200 digital pathology scanner. Control sections were used as reference for adjusting the exposure times and grey scale balance for optimal image quality, once set, these parameters were fixed and used for image acquisition of the reminder of both control and experimental groups. Three channels were collected for each coronal section. Blue: 405 nm (DAPI), red: 594 nm (NOX1), and green: 488nm [cell specific marker GFAP (astrocytes), Iba1 (microglia), and NeuN (neurons)]. Authors then manually outlined the regions of interest in different brain structures and the fluorescence intensities in each brain region were quantitated using FLAreaQuantV1

algorithm (Leica Biosystems) and expressed as average fluorescence intensity/unit stained area. For each channel, a minimum intensity threshold value was set using control sections as reference that will exclude any background fluorescence caused by nonspecific binding of fluorescent secondary antibody, and the same threshold values were used to quantify both control and experimental groups. A maximum intensity threshold was also set to remove any oversaturation due to excess fluorescent dye. The algorithm outputs the area of positive staining for each brain region, the average intensity of each channel, and intensity profile of each protein.

4.2.7 Statistical Analysis

Data are presented as mean ± standard error of the mean (SEM). Between-group comparisons were made by one-way analysis of ANOVA with a post-hoc test (Bonferroni) to determine individual group differences. Differences between means were assessed at the probability level of $p \leq 0.05$, 0.01, and 0.001. GraphPad Prism 6.0 software was used in all analyses and preparation of plots.

4.3 Results

4.3.1 Moderate Blast Overpressure Increases Protein Levels of NOX1 and NOX2

Previous studies in this laboratory identified increased oxidative and nitrosative stress factors in the cerebral cortex in rats exposed to mild-bTBI[65,86]. This study further evaluated the effect of moderate blast (180kPa peak overpressure) on the early evolution of the protein expression of NOX isoforms (NOX1 and NOX2). Immunoblot analysis of NOX1 and NOX2 in the whole cerebral hemisphere showed a significant increase (87%,

and 52%, respectively, $p<0.05$) (Figure 4.2). In order to assess the diffuse nature of primary blast (shockwave) in the posterior region of the brain, NOX1 and NOX2 protein levels were also determined in cerebellum, and, similar to cerebral hemisphere, cerebellar levels of NOX1 and NOX2 protein were significantly increased (60% and 40%, respectively, $p<0.05$) (Figure 4.2).

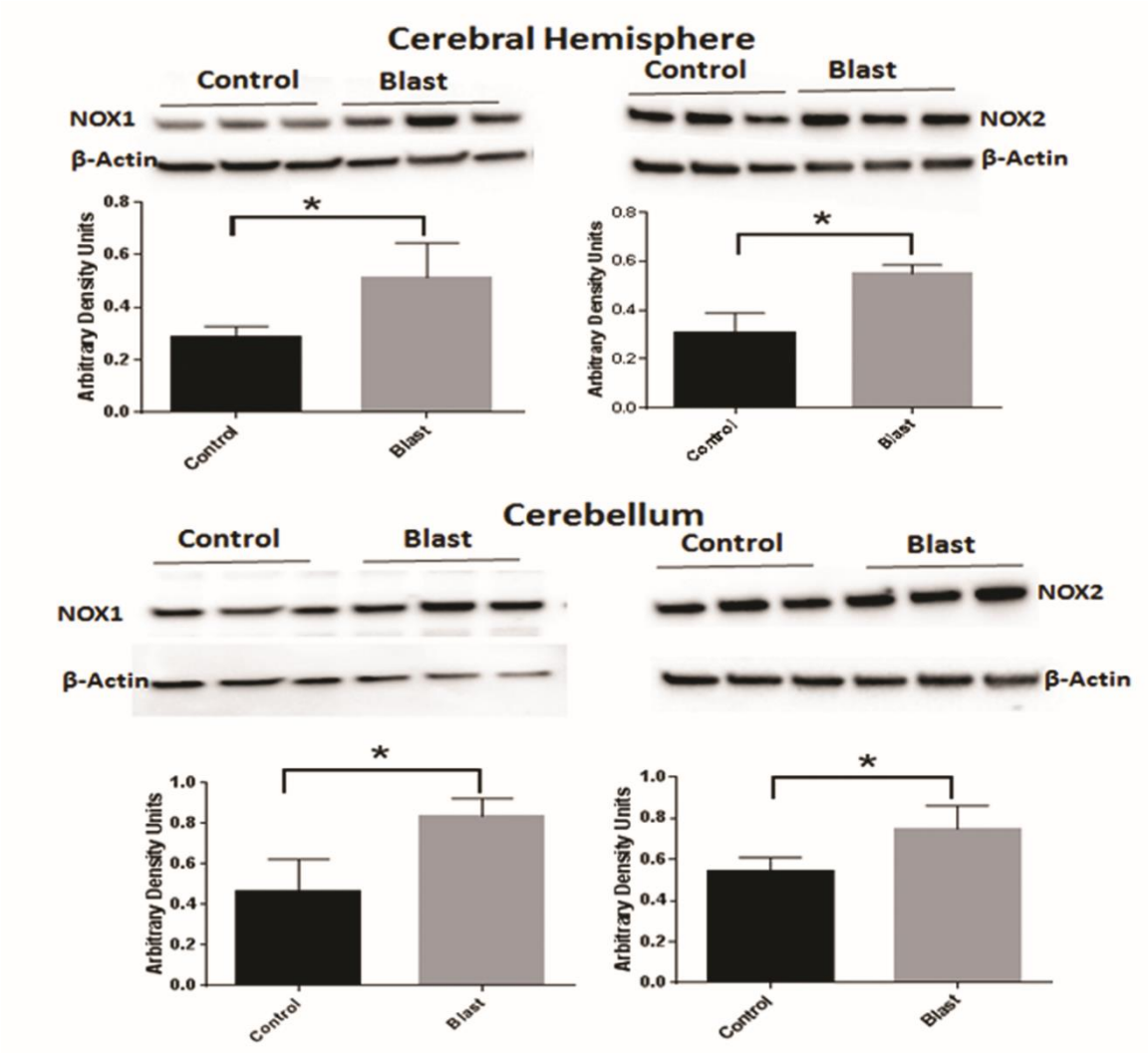

Figure 4.2 Blast increases the expression of NOX isoforms. Immunoblots of NOX1 and NOX2 isoforms in cerebral hemisphere and cerebellum 4h after blast at 180kPa blast over pressure. There was significant increase (80%) in NOX1 in both cerebral hemispheres and cerebellum, while NOX2 increased by 83% in cerebral hemispheres and 38% in cerebellum, n=3, [*] indicates a difference in intensity compared with control with a statistical significance of $p<0.05$.

4.3.2 Differential Changes in NOX Isoform Expression in Different Brain Regions

Authors next examined regional variations in NOX1 and NOX2 protein levels in the following brain structures: frontal cortex, striatum, hippocampus, thalamus, and cerebellum. The rationale in examining these regions is as follows: a) NOX1 and NOX 2 isoforms are ubiquitously expressed in all brain regions, b) the effect of shockwave propagation over the entire brain is not known and c) to use NOX1 and NOX2 as markers to evaluate whether there exists any selective vulnerability of various brain structures, a phenomenon which has not been previously investigated.

Under primary blast loading conditions, the pathological changes were found throughout the brain as indicated by changes in the fluorescent intensities of NOX1 and NOX 2 in different brain regions. Interestingly various regions displayed a differential response. Thus, NOX1 levels in the frontal cortex (FC) showed a 49% increase; hippocampus (HC) showed the highest degree of increase (107%) followed by thalamus displaying a 90% increase (Figure 4.3). Total NOX1 levels did not change in striatum and somatosensory barrel cortex (S1BF) (data not shown).

The regional variations in the levels of NOX2 are slightly different from that of NOX1. Total NOX2 levels were highest in frontal cortex (>2 fold) followed by striatum and hippocampus that showed the lowest increase (Figure 4.3). NOX isoform expression was also increased in other discrete brain regions from rostral and caudal areas, among which CA1 region of a hippocampus displayed the biggest increase.

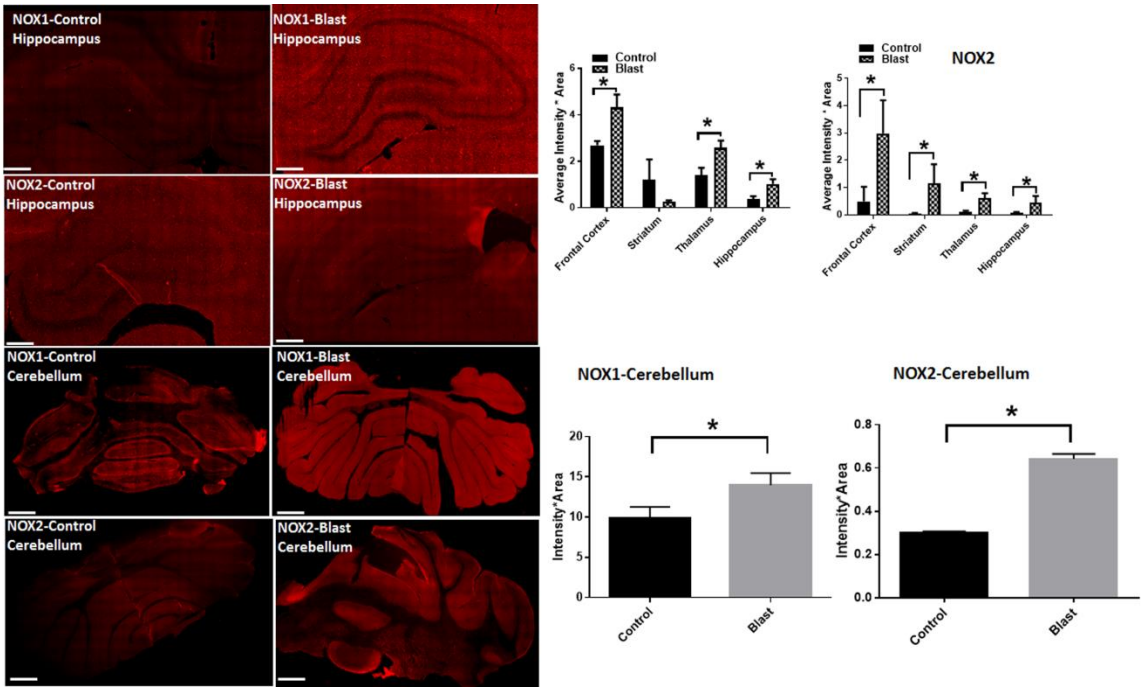

Figure 4.3 NOX isoforms show a differential increase in different brain regions. Fluorescence intensities (red) of NOX1 and NOX2 in hippocampus and cerebellum from control and blast-injury animals. Quantification of florescence intensities in different brain regions show a striking increase in NOX1 in hippocampus of blast-injured animals compared to controls. Intensities of NOX2 display a higher increase in frontal cortex compared to other regions. n=4. [*] indicates a difference in intensity compared with control with a statistical significance of $p<0.05$. Fluorescent intensities NOX1 in cerebellum display a striking increase (96%) compared to NOX2 (38%).

4.3.3 Different Neural Cell Types Display Differential Vulnerability to Oxidative Damage

To evaluate cellular vulnerability to oxidative damage resulting from primary blast, changes in NOX1 expression patterns in astrocytes, neurons and microglia were determined by double immunofluorescence staining. Additionally, simultaneous quantification of NOX immunofluorescence using cell-specific markers will provide an insight into changes in its expression in different neural cells including astrocytes, neurons and microglia.

Cell-specific analysis of increase in NOX1 and NOX2 levels following bTBI compared to their baseline expression (controls) indicate that neurons display a higher increase compared to astrocytes and microglia. Additionally, NOX1 and NOX2 increases were more pronounced in neurons in hippocampus and thalamus respectively compared to the frontal cortex. These conclusions were deduced based on the double immunofluorescence analysis showing co-localization of NOX1 with NeuN (a marker protein for neurons), with GFAP (a marker for astrocytes) and with Iba1 (a marker for microglia). (Figures 4.4 and 4.5*)*.

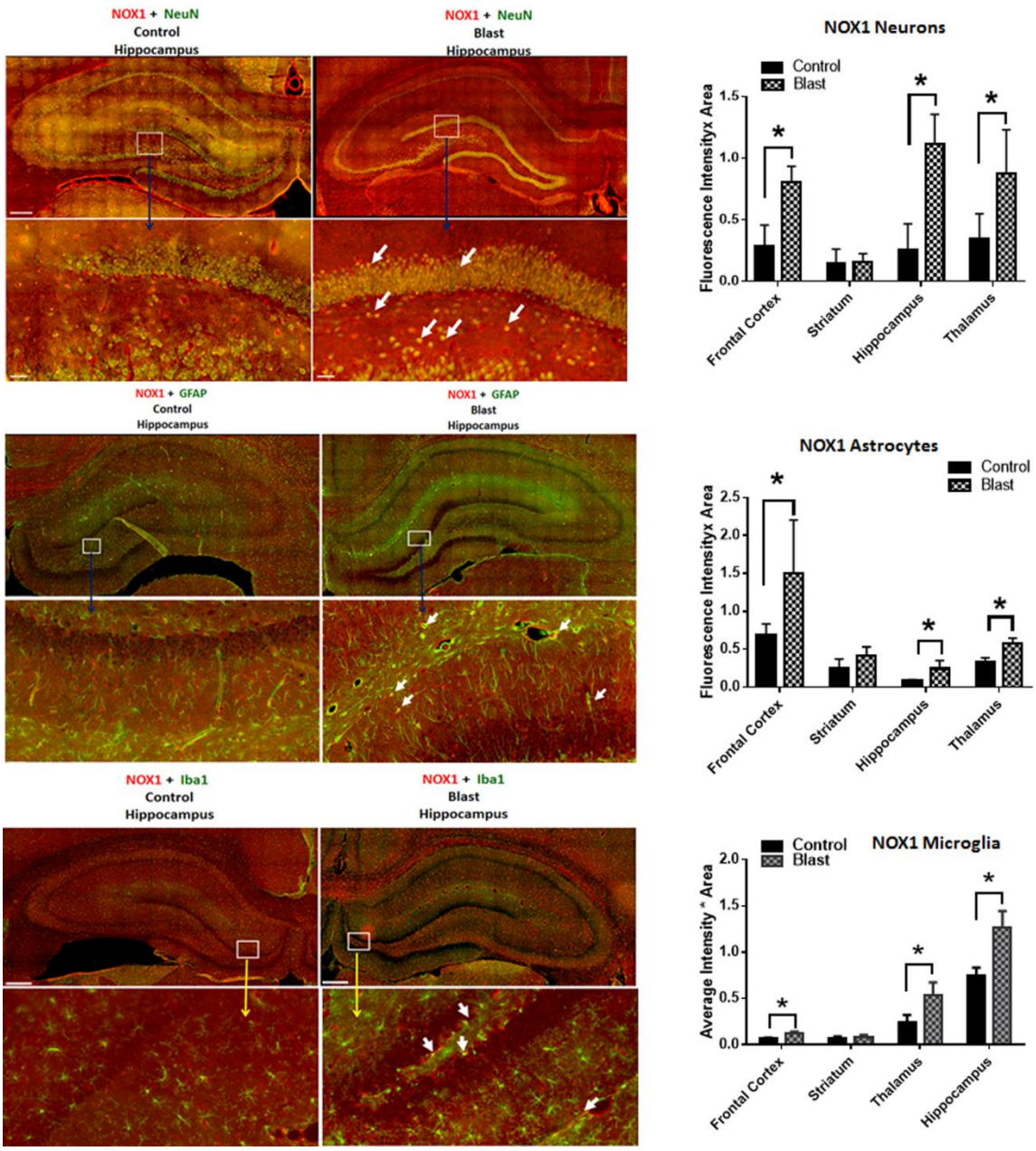

Figure 4.4 NOX1 shows greater co-localization in neurons. Representative merged images showing the co-localization of NOX1 with NeuN, GFAP and Iba1 in hippocampus indicating neuronal, astrocytic and microglia localization respectively of NOX1 in control and blast-injured animals. Majority of increase in NOX1 with respect to corresponding controls is in neurons compared to astrocytes and microglia. Quantification of florescence intensities in different brain regions show a striking increase in NOX1 fluorescence in neurons in hippocampus of blast-injured animals compared to controls. n=4, *, $p<0.01$-0.05.

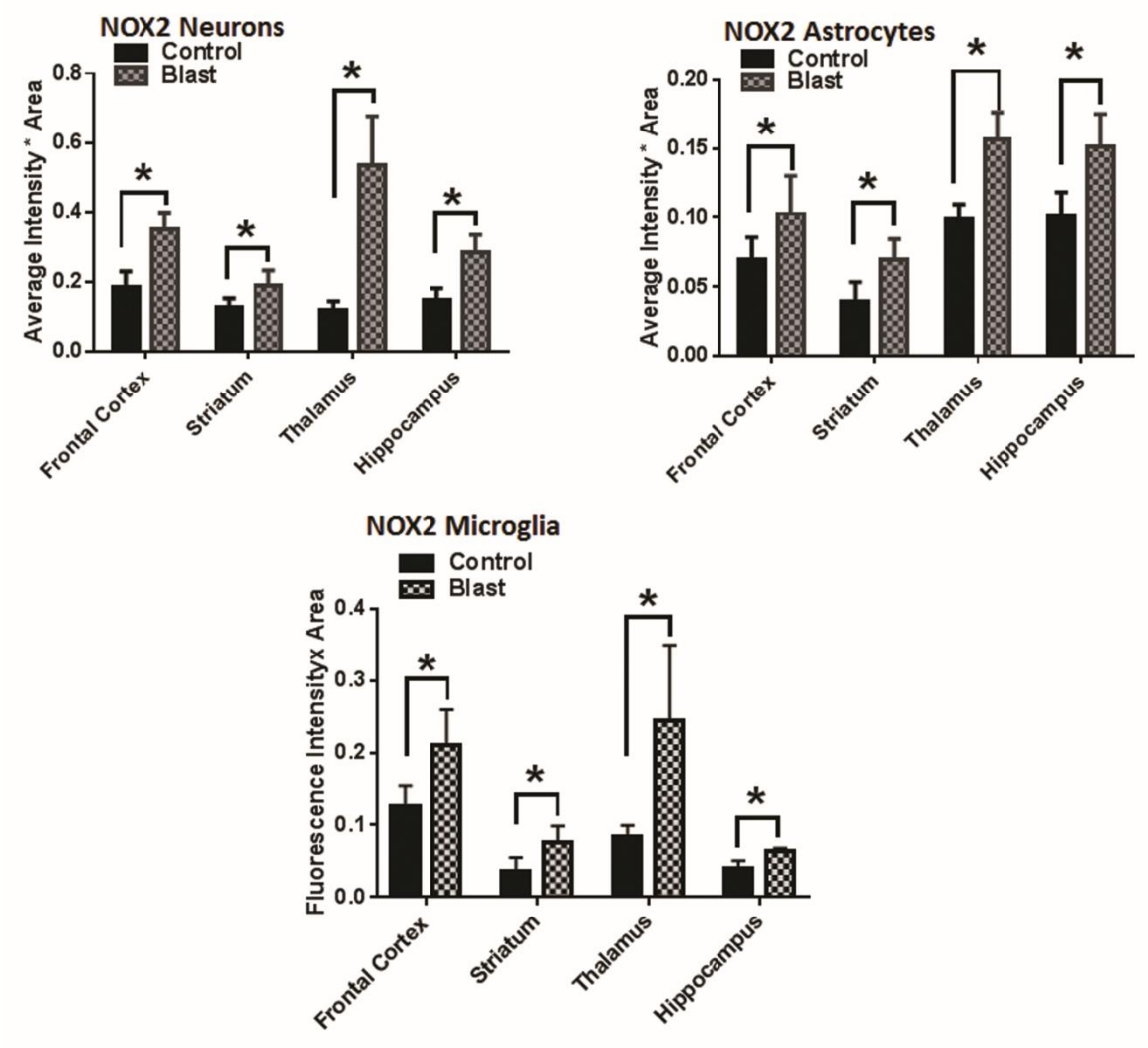

Figure 4.5 Neurons show the highest increase in NOX2 expression. Quantification of florescence intensities in different brain regions show a striking increase in NOX2 fluorescence in hippocampus and thalamus of blast-injured animals compared to other brain regions. n=4, [*] indicates a difference in intensity compared with control with a statistical significance of $p<0.05$.

4.3.4 Primary Blast Significantly Affects Posterior Brain Structures Including Cerebellum

Primary blast caused diffused pathological changes not only in the perpendicular direction (deeper brain structures, hippocampus, thalamus) but also in the parallel direction to the wave propagation from prefrontal cortex to the cerebellum. The total

tissue levels of NOX1 in the cerebellum not only increased, but this increase was highest in neurons (Figure 4.6). Such higher expression of NOX1 in neurons as compared to other neural cells also correlates with the known fact that cerebellum contains the highest density of neurons compared to other brain regions[160,161]. Similar to NOX1, elevated levels of NOX2 expression were also found to be mainly co-localized with neurons (Figure 4.7).

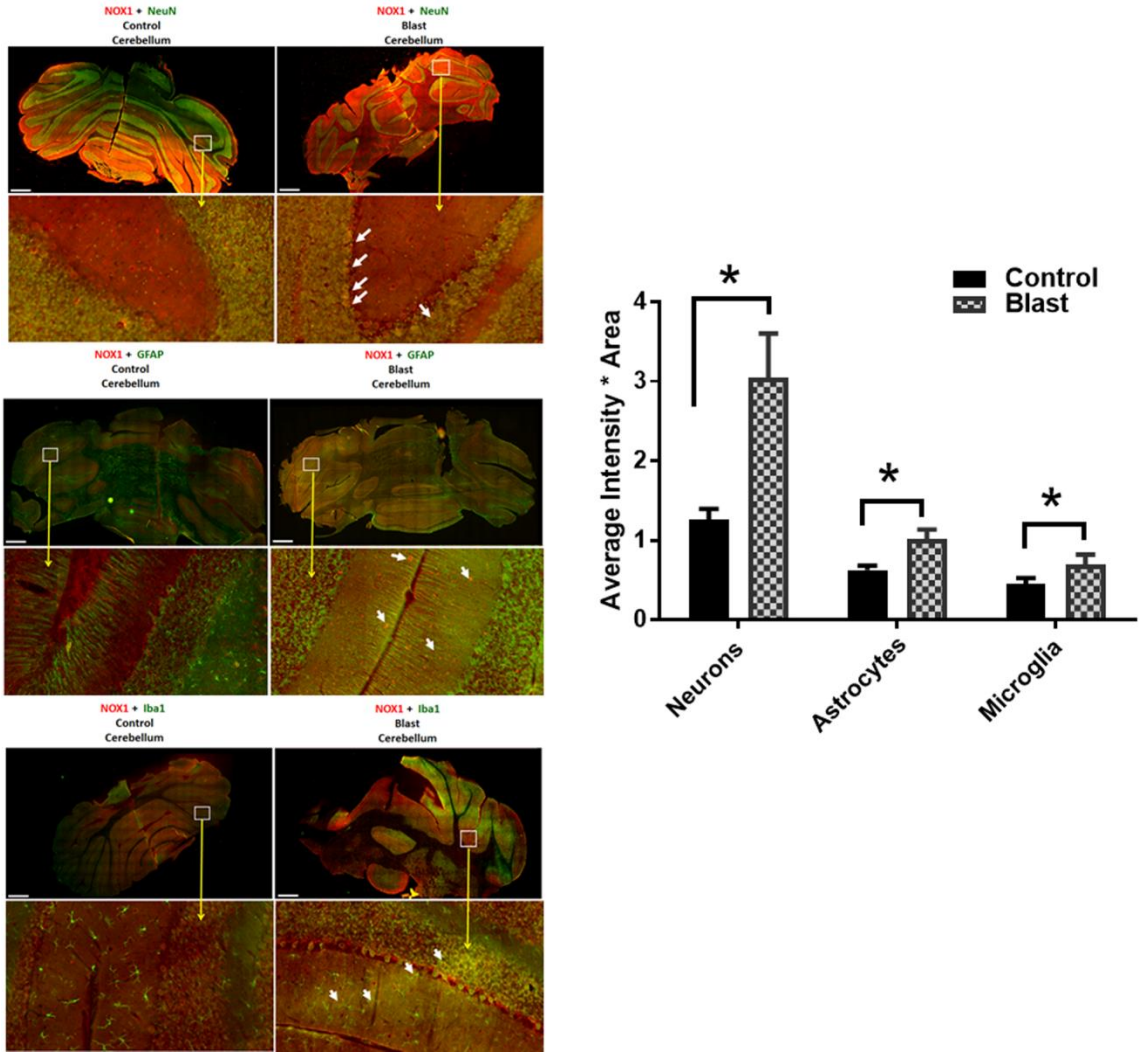

Figure 4.6 Cerebellum displays an increased NOX1 expression in neurons compared to astrocytes and microglia. Representative merged images showing the co-localization of NOX1 with NeuN, GFAP and Iba1 in cerebellum indicating neuronal, astrocytic and microglia localization respectively of NOX1 in control and blast-injured animals. n=4, [*] indicates a difference in intensity compared with control with a statistical significance of $p<0.05$.

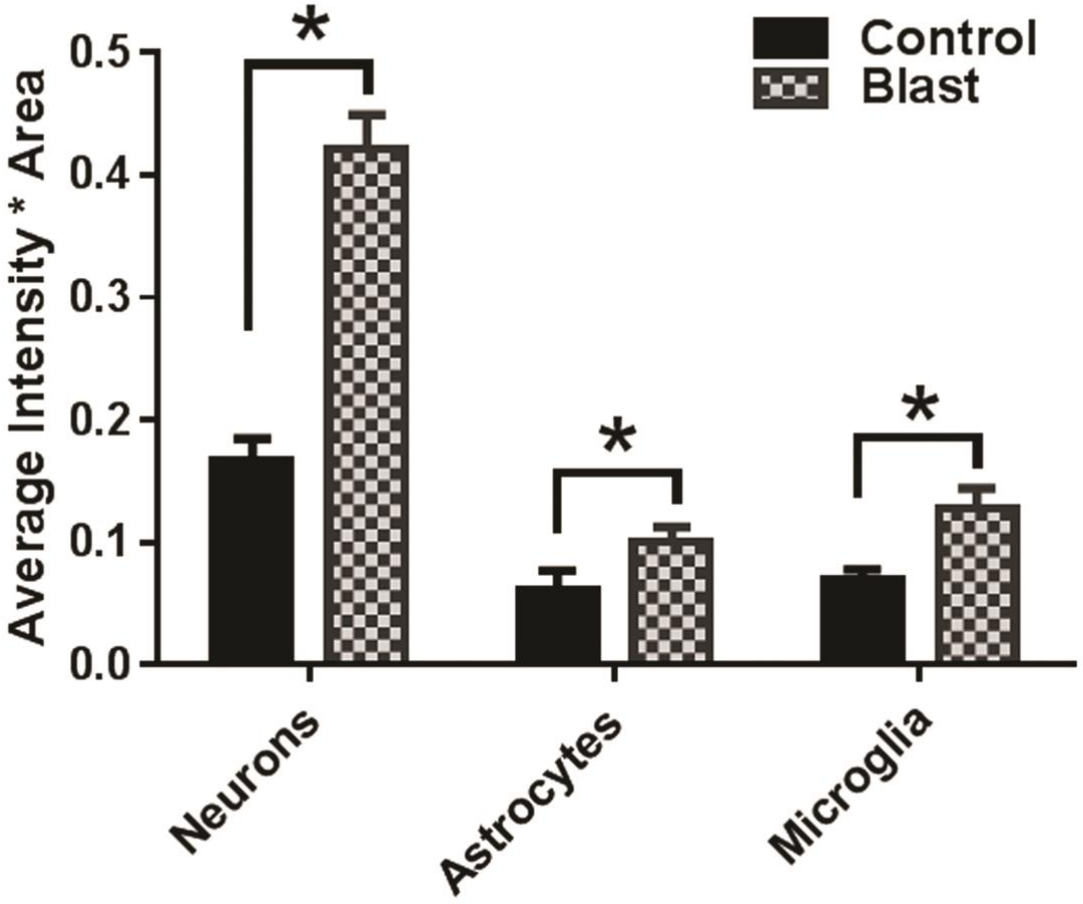

Figure 4.7 NOX2 displays a greater increase in neurons compared to astrocytes and microglia. Similar to NOX1, majority of NOX2 is localized in neurons compared to astrocytes and microglia. n=4, [*] indicates a difference in intensity compared with control with a statistical significance of $p<0.05$.

4.3.5 Primary Blast Increases Superoxide Levels in Different Brain Regions

The activation of a variety of NOX isoforms is usually associated with the increased production of superoxide[154,162]. Since the present study showed increased protein levels of NOX isoforms, authors then sought to examine whether increased NOX protein following blast has a functional significance. Accordingly, *in vivo* levels of superoxide in frontal cortex, hippocampus, thalamus and cerebellum were measured using DHE. Hippocampus displayed a robust level of the increase in superoxide (>10 fold, $p<0.001$)

followed by thalamus and frontal cortex. It is noteworthy that the extent of the rise in superoxide production in hippocampus and thalamus (Figure 4.8) correlated well with the increased degree of NOX expression. Additionally, a pretreatment of animals with apocynin, which is known to block the assembly of different NOX subunits, completely inhibited the increase in superoxide production indicating an essential role of NOX in brain superoxide production following moderate blast.

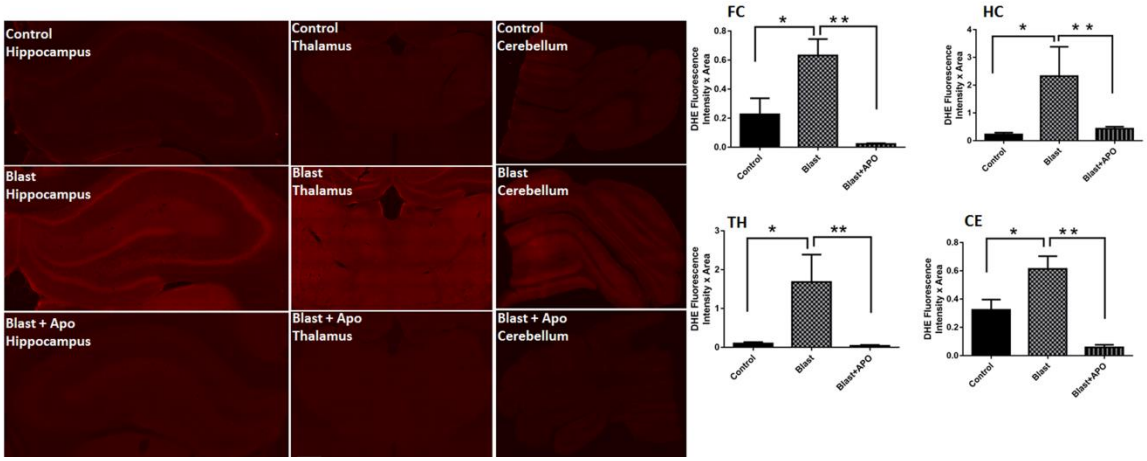

Figure 4.8 Primary blast increases superoxide levels in different brain regions. Representative fluorescent intensities (red) of DHE (dye that recognizes superoxide production) in hippocampus, thalamus and cerebellum in control, Blast-injured and blast + apocynin. Quantification of florescence intensities in different brain regions show a striking increase in DHE fluorescence in hippocampus of blast-injured animals compared to controls indicating high levels of superoxide production in hippocampus. Note that a pretreatment with apocynin (APO), an inhibitor of NOX activation completely blocks the DHE fluorescence increase indicating that the superoxide increase is mediated by activation of NOX. n=5, [*] indicates a difference in intensity compared with control with a statistical significance of $p<0.05$.

4.3.6 Primary Blast Results in Oxidative Damage and Lipid Peroxidation Products in Different Brain Structures

Several reports indicate the TBI resulting from different etiologies, including primary blast and blunt injuries display oxidative stress during the evolution of its symptoms[20,47,83,163]. Accordingly several pathways are directly involved in the induction

of oxidative stress including the activation of NADPH oxidase[155,164-166] and alterations of antioxidant defense mechanisms (a reduction in superoxide dismutase, catalase, glutathione peroxidase)[85,167].

One of the major downstream effects of oxidative stress in many neurological disorders and TBI is the formation and accumulation of lipid peroxidation products[168-170]. Lipid peroxidation is a process under which oxidants such as free radicals attack various lipids containing carbon double bonds, and the resulting aldehyde products 4-hydroxynonenal (4HNE) generated by the lipid peroxidation directly modify amino acid structures in proteins and form adducts[171].

Superoxide is one of the free radicals that can directly oxidize lipids to aldehydes that lead to the formation of protein adducts and activation of NOX produces excess levels of superoxide[162,172,173]. Since the present study clearly showed an increase in NOX proteins and increased levels of superoxide following bTBI, the levels of 4HNE adducts in discrete brain regions in rats subjected to moderate blast (180kPa, four hours) were examined. Immunoblot analysis of 4HNE products identified two major bands corresponding to molecular weights of 70 and 100kDa which showed a trend towards an increase in cerebral hemispheres, hippocampus, thalamus and cerebellum; however such changes were not significant (Figure 4.9).

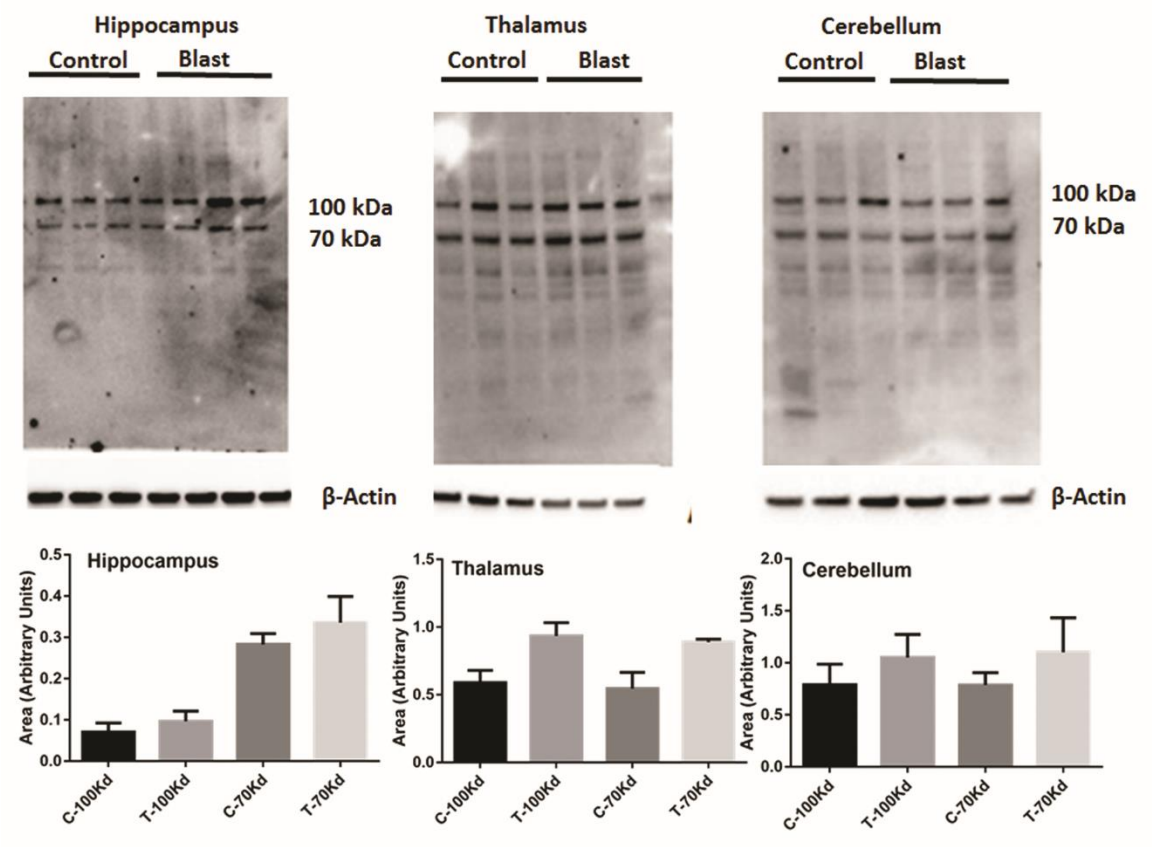

Figure 4.9 Primary blast displays a strong tendency to increase 4-HNE protein adducts. Immunoblot analysis of 4-HNE in lysates from hippocampus, thalamus and cerebellum 4hr after blast at 180kPa blast over pressure is shown. Two proteins of 100 and 70kDa show a strong tendency to increase in hippocampus and thalamus. n=3.

4.4 Discussion

This study demonstrates that protein levels of superoxide producing enzymes NOX1 and NOX2 were significantly increased to different levels in various brain regions in rats exposed to moderate primary blast overpressure. Increased NOX expression was accompanied by increased superoxide production and a strong tendency towards increased HNE adduct formation in two proteins. Together these observations strongly

indicate that there is an increase in oxidative stress and oxidative damage occurring in the early phase after a single exposure to a shock wave. This work is motivated by two related questions: 1) does the bTBI affect different brain regions equally assuming homogeneous spatial distribution of biomechanical loading and 2) does the extent of the damage vary between different brain regions containing disparate ratios of neural cells (neurons, astrocytes and microglia)? Hence, the focus was on the role of two different forms of superoxide producing enzymes and their downstream oxidative damage markers to understand both the spatial and cellular effects.

Blast-induced TBI (bTBI) has a unique pattern of biomechanical phenotype in that the external forces are dictated by the size and shape of the interacting body, in this instance skull and brain structures. Furthermore, the magnitude of forces generated depends on the contact area and interaction time that in turn determine the overall biomechanical loads at the tissue level. This loading triggers secondary biochemical cascades depending on the local tissue content. The cascade of secondary events usually develops over a period of hours to days that ultimately lead to additional neuropathological sequela[174-176]. Among many causal factors implicated in the pathophysiology of bTBI, oxidative stress represents an important early pathological outcome resulting from either the activation of free radical producing enzymes or downregulation of antioxidant defense mechanisms[47,83,163,177].

NADPH oxidase (NOX) is a superoxide producing enzyme and different isoforms of NOX, including NOX1, NOX2 and NOX4 have been identified in brain[154]. Studies reported increased activation of different isoforms of NOX in various forms of TBI. Accordingly, in a mouse model of controlled cortical impact, increased NOX2 expression

was observed at 24-48hr after injury[178] whereas Byrnes et al.[179] found a delayed increase in NOX2 activity 1 month post-injury. However, in a rat model of CCI, increased NOX activity was observed as early as 1 hour post-injury[180]. Increased NOX expression was also found in different animal models of fluid percussion injury[156,181,182]. Additionally, apocynin, an inhibitor of NOX activation showed protective effects on various models of blunt TBI[157,181]. Together these studies highlight the critical role of NADPH oxidase in the pathology of TBI.

While studies have established importance of NOX in the pathophysiology of blunt TBI, there are limited studies of NOX in bTBI[78,183,184]. This could in part be because of the lack of a true understanding the role of biomechanical loading in blast injury due to limited availability of field validated shock tube that simulates battle field injuries. In the present study authors therefore characterized the spatial resolution of two isoforms of NOX (NOX1 and NOX2) in various brain regions and their localization in neurons, astrocytes and microglia four hours following blast injury in a field validated shock tube[96,111,117].

A generalized increase in NOX protein levels by immunoblots in the present study, are comparable to previous reports from this group indicating its upregulation in the homogenates of a cerebral cortex in rats exposed to different blast overpressures[65,86]. Further, using immunofluorescence analysis, the present study identified regional variations in the expression pattern of NOX1 in that the highest increase is found in hippocampus followed by thalamus. In this study, the frontal cortex showed higher expression in NOX2 compared to that in hippocampus and thalamus. Other fine brain structures, including motor cortex, amygdala and hypothalamus also showed a significant

increase in both the isoforms of NOX with the exception that NOX2 levels were significantly lower in a motor cortex.

Interestingly, in the present study, a single blast exposure also affected distal brain structures, including the cerebellum suggesting that blast injury propagation is highly diffusive in nature. While it is interesting to observe differential vulnerability of various brain structures to blast injury, in blast, a high-velocity shock wave traverse across and through the entire body loading all the regions almost simultaneously within a matter for 5-10 milliseconds. Recent experimental evidence in animal models and human cadaveric heads has shown that the shock waves contrary to intuition is capable of passing through the skin and skull and load all the brain structures[96].

In addition to regional variations observed in NOX levels, cellular heterogeneity in the expression of NOX isoforms was also identified. Thus blast injury displayed a robust increase in the levels of both isoforms of NOX in neurons as compared to astrocytes and microglia with respect to their baseline values (controls). Studies have shown that all neural cells express different isoforms of NOX, including NOX1, NOX2 and NOX4[185]. Additionally within the neurons, NOX1 is abundantly expressed in cerebellar granule cells[186], while NOX2 has been shown to be expressed in both cerebellar granule cells as well as hippocampal neurons[187]. In addition to NOX1, the present study found a striking increase in NOX2 in neurons of hippocampus, thalamus and cerebellum as compared to microglia. These results are in slight contrast to other reports wherein NOX2 is abundantly expressed in microglia[178,188-190]. While the reason for apparent abundance of NOX2 in neurons in the present study is not known, studies report that NOX2 upregulation in hippocampal pyramidal neurons drives neuropathology

associated with psycho-social stress in rats[190,191]. Further, studies also report that cellular injury to neurons following stroke resulted in an early upregulation of NOX2 in neurons (3-6 hours following injury) whereas NOX2 was upregulated in microglia at later time points (72 hours post-injury)[192,193]. Such temporal difference in the expression pattern of NOX2 between neurons and microglia is reasonable since neurons may be far more vulnerable acutely in the evolution of the injury process whereas microglial activation could be a relatively late phenomenon.

Superoxide is a major free radical produced in the brain by a variety of reactions, including disturbances in mitochondrial oxidative phosphorylation, increased production of arachidonic acid as a consequence of activation of phospholipase A2 (PLA2), activation of xanthine oxidase as well as by the activation of NOX[194-197]. Increased superoxide production has been shown in different models of TBI[196,198-201]. The present study observed a striking increase in superoxide production in hippocampus, thalamus and frontal cortex, areas where corresponding increases in NOX levels were found. Moreover, these studies showing a complete absence of $O_2^{\cdot -}$ in animals treated with apocynin (an inhibitor of NOX activation) prior to the exposure to blast injury reinforces the finding that the increase in $O_2^{\cdot -}$ is indeed mediated by NOX activation. Results are also in agreement with previous studies showing protective effects of apocynin in attenuating oxidative damage in different models of TBI[155,157,165,181,202,203].

While in the present study, the superoxide levels were found to be strikingly increased in different brain regions, the levels of 4HNE adducts showed a trend towards the increase in two proteins with average molecular weights of 70 and 100kDa, but did not show statistically significant changes. The reason behind the lack of significant

changes is not known. However, the 4HNE products can be formed via peroxidation of unsaturated fatty acids not only by superoxide radical but also by a variety of other reactive oxygen species, including hydroxyl, peroxyl radicals as well as a variety of cyclic compounds[204]. It is therefore likely, that lipid peroxidation reaction and subsequent 4HNE formation may not have achieved a threshold as to show significant changes at four hours following blast since reactive oxygen species other than superoxide (e.g., hydroxyl radicals among others) may not have been increased in the early phase of blast injury.

Despite an observed increase in factors conducive to oxidative damage in neurons, in the present study, no neurodegeneration nor apoptotic cell death was observed as investigated by fluorescent staining for Fluorojade C and cleaved caspase-3 four hours after blast injury (data not shown). Perhaps, a four hour window of blast injury may be too early to detect neuronal death. It is also likely that moderate blast may not cause neuronal death due to the diffuse nature of the shockwave unlike blunt injuries where neuronal death was observed close to the site of injury in the acute phase of injury[205].

The selective vulnerability of neurons to oxidative damage may be dictated not only by the propagation of primary shockwave, the so-called direct mechanical impact throughout the brain regions, but also in part influenced by the cellular density and cell type's distribution in different brain regions. Recently, it has been shown that the cerebellum and hippocampus contain the highest density of neurons compared to a cerebral cortex although relative mass of hippocampus and cerebellum is far lesser than cerebral cortex[161,206]. The fact that in the present study, observation of the highest increase NOX levels in neurons in hippocampus and cerebellum following blast suggests

that neuron rich regions may be at higher risk for oxidative damage than other brain regions. This is further supported by the observation of a striking increase in superoxide levels in hippocampus following blast. Also, within hippocampus, studies have shown that neurons in CA1 region are more vulnerable to superoxide than CA3 neurons[207,208]. Moreover, it is interesting to note that NOX1 showed a greater increase in CA1 region compared to CA3. Such higher level of neuronal oxidative damage in discrete brain regions may also depend up on a number of other factors, including vascular density and associated metabolic supply and consumption of glucose and oxygen, neuronal excitability and synaptic transmission[209]. In support of this tenet, it has been shown that the density (and perhaps subsequent nutrient supply) of brain capillaries was far less in CA1 region of the hippocampus compared to CA3 region which likely places CA1 region at higher risk for ischemia and hypoxia[139].

The precise mechanism by which bTBI increases NOX isoform expression is still unknown. A shockwave passage throughout the brain during a transient period of time could initiate a mechanical disturbance to plasma membrane structures within the brain parenchyma. It is reasonable, considering the small size of the rat's brain and relatively thin skull, to assume the shockwave loading of the brain is uniform within brain structures investigated in this work (frontal cortex, striatum, hippocampus, thalamus and cerebellum). The uniformity of the pressure field within the rat brain under blast loading conditions was demonstrated in numerical model[210] and was validated via intracranial pressure measurements by the group (data not published). If this is true, i.e., the mechanical forces created by the shockwave are distributed uniformly, and considering the brain's highly anisotropic and heterogeneous organization, these data suggest the

extent of the local damage would depend on the composition and microarchitecture of a specific brain region (Figure 4.10).

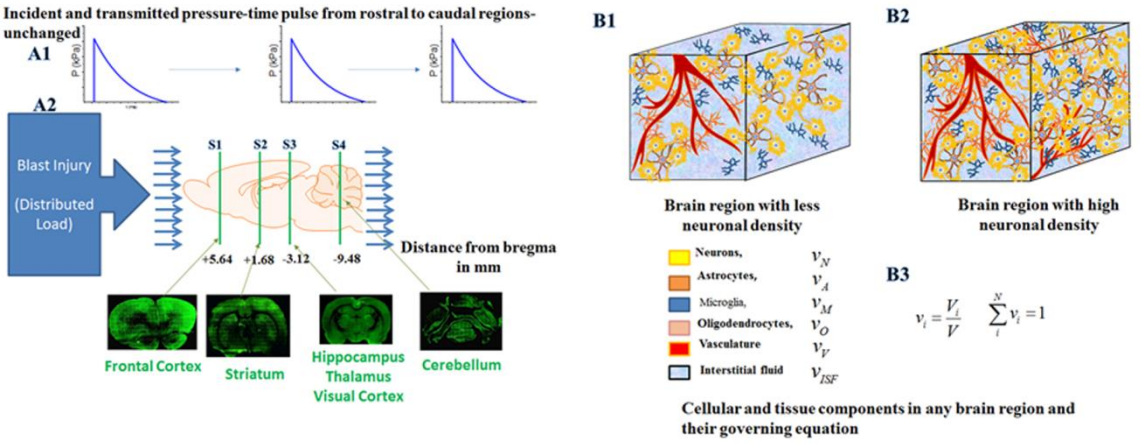

Figure 4.10 Schematic of experimental blast injury model and effective loading and tissue-specific response. (A) The top panel shows the blast overpressure-time pulse applied to the rostral to caudal to rostral regions of rodent brain travels with minimal change due to very short duration of less than a millisecond. The bottom panel shows different regions S1 to S4 analyzed in this study (B) A given brain volume comprises of the six components (neurons, astrocytes, microglia, oligodendrocyte, vasculature and interstitial/cerebrospinal fluid) that can vary from region to region. The mechanical properties of the representative volume given in B3 indicate that the effective mechanical stresses in the volume and hence the neural components will be determined by the differential volume fraction of that cell-type. The different NOX expressions seen in this work are hypothesized to be driven by this differential cell volume fraction.

In summary, the present studies demonstrate that moderate blast injury causes an increase in NOX isoforms in various brain regions to a differential degree. Increased NOX isoforms correlated with a concomitant rise in superoxide levels in corresponding regions that show a higher increase in NOX expression indicating oxidative damage. Additionally, protein oxidation product 4HNE showed a strong tendency to the increase in different brain regions. Further, higher increase in NOX isoforms in neurons compared to other brain cells strongly suggests neurons are by far more vulnerable to oxidative damage in the early evolution of injury pathology.

CHAPTER 5

ROLE OF OXIDATIVE STRESS IN THE MECHANISM OF BLOOD-BRAIN BARRIER PERMEABILITY IN BLAST-INDUCED NEUROTRAUMA

5.1 Background and Significance

Blast-induced traumatic brain injuries (bTBIs) have become the most prevalent form of neurotrauma amongst military soldiers and a growing cause of injury in civilian populations due to asymmetric warfare with increased acts of terrorism domestically and abroad[1-3,147-149]. However, in spite of the increase in BINT studies, there are still significant gaps in understanding how primary mechanical injury and subsequent secondary injuries manifest following blast. A recent survey reported that more than 30 phase III clinical trials aimed at targeting TBI have failed and, to this effect, this group has attempted to elucidate the temporal and spatial neuropathology of bTBI as it pertains to two commonly identified pathological factors: oxidative stress and blood-brain barrier (BBB) breakdown[39-42].

Oxidative stress has been implicated in multiple modes of TBI[82,83] and is mainly induced by reactive oxidative species (ROS). These include, but are not limited to, superoxide ($O2\cdot-$), hydroxyl radical ($HO\cdot$), and hydrogen peroxide (H_2O_2)[84,85]. While a basal level of ROS is to be expected due to normal reactions of oxidative phosphorylation, redox-reactions, and mechanisms of the electron transport chain, an excess amount, as seen after injury, can be harmful. NADPH oxidase (NOX) is a multi-subunit enzyme that catalyzes the formation of superoxide radicals from present molecular oxygen. As previously reported by this group and other investigators[47,86,158,211],

NOX is upregulated in different brain regions following blast injury and neurons display the highest increase in hippocampus compared to other neural cells. It is also worth noting that a single blast induces substantial increases in superoxide levels in multiple brain regions from the pre-frontal cortex to hippocampus to cerebellum, all along the direction of shock wave propagation[211].

Direct blast biomechanical loading was also recently identified as causing disruption of brain vascular integrity (blood brain barrier, BBB) in multiple brain regions within minutes of loading and that this BBB disruption further increased four hours following blast before returning to normal at 24 hours post-injury[158]. The BBB is a selectively-permeable membrane separating the brain from the circulatory system, consisting of tight junction complexes, which attach adjacent endothelial cells together, as well as a host of dynamically modulating cells including pericytes and astrocytes, which wrap around the endothelium. In recent work by this group, increased permeability of the BBB was most significantly seen four hours post-blast across the cerebral hemisphere, with most pronounced injury seen in the frontal cortex[158]. Damage to the BBB was established through extravasation of tracers Evans blue and sodium fluorescein, the dislodging of tight junction proteins, and leakage of blood-borne cells into the brain parenchyma and brain parenchymal molecules into the blood. Increased permeability of the BBB has been observed in several modes of TBI including closed cortical injuries[70-72], weight drop models[73,74], and blast models[75-80,131].

Oxidative stress is a well-known factor for BBB disruption in TBI as well as other prevalent neurological pathologies including Alzheimer's and Parkinson's disease[212-214]. Combining this with recent reports indicating concurrent increases in oxidative stress and

heightened BBB disruption four hours after injury[158,211], authors set out to investigate the interaction of these two well-known pathogenic factors in BINT. Authors hypothesize that while BBB is acutely disrupted immediate following blast injury is a through biomechanical means, heightened BBB disruption in latter stages (four hours) is due, at least in part, to contributions by NOX-mediated oxidative stress. This study therefore employed apocynin, known to block the assembly of NOX subunits and prevent activation of NOX, to eliminate superoxide production and thus nullify NOX-mediated breakdown of the BBB.

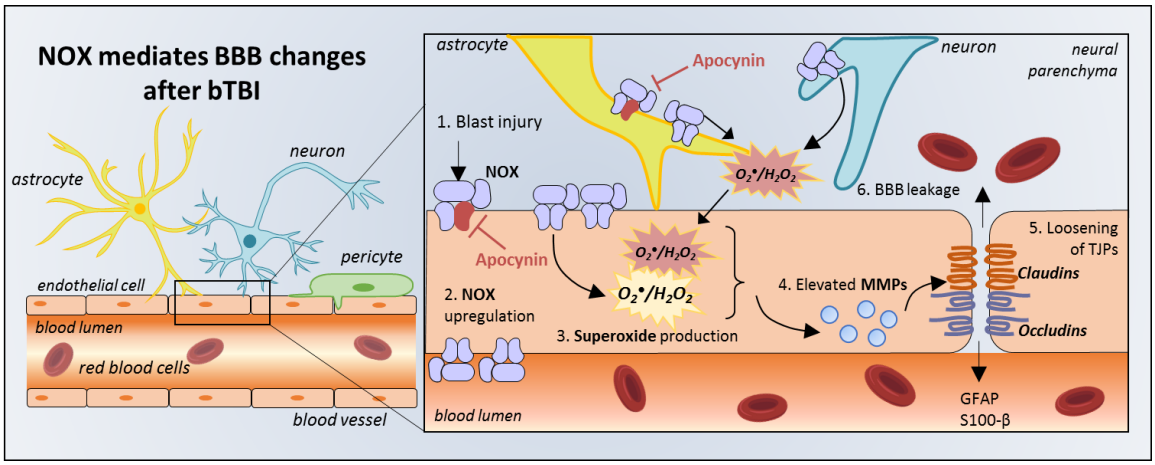

Figure 5.1 Pathway schematic of role of NOX in BBB permeability following blast. Upregulation of NOX on neurovascular endothelial cells (and other neural cells) cause increased superoxide production both within and outside the endothelial cells. This superoxide elevates MMP production, which breaks down the tight junction complexes connecting adjacent endothelial cells, causing increased permeability of the BBB. Use of apocynin prevents the translocation of the NOX p47 phox subunit, thereby preventing the increase in superoxide production and, eventually, BBB permeability.

5.2 Materials and Methods

5.2.1 Animal Preparation

Adult (10-week old), male Sprague-dawley rats (Charles River Laboratories) weighing between 350 $\pm$ 50g were used throughout this study (n = 54), in accordance with protocols approved by Rutgers University Institutional Animal Care and Use Committee (IACUC). Animals were housed at 22° C with free access to food and water in a 12 hour light-dark cycle. Animals were divided among sham, blast, and treatment groups, all to be sacrificed four hours post-blast (or, in the case of sham animals, noise exposure). All methods used throughout the study were performed in accordance with protocols, guidelines, and regulations approved by Rutgers University IACUC.

5.2.2 Exposure to Blast and Apocynin Pre-Treatment

Rats were exposed to a single shock wave at the New Jersey Institute of Technology (Center for Injury Biomechanics, Materials, and Medicine) in the modular, field-validated shock tube described in previous publications[86,96,110,111]. Based on results from previous work from this group, an $n \geq 4$, was used for both sham and blast groups (power value of 0.8, α=0.05) based on a priori power analysis. Prior to blast exposure, animals were anesthetized with 5% isoflurane, released in a chamber containing 95% air and 5% CO_2, until rats were unresponsive to noxious stimulation. An additional group of animals (n = 4) received an intraperitoneal injection of apocynin (5mg/kg, Sigma-Aldrich) 30 min prior to blast exposure. At this point the rats were mounted and immobilized on a custom rat-holder in the test section of the shock tube. Sham animals were anesthetized and received noise exposure, but kept outside of the shock tube, away from the shock wave. Following blast injury, animals were closely monitored for any signs of trauma-related

distress (apnea, loss of motor coordination). Neurological severity score was conducted five minutes post exposure and none of the animals included in this study displayed scores that differed from sham animals. Exposed animals were subjected to a single blast of 180kPa peak overpressure and euthanized via transcardial perfusion-fixation four hours post-injury. Prior to initiation of perfusion, CSF was extracted from the cisterna magna using a 25 gauge butterfly needle from scalp vein set (Exelint International, CA) and was freely allowed to collect into catheter (sans any pulling force). Blood (about 4ml) was collected by cardiac puncture (left ventricle) and allowed to settle in vacutainer tubes (BD Bioscience) containing 3.2% sodium citrate for 10 minutes. Plasma was separated from blood by centrifuging at 2000 g. For extravasation studies, Evans blue (2% solution dissolved in PBS, .002g/ml, 0.7ml delivered) was injected intravenously through tail vein two hours prior to euthanasia (two hours post-blast). Two hours were given as to give sufficient time for the tracers to circulate the body multiple times and perfuse even deeper neurovasculature across all experimental groups. Other groups have used both these dyes to assess BBB permeability up to four hours following tracer administration[69,112].

As a quality control measure, high-speed video was monitored and recorded with a Photron FASTCAM Mini UX100 operating at a framerate of 5000fps to capture any substantial head/body movement during blast, in order to exclude the effects of secondary/tertiary injury from this study. Approximately two seconds of video footage were recorded per exposure and then saved via PFV (Photron FASTCAM Viewer) 3.3.5 software. Incident overpressure at the location of the animals in the test section of the shock tube was recorded at 1.0 MHz sampling frequency by a custom LabView program

running on in-house built data acquisition system based on National Instruments PXI-6133 32 MS Memory S Series Multifunction DAQ Modules and PXIe-1082 PXI Express Chassis. PCB Piezotronics (Depew, NY) model 134A24 pressure sensors were used in all experiments.

5.2.3 Immunofluorescence and Microscopy

In order to evaluate the increase in NOX1 expression in vascular endothelial cells following blast injury, double immunofluorescence studies were conducted for NOX1 and RECA-1 a marker of endothelial cells) in the frontal cortex. Briefly, four hours post-injury, both sham and injured animals were transcardially perfused with PBS and brains were fixed with 4% paraformaldehyde (PFA). Brains were separated from cranial vaults and incubated in 4% PFA for additional 48 hours and cryoprotected by immersing in 30% sucrose. Brains were then dissected into 2 mm thick sections using rat brain slicer (Kent Scientific Corp.) and embedded in OCT (Optimal Cutting Temperature) media and quickly frozen in isopentane cooled to liquid nitrogen temperature. Frozen sections were stored at –80 °C until ready for sectioning. Brain sections (20 μm thick) were prepared from the frozen tissue blocks, using Leica CM3050 cryostat and immunofluorescence was performed. The frontal cortex of each animal offered 24 sections for analysis. Tissue sections were mounted on glass slides (2-3 sections per slide) prepared from individual animals in each group were washed with 10 mM phosphate buffered saline (PBS), fixed in ice-cold methanol (100%) solution for 10 minutes at –20 °C. The tissue sections were blocked with 10% donkey serum at room temperature for 1 hour in PBS containing 0.03% Triton X-100. Fixed tissues were incubated overnight at 4 °C with respective primary antibodies to NOX1 (Rabbit

polyclonal, Sigma-Aldrich, 1:400) and RECA-1 (Mouse monoclonal, Abcam, 1:50). Double immunofluorescence was performed using Alexafluor 488 for NOX1 and Alexafluor 594 for RECA-1. Slides containing brain regions were digitized (20x magnification) using Leica Aperio Versa 200 fluorescent microscope and slide scanner. Fluorescence intensities in regions of interest were quantitated using AreaQuant software (Leica Biosystems) and expressed as average fluorescence intensity/unit area.

5.2.4 Superoxide Production

Superoxide ($O_{2.}^-$) levels in different brain regions were measured using dihydroethidium (DHE) following the method of Kim et al.[159], and previously described[211]. Briefly, animals were injected with 5mg/kg DHE (Molecular probes, MA, dissolved in DMSO) intraperitoneally 30 minutes prior to blast and, four hours after exposure, animals were transcardially perfused first with PBS followed by 4% PFA (n=6, per group). Brains were extracted and 50 µm sections were cut using Leica VT 1000S vibratome and mounted. DHE immunofluorescence in each region was visualized and quantified as described above.

5.2.5 ELISA

As a means to determine the abundance of tight junction proteins and matrix metalloproteinases in the brain tissue, GFAP in the blood plasma, and albumin in the cerebrospinal fluid, ELISAs were performed in the cerebral hemisphere. Following perfusion with PBS, brains were excised from the skull and cerebrum was homogenized in CellLytic-M (Sigma) using sonicator with probe amplitude set to 45% on ice. Samples were then centrifuged at 14,000g at 4°C. The protein concentration in the samples was estimated bicinochoninic acid (BCA) method (Thermo Scientific, Rockford, IL).

Subsequently, samples were diluted in PBS and loaded onto specific ELISA plates for MMP3, MMP9, occludin, and claudin-5 (LSBio, Seattle, WA). Plates were read in microplate reader (Spectra Max i3, Molecular Devices) at wavelength of 450nm. Steps of ELISA were conducted in accordance with manufacturer instructions and samples plotted against a standard curve made up of eight samples (R^2 = 0.980, 0.985, 0.995, 0.999 for MMP3, MMP9, occludin, and claudin-5 respectively) using SoftMax Pro 6.5 software.

5.2.6 Ex-Vivo Imaging and Analysis

Slides containing EB extravasated tissue sections were digitized (10x magnification) using Leica Aperio Versa 200 digital pathology grade slide scanner. Fluroescent intensities were quantified after excitation at 594 nm, 125 ms exposure, using AreaQuant, software specifically designed for this imaging application (Leica Biosystems) and expressed as average fluorescence intensity/ unit area. This imaging technique allows for visualization of micro-structural details and digital scanning affords the ability to image large brain regions with no loss of resolution. In order to quantify fluorescence intensities, regions of interest were manually outlined in different brain section. For the given channel, a minimum intensity threshold value was selected to exclude any background fluorescence from relevant calculations. The AreaQuant algorithm then determines if the intensity value of each pixel enclosed in the outlined region exceeds the minimum intensity threshold and outputs the total area of positive stain for each section, the average intensity in each channel, and the expression profile of the tracer.

5.2.7 Statistical Analysis

Data are presented as mean $\pm$ standard error of the mean. Statistical significance was determined using one-way analysis of variance (ANOVA) to compare mean fluorescence

intensities of between control, blast, and blast + treatment groups with a Tukey pairwise test done to determine differences between individual groups. Normalcy and population variance homogeneity were assessed with Shapiro-Wilk and Levene's tests respectively. Differences between means were assessed and probability levels of $p < 0.05$ were considered statistically significant. Minitab 17 Statistical Software was used for all analyses and Origin 2017 was used for generation of bar plots. Bar plots presented in semi-log scale are done so in order to capture magnitudinal differences between groups. Fluorescent images were taken using Aperio Versa software and analysis and export done via ImageScope software (LEICA Corp.).

5.3 Results

5.3.1 NOX1 is Upregulated in Neurovascular Endothelial Cells Four Hours Following Moderate Blast Injury

Previous studies in this laboratory identified increased levels of NOX1 and NOX2 in neurons, astrocytes, and microglia following moderate blast injury (180kPa) across the cerebral hemisphere and cerebellum[211]. In the present study, levels of NOX1 in brain endothelial cells in the frontal cortex in vascular endothelial cells were examined. The double immunofluorescence for NOX1 and RECA-1 (endothelial cell marker) showed a significant increase in amount of colocalization following moderate blast (Figure 5.2). Fifteen minutes post-exposure, a statistically insignificant increase in colocalized NOX1 compared to controls was observed (post-ANOVA Tukey test, $p > 0.05$, Figure 2B). Four hours after blast, which previous work from this group has shown as the peak time for

BBB permeability following blast injury, a robust increase (ten-fold) in NOX1 concentration in vascular endothelial cells was observed (Tukey test, p=0.023).

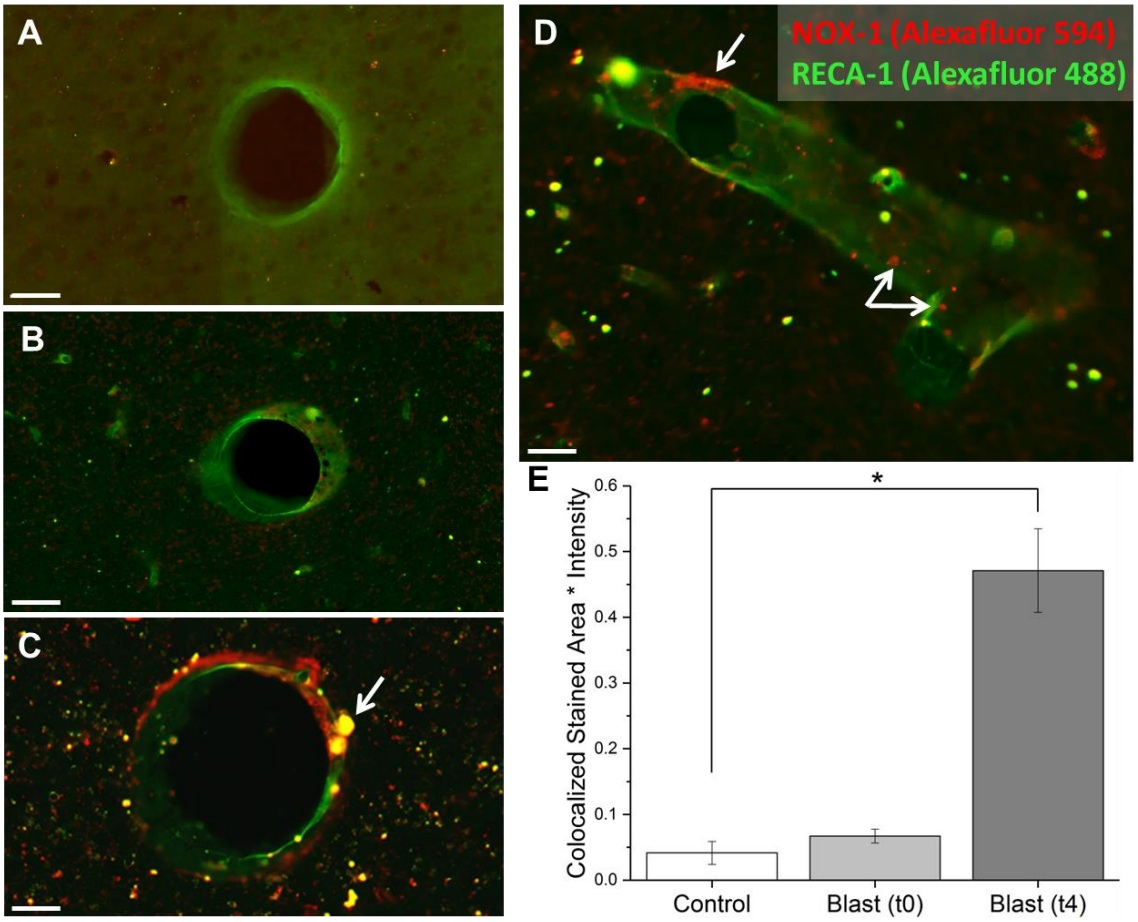

Figure 5.2 Colocalization of NOX-1 (red) and RECA-1 (green) on vascular endothelial cells in the frontal cortex. (A) controls show very little NOX-1 on vascular endothelial cells while (B) there is a slight increase in colocalization fifteen minutes following moderate blast exposure. (C**)** four hours following blast, there is a significant upregulation of NOX-1 on marked endothelial cells, with the yellow indicating an overlap of NOX-1 and RECA-1. (D) shows an alternative view of the vessel in order to show that NOX-1 is upregulated across the length of the vessel lumen, as indicated by the arrows. (E) shows the quantitation of the colocalization between control, 15 minutes post-blast, and four hours post-blast groups. Scale bars equal 30μm. [*] indicates a difference in intensity compared with control with a statistical significance of $p < 0.05$.

5.3.2 Apocynin Significantly Reduces Superoxide Production Following Blast Injury

Several groups have demonstrated that activation of NOX results in increased superoxide production[154,162]. After demonstrating the increase in NOX1 concentration in

neurovasculature in the frontal cortex, authors sought to determine if this results in an increase of superoxide production. *In-vivo* levels of superoxide were measured using DHE and a clear increase in superoxide produced in the frontal cortex was observed, which corroborated well with the upregulation of NOX1 (Figure 5.3). Differences between control and blast groups (Tukey test, p=0.004) and blast and treatment groups (Tukey test, p=0.001) were found to be statistically significant.

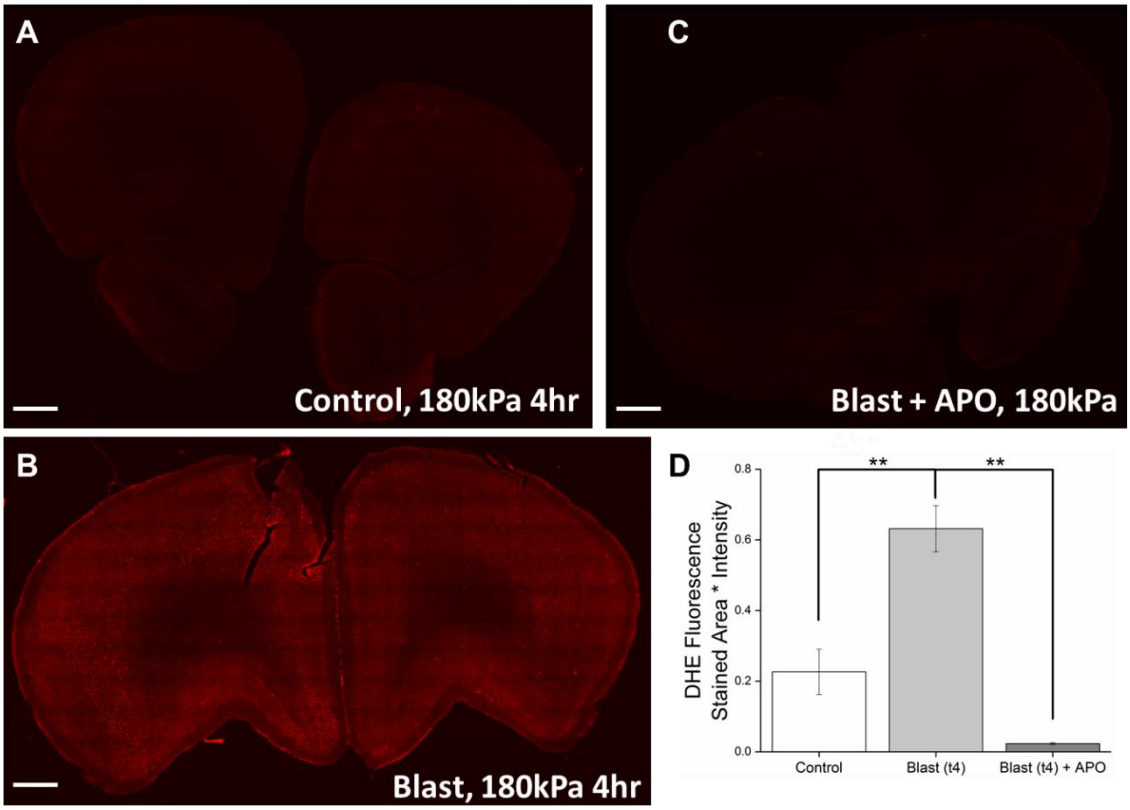

Figure 5.3 DHE stain to observe superoxide concentration in the frontal cortex. (A) superoxide levels in control tissue, basal level of superoxide. (B) levels of superoxide robustly increase four hours following blast exposure, but are brought back down to basal levels with pretreatment of apocynin (C). (D) quantitation of DHE fluorescence intensity for the three aforementioned groups. Scale bars equal 1mm. [**] indicates a difference between control and blast groups as well as blast and treatment groups with a statistical significance of $p < 0.01$.

5.3.3 Apocynin Significantly Reduces Tight Junction Degradation Following Blast Injury

In order to determine the degree of BBB breakdown following blast injury, ELISA was conducted for tight junction proteins occludin and claudin-5 for control, blast, and blast + apocynin groups (n=3, Figure 5.4). Occludin decreased by 20.31% four hours post-blast compared to controls (ANOVA followed by Tukey test, $p = 0.002$) but barely changed in animals treated with apocynin (Tukey test, $p = 0.946$). The difference between the blast group and the treatment group was also significant (Tukey test, $p=0.001$). Claudin-5 decreased by 12.40% four hours post-blast compared to controls (Tukey test, $p=0.001$), but like occludin, displayed only a negligible decrease in the treatment group (Tukey test, $p = 0.362$). The difference between blast and treatment groups was statistically significant (Tukey test, $p=.007$).

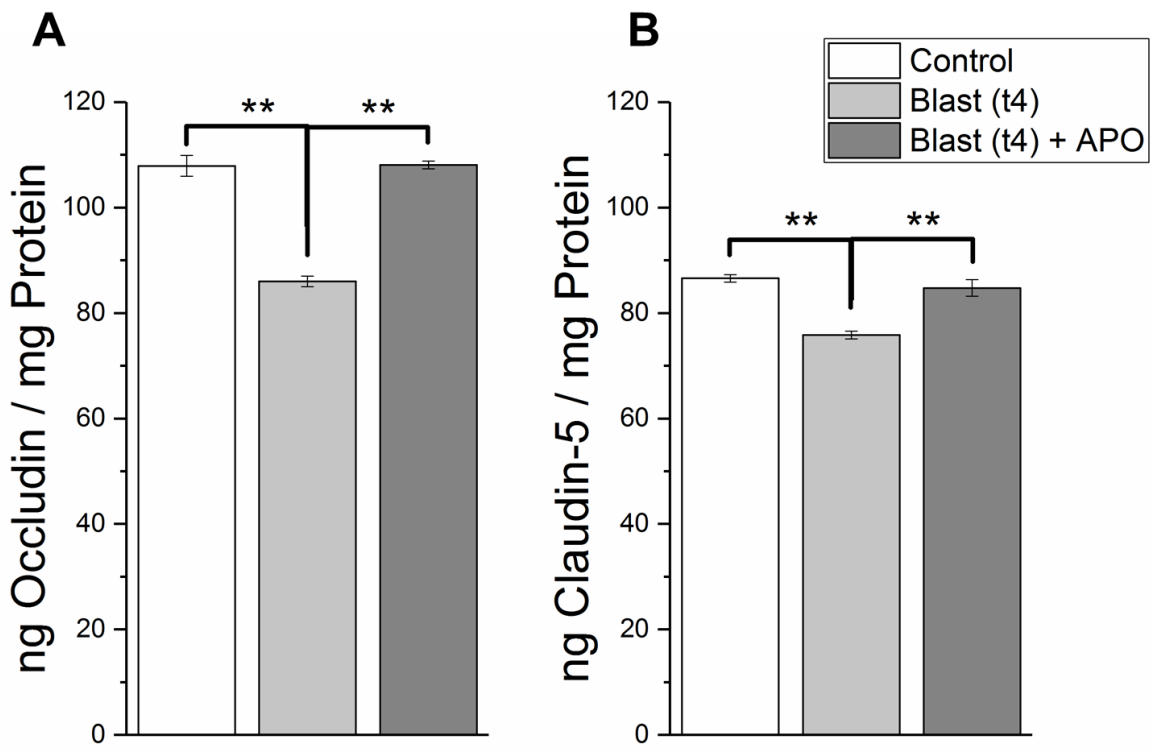

Figure 5.4 ELISA results for tight junction proteins, occludin (A) and claudin-5 (B) in control, blast, and treatment groups. [**] indicates a difference in intensity with a statistical significance of $p < 0.01$.

5.3.4 Apocynin Significantly Decreases Blood-Brain Barrier Permeability Following Blast Injury

The extent of extravasation was evaluated in the frontal cortex at both fifteen minutes and four hours post-blast injury (Figure 5.5). This group previously displayed that extravasation of Evans blue was significant at both time points post-moderate blast injury and current results support that. Significant extravasation was observed in both injured and treatment groups at the acute stage ($p=0.006$, $p=0.004$, respectively), with no statistically significant difference between them. EB presence in the brain parenchyma increased by 1300-fold four hours following moderate blast over the control in the frontal cortex (ANOVA followed by Tukey test, $p < 0.01$) and over the blast + apocynin group (75 fold, Tukey test, $p < 0.01$). Interestingly, there was no statistically significant

difference between the control group and the treated group (Tukey test, $p > 0.05$). Four animals were used per group in this phase of the study ($n = 4$).

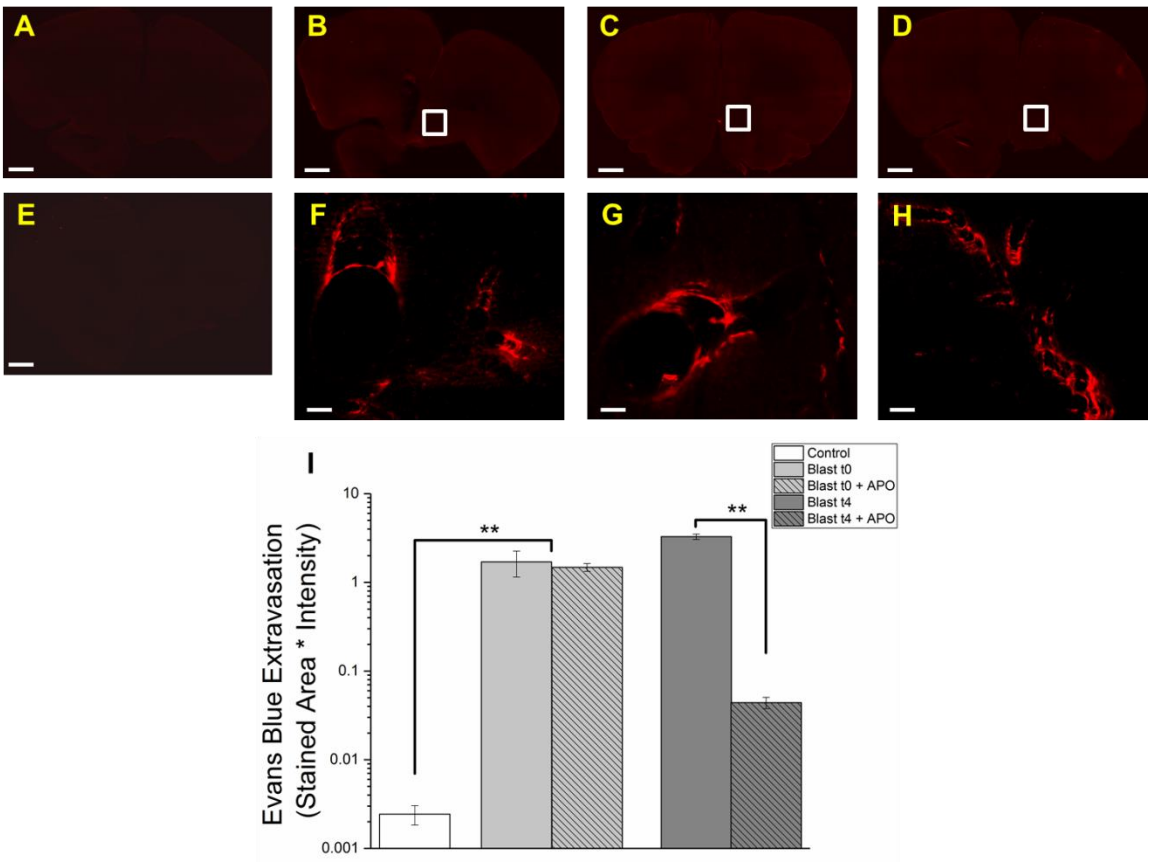

Figure 5.5 Fluorescent images of Evans blue extravasation. Images show whole coronal sections as well as zoomed in 20x images in the frontal cortex. (A) shows a cortical section of a control animal, with almost no observable extravasation of leakage, (B) shows a coronal section from injured animal (180kPa BOP), acutely (15 minutes) following blast exposure with a significant amount of leakage observed around the blood vessels, (C) shows a coronal section from an injured animal at the same time point, but pretreated with apocynin thirty minutes prior to blast, with extravasation levels similar to control animals. (D) shows a coronal section from injured animal four hours post-exposure with an even greater amount of leakage than at the acute time point and (E) shows an animal at the same time point with apocynin pretreatment. F, G, H show zoomed in, 20x images from images (B, C, and D), respectively. (I) Quantitation of extravasation is shown using a semilog plot in order to capture magnitudinal differences. Scale bars equal 2mm for coronal sections (A-E), 30μm for 20x images. [**] indicates a difference in intensity with a statistical significance of $p < 0.01$.

5.3.5 Moderate Blast Induces Translocation of Glial Fibrillary Acidic Protein into the Blood Stream

Concentration of GFAP in the blood plasma was determined via ELISA (Figure 5.6). Statistically significant increase in GFAP concentration was seen compared to controls in both blast and treatment groups 15 minutes after injury (Tukey test, $p = 0.016$ and $p = 0.002$, respectively), but no difference between blast and treatment group. At four hours post-blast, there is a further increase in GFAP concentration in blood plasma (Tukey test, $p = 0.002$), but with apocynin, the values drop back to control levels (Tukey test, $p > 0.05$). Intergroup comparison reveals a statistically significant difference between blast and treatment groups four hours after injury (Tukey test, $p = 0.001$).

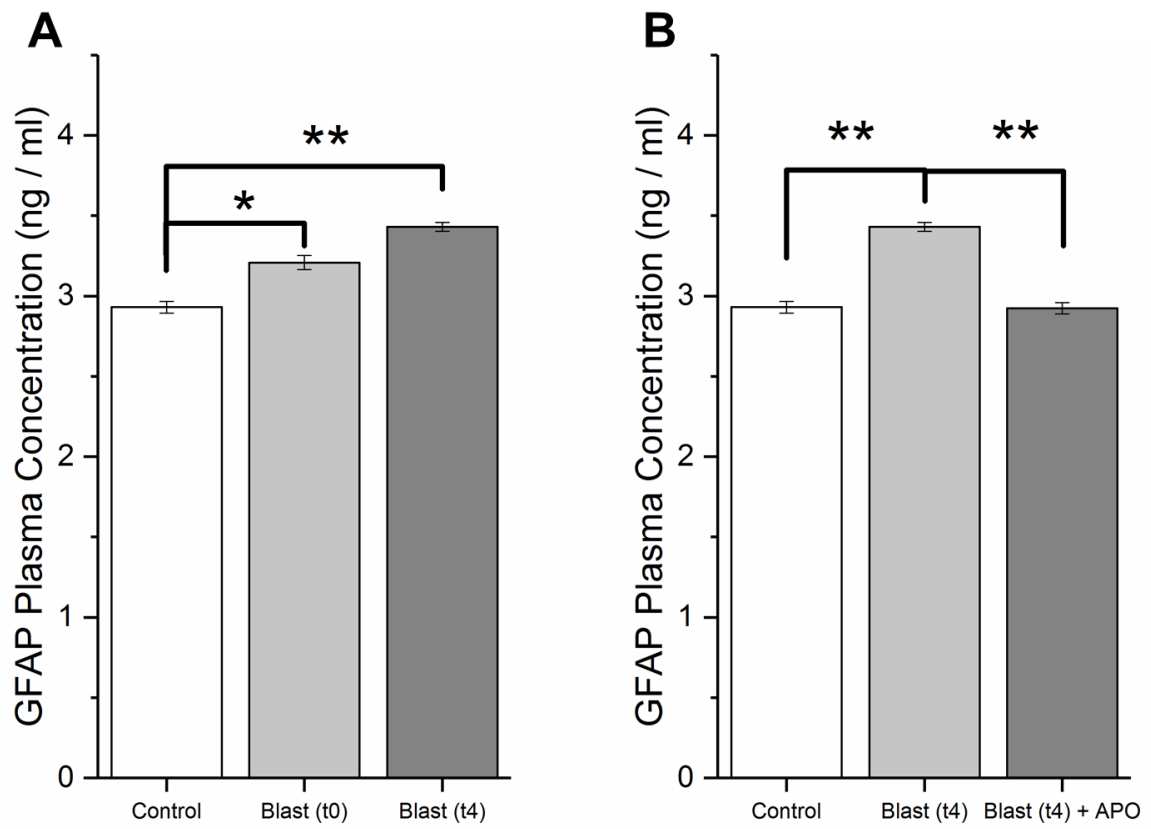

Figure 5.6 ELISA results for GFAP concentration in blood plasma. **(A)** compares control levels with levels 15 minutes and four hours following blast and (B) compares control levels with levels four hours following blast with and without apocynin pretreatment. [*] indicates a difference in intensity with a statistical significance of $p < 0.05$, [**] indicates $p < 0.01$.

5.3.6 CSF-Plasma Ratio of Albumin Increases Following Moderate Blast Injury

In order to determine the ratio of albumin in the CSF and blood plasma, another ELISA was conducted on both samples (Figure 5.7). While an increase in the CSF-Plasma albumin ratio was observed acutely (fifteen minutes post-blast) for both blast and treatment groups, statistical significance was not achieved in either ($p > 0.05$). Four hours following blast, a statistically significant increase over control was observed in the injured group (Tukey test, $p = 0.044$). Comparison between blast and treatment group at this point also revealed statistically significant difference (Tukey test, $p = 0.048$).

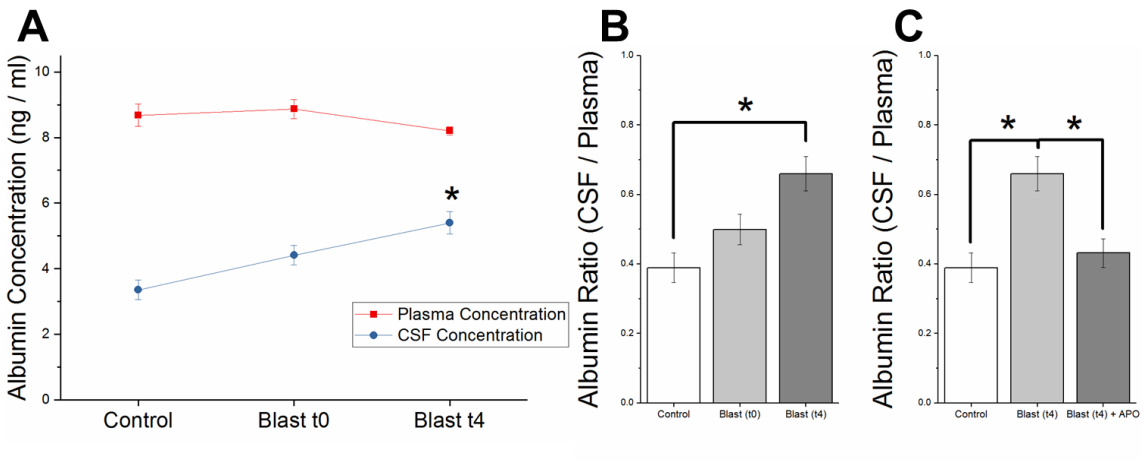

Figure 5.7 (A) ELISA results for albumin concentration in CSF and blood plasma. [*] indicates a difference in intensity compared with control with a statistical significance of $p < 0.05$. (B&C) present results as ratios of albumin concentration in CSF and blood plasma, (B) compares control levels with levels 15 minutes and four hours following blast and (C) compares control levels with levels four hours following blast with and without apocynin pretreatment. [*] indicates a difference in intensity with a statistical significance of $p < 0.05$.

5.3.7 Apocynin Mitigates the Activation of Matrix Metalloproteinase 3 and 9 Following Blast Injury

Given the number of groups that link increased ROS activity with increased MMP production, ELISAs were conducted for MMPs 3 & 9 for control, blast, and blast + apocynin groups (n=4, Figure 5.8). MMP3 increased by 105% (ANOVA followed by Tukey test, $p = 0.020$) compared to controls in the injured group, while the difference between the blast + apocynin and control groups was not statistically significant (Tukey test, $p > 0.05$). Similarly, MMP9 increased by 115% (Tukey test, $p = 0.007$) compared to the controls in the injured group, but the difference between blast + apocynin and control groups was not statistically significant (Tukey test, $p > 0.05$). However, it is important to note that there is still an observed increase in both MMP3 and MMP9 in the blast + apocynin groups, meaning that the pretreatment was not enough to completely mitigate

the increased production of these matrix metalloproteinases, although this relative increase is not statistically significant.

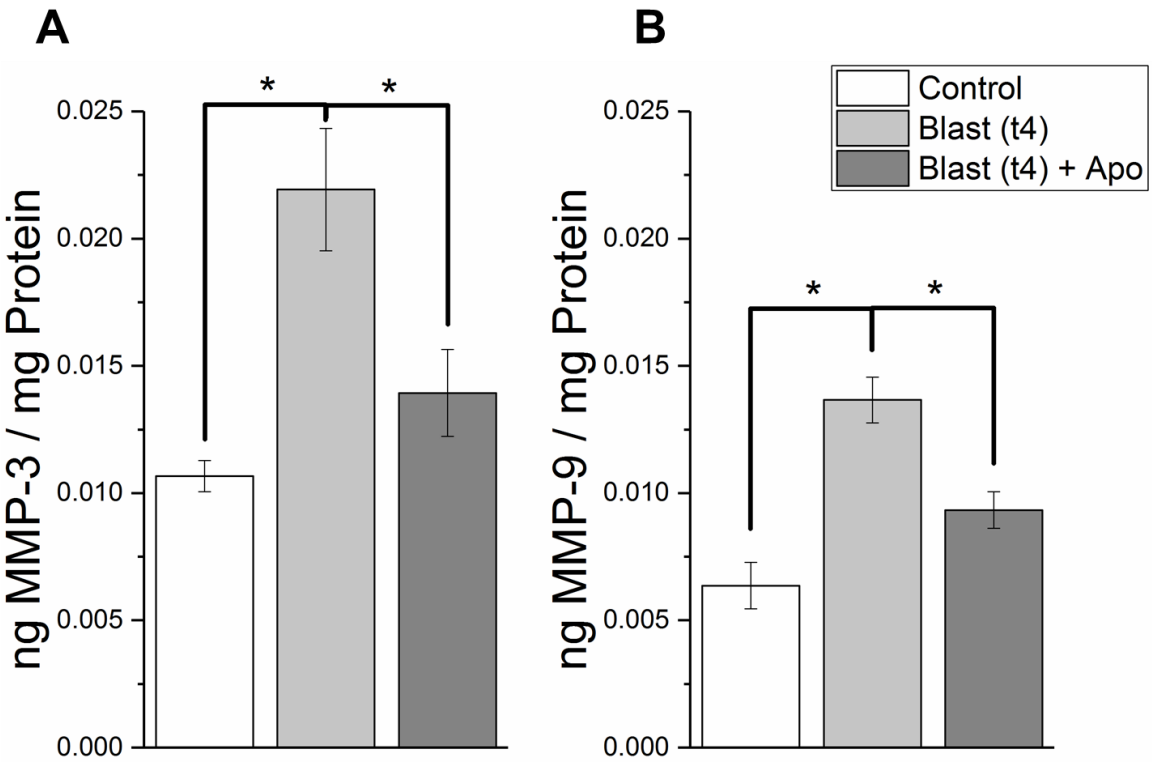

Figure 5.8 ELISA results for matrix metalloproteinases 3 (A) and 9 (B) in control, blast, and treatment groups. [*] indicates a difference in intensity with a statistical significance of $p < 0.05$.

5.4 Discussion

This work aims to investigate the role of oxidative stress in the mechanism of increased BBB permeability in the neuropathology of blast-induced traumatic brain injury. Based on previous studies from this group, the frontal cortex has been determined as the most vulnerable region to BBB extravasation in this blast injury model for an overpressure of 180kPa. This group has previously demonstrated that moderate levels of blast can acutely disrupt the BBB, but that maximum permeability is seen four hours after injury and that

there is an upregulation in NADPH-oxidase abundance across the brain following blast at the same time point[158,211]. Given these facts, authors hypothesize that oxidative stress plays a role in the increased permeability seen four hours post-blast. A schematic diagram depicting various events that are induced by oxidative stress ultimately leading to BBB disruption is illustrated in Figure 5.1.

In the present study, a robust (10-fold) increase in NOX1 expression four hours following blast injury was observed in endothelial cells in the frontal cortex as demonstrated by double immunofluorescence staining of NOX1 with RECA-1, an endothelial cell marker (Figure 5.2). Recent observations along with other investigations also report increased activation of NOX1 between four hours and a few days after various forms of TBI[47,155,157,181,211]. This gives credence to the belief that increased NOX expression and associated, heighted oxidative stress represent secondary injury events that likely occur a few hours following blast TBI.

In order to confirm that increased NOX1 expression activates downstream pathways, superoxide production was examined by prior administration of dihydroethidium (DHE). There was a robust increase in superoxide production in animals subjected to blast injury, which corroborates the increased NOX1 expression on vascular endothelial cells (Figure 5.3). It is important to note that both superoxide produced in vascular endothelial cells, as well as that produced in neural cells (neurons, astrocytes, microglia)[211] can contribute to downstream BBB disruption. Authors further established that the superoxide production is indeed mediated by NOX1 expression by using apocynin, that inhibits assembly of NOX subunits and renders NOX functionally inactive and found that animals pretreated with an apocynin bolus show a complete absence of

superoxide four hours post-injury (Figure 5.3), which is consistent with this group's previous work[211]. It should be mentioned that the use of apocynin as a NOX inhibitor following TBI has been well established[155,165,202,203].

It is interesting to note that the present study observed a close correlation between increased NOX1 expression, its associated increase in superoxide production, and the heightened disruption of the BBB four hours after blast injury. The integrity of the BBB was assessed in the presence and the absence of apocynin (Figure 5.5). A robust extravasation of EB was observed in animals four hours following blast injury and such increased extravasation was completely blocked by apocynin. Additionally, levels of tight junction proteins (TJPs) occludin and claudin-5 were also quantified as another means to determine BBB integrity. Tight junctions are water-tight seals that attach adjacent endothelial cells together and occludins and claudins represent the major families of TJPs[46,48]. Results indicate a significant reduction of both occludin and claudin-5, four hours after blast injury (Figure 5.4). Occludin abundance was reduced by 20.31% ($p = 0.002$) and claudin-5 reduced by 12.40% ($p = 0.001$) which is consistent with extravasation of tracers since loss of tight junction protein integrity is well known to allow leakage of tracers to penetrate into brain parenchyma[158]. Moreover, increased presence of astrocytic protein, GFAP, in plasma as well as the increased CSF-blood ratio of albumin observed in the present study (Figures 5.6 and 5.7) not only establish BBB disruption but also confirm the reciprocal translocation of brain and blood-borne macromolecules as a result of BBB disruption. Noteworthy that a pretreatment with apocynin significantly attenuated the extravasation of tracers, restored the levels of TJPs and CSF-blood albumin ratio to that of controls, as well as attenuated increased presence

of GFAP in plasma. Together these data strongly suggest that NOX-mediated oxidative stress contributes to heightened BBB disruption (four hours) following blast injury.

Several groups have attempted to establish a connection between oxidative stress and BBB breakdown by a means involving matrix metalloproteinases (MMPs)[47,91-95]. MMPs are endopeptidases that degrade the extracellular matrix (ECM) of various cell types. While the activity of MMPs are tightly controlled in normal, "uninjured" conditions by MMP inhibitors, uncontrolled activation has been observed due to oxidative stress[47,87-90]. This in-turn degrades the brain endothelium and substantially increases the permeability of the BBB. The role of MMPs in BBB degradation has been well-investigated[47,91-95]. As a means to assess the role of NOX-mediated oxidative stress (increased superoxide production), ELISAs were run for two matrix metalloproteinase isoforms (III&IX) commonly implicated in BBB degradation and endogenous to vascular endothelial cells. Levels of both MMP3 and MMP9 significantly increased over controls four hours after blast exposure (Figures 5.8A & 5.8B). Rats pretreated with apocynin displayed significant reduction in the levels of MMPs as compared to animals subjected to blast injury (Figure 5.8), which indicates that NOX-mediated oxidative stress contributes to increased MMPs. The data presented in this study showing the protective effect of apocynin against increased extravasation of tracers, reduction of TJPs and associated changes in the translocation of macromolecules between the brain and blood, in conjunction with the ability of apocynin to indirectly inhibit MMPs, strongly suggest that the activation of MMPs are likely NOX-mediated and induce BBB disruption via degradation of TJPs.

While it is strongly suggested that oxidative stress is a secondary event that contributes to heightened BBB disruption in the latter stages after blast injury, authors further extended studies to question whether BBB disruption immediately after blast injury is caused by a direct mechanical loading or in part mediated by any presence of oxidative stress. Time course for NOX1 protein levels in endothelial cells was examined by double immunofluorescence in sections obtained from animals euthanized immediately (approximately fifteen minutes) after blast injury. Staining was performed as early as fifteen minutes after injury (t0). Moreover, this was the earliest time studies could be performed since fifteen minutes represents the time necessary to remove the animal from the shock tube and complete transcardial perfusion-fixation. At this acute time point, there is a negligible difference in the amount of NOX1 colocalized on endothelial cells (Figure 5.2). These data in conjunction with observations of robust increase in NOX1 four hours after blast strongly suggest that oxidative stress is a secondary event occurring following blast injury. Lack of evidence of increased NOX1 levels immediately following blast injury not only suggest that oxidative stress appears a secondary factor but also adds credence to the tenet that the disruption of BBB immediately after blast is indeed mediated by a direct mechanical effect created by shockwave loading. This also corroborates extravasation results at t0, where apocynin has no effect on amount of EB that leaks into the brain parenchyma (Figure 5.5). The degree of BBB permeability is significant at this acute time point (based on extravasation results as well as translocation of GFAP and albumin), but NOX-mediated oxidative stress does not contribute to this change.

In summary, these studies demonstrate that moderate blast injury causes an a disruption of BBB by loss of TJPs and results in leakage of macromolecules across brain-to-blood as well as increase in NOX expression on vascular endothelial cells and associated increased production of superoxide 4h after blast injury. These events corroborate with the heightened activation of matrix metalloproteinases III & IX. Pretreatment with NOX inhibitor (apocynin), BBB permeability is significantly reduced and MMPs levels were restored to that of controls. This study therefore indicates a strong relationship between NOX-mediated oxidative stress and blood brain barrier breakdown, which may lead to further investigation delineating relationships between other injury mechanisms, a prerequisite for better therapeutic interventions.

CHAPTER 6

SUMMARY AND FUTURE WORK

Exposure to shock waves is the leading cause of traumatic brain injury (TBI) in military personnel and blast-induced traumatic brain injury (bTBI) is considered the signature wound in recent military conflicts in Iraq and Afghanistan. Many researchers attempt to replicate field-relevant shock waves in laboratory settings through the use of shock tubes in order to investigate the generation and propagation of shock waves and possible mechanisms of bTBI. Among several injury mechanisms, damage to the blood-brain barrier (BBB) has been identified as a potential candidate and has been a focus of several clinical and experimental investigations aimed to establish injury baselines and discover timelines for therapeutic intervention for neurotrauma. In this work, the shock tube housed at the New Jersey Institute of Technology is characterized and effects of an end reflector plate on shock loading investigated, prior to using this model in the study of BBB permeability post-blast injury. Barrier breakdown is studied across the frontal cortex, striatum, somatosensory barrel field cortex, thalamus, hippocampus, and cerebellum at fifteen minutes, four, and twenty-four hours at 35, 70, 130, and 180kPa through the use of extravasation of tracers into the brain, quantification of tight junction proteins in the brain and the blood, and tracking of specific blood-borne molecules into the brain and brain-specific proteins into the blood. Finally, effects of oxidative stress on BBB permeability are delineated at four hours for an 180kPa blast overpressure in the frontal cortex, as well as the introduction of a potential treatment, apocynin, for NADPH-mediated BBB damage following blast injury.

End effector studies are conducted with the use of four different end plate configurations (0.625, two, four inches, and an open end). Use of end reflector plate allows for precise control over the intensity of reflected waves penetrating into the shock tube and, at a calculated optimized distance, can eliminate secondary waves from the test section, confirmed by pressure sensor recordings. Numerical simulations combined with experimental data offer detailed insight into spatiotemporal dynamics of shock waves and wave attenuation via internal pressure expansion. Diffusion of the driver gas inside of the shock tube is responsible for velocity increase of reflected shock waves. Results indicate that the end of the shock tube is a less favorable location to the test specimen, due to the complexity of loading conditions. The incident shock wave exiting the shock tube results in formation of underpressure waves, while reflected pressure waves are created when the end is fully closed or the reflector plate is positioned close to the muzzle of the shock tube. This experimental investigation should serve as a strong starting point for researchers attempting to ensure accurate loading of test subjects in compressed-gas driven shock tubes.

Following the characterization and validation of the shock tube, blood-brain barrier permeability is primarily assessed by extravasation of sodium fluorescein and Evans blue into brain parenchyma. Maximum extravasation of tracers (and hence BBB permeability) occurs in the frontal cortex at four hours following injury and increases with increasing blast overpressure. Abundance of tight junction proteins occludin and claudin-5 is also measured at different time-points after injury both in the brain and in blood serum. Significant extravasation is observed immediately after blast across several brain regions, suggesting a shockwave-induced mechanical disruption of the BBB even at

mild overpressures. This force is enough to dislodge the tight junction proteins from neurovascular endothelial cells and which are then taken up by circulation. The presence of s100-β in the blood serum as well as monocyte infiltration into the brain parenchyma were observed, further validating increased BBB permeability. Within 24 hours, extravasation of sodium fluorescein and Evans blue returns close to control values across all brain regions studied.

NADPH-oxidase (NOX) is shown to be upregulated in vascular endothelial cells, resulting in an increase in superoxide production at four hours post-blast. This leads to increased activation of matrix metalloproteinase III and IX, which degrade vascular tight junction complexes. The decrease in tight junction proteins occludin and claudin-5 contribute to the decreased integrity of the BBB, functionally assayed through the extravasation of Evans blue. However, the use of apocynin, a selective NOX inhibitor, thirty minutes before blast injury is shown to ameliorate production of superoxide and thereby significantly reduce MMP activity, tight junction breakdown, and BBB extravasation. These studies indicate and explicate a clear relationship between NOX-mediated oxidative stress and BBB breakdown, which may lead to further investigations delineating relationships between other injury mechanisms, a prerequisite to therapeutic and treatment development.

This work should serve as the foundation for continued investigation of primary blast-induced neurotrauma. More experimental work needs to be done in order to elucidate the mechanisms of BBB restoration between four and twenty-four hours post-blast. While increased tight junction protein production is observed, the pathway for this increase is not yet understood. Members of our laboratory are beginning to examine other

biochemical injury sequelae (neuroinflammation, excitotoxicity, etc.) and their relation to increased BBB permeability. It would be interesting to know if these injury cascades follow similar temporal and spatial profiles in the exacerbation of bTBI pathology.

In these studies, the roles of brain and blood-borne particles crossing over the BBB were not investigated in the long term neuropathology following BBB disruption. It is quite possible that the presence of these foreign molecules exacerbates injury even after the BBB has been resealed. The closing of the barrier prevents further leakage, but does not necessarily resolve the consequences of the leakage within the first twenty-four hours after blast injury.

This dissertation represents the cumulative completion of three specific experimental aims: 1) the characterization and validation of the blast injury model, which includes the detailed investigation on shock wave propagation and pressure transmission within the shock tube, 2) the use of this model in the study of the temporal and spatial effects of blast overpressure on blood-brain barrier permeability following blast-induced traumatic brain injury, and 3) the examination of the intertwined roles of oxidative stress and BBB breakdown following injury, with a closer look at a potential preventative intervention for blast-induced neurotrauma. All three of these aims have either resulted in publications in peer-reviewed journals or are currently under review for publication.

REFERENCES

1. Ling, G. S., Hawley, J., Grimes, J., Macedonia, C., Hancock, J., Jaffee, M., Dombroski, T. & Ecklund, J. M. Traumatic brain injury in modern war. *Current Opinion in Anesthesiology* **24**, 124-130 (2013).

2. Mathews, Z. R. & Koyfman, A. Blast injuries. *The Journal of Emergency Medicine* **49**, 573-587 (2015).

3. Moore, B. Blast injuries-a prehospital perspective. *Australasian Journal of Paramedicine* **4** (2015).

4. Elder, G. A. & Cristian, A. Blast-related mild traumatic brain injury: mechanisms of injury and impact on clinical care. *Mount Sinai Journal of Medicine* **76**, 111-118, doi:10.1002/msj.20098 (2009).

5. Elder, G. A., Stone, J. R. & Ahlers, S. T. Effects of low-level blast exposure on the nervous system: Is there really a controversy? *Frontiers in Neurology* **5**, 269, doi:10.3389/fneur.2014.00269 (2014).

6. DePalma, R. G., Burris, D. G., Champion, H. R. & Hodgson, M. J. Blast injuries. *The New England Journal of Medicine* **352**, 1335-1342 (2005).

7. Hoge, C. W., McGurk, D., Thomas, J. L., Cox, A. L., Engel, C. C. & Castro, C. A. Mild traumatic brain injury in U.S. soldiers returning from Iraq. *The New England Journal of Medicine* **358**, 453-463, doi:10.1056/NEJMoa072972 (2008).

8. Vanderploeg, R. D., Belanger, H. G., Horner, R. D., Spehar, A. M., Powell-Cope, G., Luther, S. L. & Scott, S. G. Health outcomes associated with military deployment: mild traumatic brain injury, blast, trauma, and combat associations in the Florida national guard. *Archives of Physical Medicine and Rehabilitation* **93**, 1887-1895, doi:10.1016/j.apmr.2012.05.024 (2012).

9. Gould, K. E. High-explosive field tests, explosion phenomena and environmental impacts. Defense Technical Information Center, Santa Barbara, CA. (1981).

10. Cernak, I. in *Brain Neurotrauma: Molecular, Neuropsychological, and Rehabilitation Aspects. Frontiers in Neuroengineering* (ed F. H. Kobeissy) Ch. 45, Boca Raton, FL: CRC Press, (2015).

11. Knudsen, S. K. & Oen, E. O. Blast-induced neurotrauma in whales. *Neuroscience Research* **46**, 377-386 (2003).

12. Bolander, R., Mathie, B., Bir, C., Ritzel, D. & VandeVord, P. Skull flexure as a contributing factor in the mechanism of injury in the rat when exposed to a shock wave. *Annals of Biomedical Engineering* **39**, 2550-2559 (2011).

13. Cernak, I., Merkle, A. C., Koliatsos, V. E., Bilik, J. M., Luong, Q. T., Mahota, T. M., Xu, L., Slack, N., Windle, D. & Ahmed, F. A. The pathobiology of blast injuries and blast-induced neurotrauma as identified using a new experimental model of injury in mice. *Neurobiology of Disease* **41**, 538-551 (2011).

14. Chavko, M., Watanabe, T., Adeeb, S., Lankasky, J., Ahlers, S. T. & McCarron, R. M. Relationship between orientation to a blast and pressure wave propagation inside the rat brain. *Journal of Neuroscience Methods* **195**, 61-66 (2011).

15. Rafaels, K. A. Blast brain injury risk from primary blast. *Journal of Trauma and Acute Care Surgery* **73**, 895-901 (2012).

16. Reneer, D. V., Hisel, R. D., Hoffman, J. M., Kryscio, R. J., Lusk, B. T. & Geddes, J. W. A multi-mode shock tube for investigation of blast-induced traumatic brain injury. *Journal of Neurotrauma* **28**, 95-104 (2011).

17. Svetlov, S. I., Prima, V., Kirk, D. R., Gutierrez, H., Curley, K. C., Hayes, R. L. & Wang, K. K. Morphologic and biochemical characterization of brain injury in a model of controlled blast overpressure exposure. *Journal of Trauma and Acute Care Surgery* **69**, 795-804 (2010).

18. Bell, R. S., Vo, A. H., Neal, C. J., Tigno, J., Roberts, R., Mossop, C., Dunne, J. R. & Armonda, R. A. Military traumatic brain and spinal column injury: a 5-year study of the impact blast and other military grade weaponry on the central nervous system. *Journal of Trauma* **66**, S104-111, doi:10.1097/TA.0b013e31819d88c8 (2009).

19. Yattoo, G. & Tabish, A. The profile of head injuries and traumatic brain injury deaths in Kashmir. *Journal of Trauma Management & Outcomes* **2**, 5, doi:10.1186/1752-2897-2-5 (2008).

20. Cernak, I., Savic, V. J., Kotur, J., Prokic, V., Veljovic, M. & Grbovic, D. Characterization of plasma magnesium concentration and oxidative stress following graded traumatic brain injury in humans. *Journal of Neurotrauma* **17**, 53-68 (2000).

21. Needham, C. E., Ritzel, D., Rule, G. T., Wiri, S. & Young, L. Blast testing issues and TBI: Experimental models that lead to wrong conclusions. *Frontiers of Neurology* **6**, 72, doi:10.3389/fneur.2015.00072 (2015).

22. Sundaramurthy, A., Alai, A., Ganpule, S., Holmberg, A., Plougonven, E. & Chandra, N. Blast-induced biomechanical loading of the rat: an experimental and anatomically accurate computational blast injury model. *Journal of Neurotrauma* **29**, 2352-2364, doi:10.1089/neu.2012.2413 (2012).

23. Vieille, P. Sur les discontinuités produites par la détente brusque de gaz comprimes. *Comptes Rendus de l'Académie des Sciences* **A 129**, 1228-1230 (1899).

24. Park, C. & Appleton, J. P. Shock-tube measurements of soot oxidation rates. *Combustion and Flame* **20**, 369-379 (1973).

25. Kiefer, J., Mizerka, L., Patel, M. & Wei, H. A shock tube investigation of major pathways in the high-temperature pyrolysis of benzene. *The Journal of Physical Chemistry* **89**, 2013-2019 (1985).

26. Hooker, W. J. & Millikan, R. C. Shock-tube study of vibrational relaxation in carbon monoxide for the fundamental and first overtone. *The Journal of Chemical Physics* **38**, 214-220 (1963).

27. Dryer, M., Merritt, D. L. & Aronson, P. M. Interaction of a plasma cloud with the Earth's magnetosphere. *Journal of Geophysical Research* **72**, 2955-2962, doi:10.1029/JZ072i011p02955 (1967).

28. Cernak, I., Wang, Z., Jiang, J., Bian, X. & Savic, J. Ultrastructural and functional characteristics of blast injury-induced neurotrauma. *Journal of Trauma* **50**, 695-706 (2001).

29. Cernak, I., Wang, Z., Jiang, J., Bian, X. & Savic, J. Cognitive deficits following blast injury-induced neurotrauma: possible involvement of nitric oxide. *Brain Injury* **15**, 593-612, doi:10.1080/02699050010009559 (2001).

30. Saljo, A., Arrhen, F., Bolouri, H., Mayorga, M. & Hamberger, A. Neuropathology and pressure in the pig brain resulting from low-impulse noise exposure. *Journal of Neurotrauma* **25**, 1397-1406, doi:10.1089/neu.2008.0602 (2008).

31. Saljo, A., Svensson, B., Mayorga, M., Hamberger, A. & Bolouri, H. Low-level blasts raise intracranial pressure and impair cognitive function in rats. *Journal of Neurotrauma* **26**, 1345-1352, doi:10.1089/neu.2008-0856 (2009).

32. Stuhmiller, J. H., Phillips, Y. & Richmond, D. The physics and mechanisms of primary blast injury. *Conventional Warfare: Ballistic, Blast, and Burn Injuries*, 241-270 (1991).

33. Moore, D. F., Radovitzky, R. A., Shupenko, L., Klinoff, A., Jaffee, M. S. & Rosen, J. M. Blast physics and central nervous system injury. *Future Neurology* **3**, 243-250, doi:10.2217/14796708.3.3.243 (2008).

34. Cullis, I. Blast waves and how they interact with structures. *Journal of the Royal Army Medical Corps* **147**, 16-26 (2001).

35. Miura, H. Decay of shock waves in a dusty-gas shock tube. *Fluid Dynamics Research* **6**, 251 (1990).

36. Sommerfeld, M. The unsteadiness of shock waves propagating through gas-particle mixtures. *Experiments in Fluids* **3**, 197-206 (1985).

37. Newman, A. J. & Mollendorf, J. C. The peak overpressure field resulting from shocks emerging from circular shock tubes. *Journal of Fluids Engineering* **132**, 081204-081204, doi:10.1115/1.4002183 (2010).

38. Effgen, G. B., Hue, C. D., Vogel, E., 3rd, Panzer, M. B., Meaney, D. F., Bass, C. R. & Morrison, B., 3rd. A multiscale approach to blast neurotrauma modeling: Part II: Methodology for inducing blast injury to in vitro models. *Frontiers in Neurology* **3**, 23, doi:10.3389/fneur.2012.00023 (2012).

39. Loane, D. J. & Faden, A. I. Neuroprotection for traumatic brain injury: translational challenges and emerging therapeutic strategies. *Trends in Pharmacological Sciences* **31**, 596-604, doi:10.1016/j.tips.2010.09.005 (2010).

40. Maas, A. I., Roozenbeek, B. & Manley, G. T. Clinical trials in traumatic brain injury: past experience and current developments. *Neurotherapeutics* **7**, 115-126 (2010).

41. Narayan, R. K., Michel, M. E., Ansell, B., Baethmann, A., Biegon, A., Bracken, M. B., Bullock, M. R., Choi, S. C., Clifton, G. L. & Contant, C. F. Clinical trials in head injury. *Journal of Neurotrauma* **19**, 503-557 (2002).

42. Schouten, J. W. Neuroprotection in traumatic brain injury: a complex struggle against the biology of nature. *Current Opinion in Critical Care* **13**, 134-142 (2007).

43. Chodobski, A., Zink, B. J. & Szmydynger-Chodobska, J. Blood–brain barrier pathophysiology in traumatic brain injury. *Translational Stroke Research* **2**, 492-516 (2011).

44. Hayes, R. L. & Dixon, C. E. in *Seminars in Neurology*. 25-31 (Thieme Medical Publishers).

45. Abbott, N. J. Inflammatory mediators and modulation of blood-brain barrier permeability. *Cellular and Molecular Neurobiology* **20**, 131-147, doi:10.1023/a:1007074420772 (2000).

46. Abbott, N. J., Patabendige, A. A., Dolman, D. E., Yusof, S. R. & Begley, D. J. Structure and function of the blood-brain barrier. *Neurobiology of Disease* **37**, 13-25, doi:10.1016/j.nbd.2009.07.030 (2010).

47. Abdul-Muneer, P. M., Chandra, N. & Haorah, J. Interactions of oxidative stress and neurovascular inflammation in the pathogenesis of traumatic brain injury. *Molecular Neurobiology* **51**, 966-979, doi:10.1007/s12035-014-8752-3 (2015).

48. Ballabh, P., Braun, A. & Nedergaard, M. The blood–brain barrier: an overview: structure, regulation, and clinical implications. *Neurobiology of Disease* **16**, 1-13 (2004).

49. Hawkins, B. T. & Davis, T. P. The blood-brain barrier/neurovascular unit in health and disease. *Pharmacological Reviews* **57**, 173-185 (2005).

50. Obermeier, B., Daneman, R. & Ransohoff, R. M. Development, maintenance and disruption of the blood-brain barrier. *Nature Medicine* **19**, 1584-1596, doi:10.1038/nm.3407 (2013).

51. Zlokovic, B. V. The blood-brain barrier in health and chronic neurodegenerative disorders. *Neuron* **57**, 178-201 (2008).

52. Abbruscato, T. J., Lopez, S. P., Roder, K. & Paulson, J. R. Regulation of blood-brain barrier Na, K, 2Cl-cotransporter through phosphorylation during in vitro stroke conditions and nicotine exposure. *Journal of Pharmacology and Experimental Therapeutics* **310**, 459-468 (2004).

53. Iłzecka, J. in *Annales Universitatis Mariae Curie-Sklodowska. Sectio D: Medicina.* 123-127.

54. Khatri, R., McKinney, A. M., Swenson, B. & Janardhan, V. Blood–brain barrier, reperfusion injury, and hemorrhagic transformation in acute ischemic stroke. *Neurology* **79**, S52-S57 (2012).

55. Sandoval, K. E. & Witt, K. A. Blood-brain barrier tight junction permeability and ischemic stroke. *Neurobiology of Disease* **32**, 200-219, doi:10.1016/j.nbd.2008.08.005 (2008).

56. Fiala, M., Liu, Q., Sayre, J., Pop, V., Brahmandam, V., Graves, M. & Vinters, H. Cyclooxygenase-2-positive macrophages infiltrate the Alzheimer's disease brain and damage the blood–brain barrier. *European Journal of Clinical Investigation* **32**, 360-371 (2002).

57. Zlokovic, B. V. Neurovascular pathways to neurodegeneration in Alzheimer's disease and other disorders. *Nature Reviews Neuroscience* **12**, 723-738, doi:10.1038/nrn3114 (2011).

58. Desai, B. S., Monahan, A. J., Carvey, P. M. & Hendey, B. Blood–brain barrier pathology in Alzheimer's and Parkinson's disease: implications for drug therapy. *Cell Transplantation* **16**, 285-299 (2007).

59. Persidsky, Y., Heilman, D., Haorah, J., Zelivyanskaya, M., Persidsky, R., Weber, G. A., Shimokawa, H., Kaibuchi, K. & Ikezu, T. Rho-mediated regulation of tight junctions during monocyte migration across the blood-brain barrier in HIV-1 encephalitis (HIVE). *Blood* **107**, 4770-4780 (2006).

60. Oby, E. & Janigro, D. The blood–brain barrier and epilepsy. *Epilepsia* **47**, 1761-1774 (2006).

61. Remy, S. & Beck, H. Molecular and cellular mechanisms of pharmacoresistance in epilepsy. *Brain* **129**, 18-35 (2006).

62. Correale, J. & Villa, A. The blood–brain-barrier in multiple sclerosis: functional roles and therapeutic targeting. *Autoimmunity* **40**, 148-160 (2007).

63. de Vries, H. E. & Dijkstra, D. Mononuclear phagocytes at the blood-brain barrier in multiple sclerosis. *Blood-Spinal Cord and Brain Barriers in Health and Disease*, 409-417 (2004).

64. Opdenakker, G., Nelissen, I. & Van Damme, J. Functional roles and therapeutic targeting of gelatinase B and chemokines in multiple sclerosis. *The Lancet Neurology* **2**, 747-756 (2003).

65. Abdul-Muneer, P. M., Schuetz, H., Wang, F., Skotak, M., Jones, J., Gorantla, S., Zimmerman, M. C., Chandra, N. & Haorah, J. Induction of oxidative and nitrosative damage leads to cerebrovascular inflammation in an animal model of mild traumatic brain injury induced by primary blast. *Free Radical Biology & Medicine* **60**, 282-291, doi:10.1016/j.freeradbiomed.2013.02.029 (2013).

66. Chen, Y. & Huang, W. Non-impact, blast-induced mild TBI and PTSD: concepts and caveats. *Brain Injury* **25**, 641-650 (2011).

67. Haorah, J., Heilman, D., Knipe, B., Chrastil, J., Leibhart, J., Ghorpade, A., Miller, D. W. & Persidsky, Y. Ethanol-induced activation of myosin light chain kinase leads to dysfunction of tight junctions and blood-brain barrier compromise. *Alcoholism: Clinical and Experimental Research* **29**, 999-1009 (2005).

68. Haorah, J., Ramirez, S. H., Schall, K., Smith, D., Pandya, R. & Persidsky, Y. Oxidative stress activates protein tyrosine kinase and matrix metalloproteinases leading to blood–brain barrier dysfunction. *Journal of Neurochemistry* **101**, 566-576 (2007).

69. Hue, C. D., Cho, F. S., Cao, S., Nicholls, R. E., Vogel Iii, E. W., Sibindi, C., Arancio, O., Dale Bass, C. R., Meaney, D. F. & Morrison Iii, B. Time course and size of blood-brain barrier opening in a mouse model of blast-induced traumatic brain injury. *Journal of Neurotrauma*, doi:10.1089/neu.2015.4067 (2015).

70. Baldwin, S. A., Fugaccia, I., Brown, D. R., Brown, L. V. & Scheff, S. W. Blood-brain barrier breach following cortical contusion in the rat. *Journal of Neurosurgery* **85**, 476-481 (1996).

71. Başkaya, M. K., Rao, A. M., Doğan, A., Donaldson, D. & Dempsey, R. J. The biphasic opening of the blood–brain barrier in the cortex and hippocampus after traumatic brain injury in rats. *Neuroscience Letters* **226**, 33-36 (1997).

72. Hicks, R. R., Baldwin, S. A. & Scheff, S. W. Serum extravasation and cytoskeletal alterations following traumatic brain injury in rats. *Molecular and Chemical Neuropathology* **32**, 1-16 (1997).

73. Higashida, T., Kreipke, C. W., Rafols, J. A., Peng, C., Schafer, S., Schafer, P., Ding, J. Y., Dornbos III, D., Li, X. & Guthikonda, M. The role of hypoxia-inducible factor-1α, aquaporin-4, and matrix metalloproteinase-9 in blood-brain barrier disruption and brain edema after traumatic brain injury: laboratory investigation. *Journal of Neurosurgery* **114**, 92-101 (2011).

74. Shapira, Y., Setton, D., Artru, A. A. & Shohami, E. Blood-brain barrier permeability, cerebral edema, and neurologic function after closed head injury in rats. *Anesthesia & Analgesia* **77**, 141-148 (1993).

75. Elder, G. A., Gama Sosa, M. A., De Gasperi, R., Stone, J. R., Dickstein, D. L., Haghighi, F., Hof, P. R. & Ahlers, S. T. Vascular and inflammatory factors in the pathophysiology of blast-induced brain injury. *Frontiers in Neurolology* **6**, 48, doi:10.3389/fneur.2015.00048 (2015).

76. Hue, C. D., Cho, F. S., Cao, S., Cameron, R., Meaney, D. F. & Morrison, B. Dexamethasone potentiates in vitro blood-brain barrier recovery after primary blast injury by glucocorticoid receptor-mediated upregulation of ZO-1 tight junction protein. *Journal of Cerebral Blood Flow & Metabolism* **35**, 1191-1198 (2015).

77. Kawoos, U., Gu, M., Lankasky, J., McCarron, R. M. & Chavko, M. Effects of exposure to blast overpressure on intracranial pressure and blood-brain barrier permeability in a rat model. *PloS One* **11**, e0167510 (2016).

78. Readnower, R. D., Chavko, M., Adeeb, S., Conroy, M. D., Pauly, J. R., McCarron, R. M. & Sullivan, P. G. Increase in blood-brain barrier permeability, oxidative stress, and activated microglia in a rat model of blast-induced traumatic brain injury. *Journal of Neuroscience Research* **88**, 3530-3539, doi:10.1002/jnr.22510 (2010).

79. Shetty, A. K., Mishra, V., Kodali, M. & Hattiangady, B. Blood brain barrier dysfunction and delayed neurological deficits in mild traumatic brain injury induced by blast shock waves. *Frontiers in Cellular Neuroscience* **8** (2014).

80. Yeoh, S., Bell, E. D. & Monson, K. L. Distribution of blood-brain barrier disruption in primary blast injury. *Annals of Biomedical Engineering* **41**, 2206-2214, doi:10.1007/s10439-013-0805-7 (2013).

81. Skotak, M., Alay, E. & Chandra, N. On the accurate determination of shock wave time-pressure profile in the experimental models of blast induced neurotrauma. *Frontiers in Neurology* **9**, 52 (2018).

82. Bayir, H., Kochanek, P. M. & Kagan, V. E. Oxidative stress in immature brain after traumatic brain injury. *Developmental Neuroscience* **28**, 420-431, doi:10.1159/000094168 (2006).

83. Cornelius, C., Crupi, R., Calabrese, V., Graziano, A., Milone, P., Pennisi, G., Radak, Z., Calabrese, E. J. & Cuzzocrea, S. Traumatic brain injury: oxidative stress and neuroprotection. *Antioxidant & Redox Signaling* **19**, 836-853, doi:10.1089/ars.2012.4981 (2013).

84. Koppula, S., Kumar, H., Kim, I. S. & Choi, D. K. Reactive oxygen species and inhibitors of inflammatory enzymes, NADPH oxidase, and iNOS in experimental models of Parkinson's disease. *Mediators of Inflammation* **2012**, 823902, doi:10.1155/2012/823902 (2012).

85. Lewen, A. & Hillered, L. Involvement of reactive oxygen species in membrane phospholipid breakdown and energy perturbation after traumatic brain injury in the rat. *Journal of Neurotrauma* **15**, 521-530 (1998).

86. Mishra, V., Skotak, M., Schuetz, H., Heller, A., Haorah, J. & Chandra, N. Primary blast causes mild, moderate, severe and lethal TBI with increasing blast overpressures: Experimental rat injury model. *Scientific Reports* **6**, 26992, doi:10.1038/srep26992 (2016).

87. Galli, A., Svegliati-Baroni, G., Ceni, E., Milani, S., Ridolfi, F., Salzano, R., Tarocchi, M., Grappone, C., Pellegrini, G. & Benedetti, A. Oxidative stress stimulates proliferation and invasiveness of hepatic stellate cells via a MMP2-mediated mechanism. *Hepatology* **41**, 1074-1084 (2005).

88. Gasche, Y., Fujimura, M., Morita-Fujimura, Y., Copin, J.-C., Kawase, M., Massengale, J. & Chan, P. H. Early appearance of activated matrix metalloproteinase-9 after focal cerebral ischemia in mice: a possible role in blood—brain barrier dysfunction. *Journal of Cerebral Blood Flow & Metabolism* **19**, 1020-1028 (1999).

89. Kim, G. W., Gasche, Y., Grzeschik, S., Copin, J.-C., Maier, C. M. & Chan, P. H. Neurodegeneration in striatum induced by the mitochondrial toxin 3-nitropropionic acid: role of matrix metalloproteinase-9 in early blood-brain barrier disruption? *Journal of Neuroscience* **23**, 8733-8742 (2003).

90. Machado, L. S., Kozak, A., Ergul, A., Hess, D. C., Borlongan, C. V. & Fagan, S. C. Delayed minocycline inhibits ischemia-activated matrix metalloproteinases 2 and 9 after experimental stroke. *BMC Neuroscience* **7**, 56 (2006).

91. Grossetete, M., Phelps, J., Arko, L., Yonas, H. & Rosenberg, G. A. Elevation of matrix metalloproteinases 3 and 9 in cerebrospinal fluid and blood in patients with severe traumatic brain injury. *Neurosurgery* **65**, 702-708 (2009).

92. Hanumegowda, U. M., Copple, B. L., Shibuya, M., Malle, E., Ganey, P. E. & Roth, R. A. Basement membrane and matrix metalloproteinases in monocrotaline-induced liver injury. *Toxicological Sciences* **76**, 237-246 (2003).

93. Jia, F., Pan, Y.-h., Mao, Q., Liang, Y.-m. & Jiang, J.-y. Matrix metalloproteinase-9 expression and protein levels after fluid percussion injury in rats: the effect of injury severity and brain temperature. *Journal of Neurotrauma* **27**, 1059-1068 (2010).

94. Reijerkerk, A., Kooij, G., van der Pol, S. M., Khazen, S., Dijkstra, C. D. & de Vries, H. E. Diapedesis of monocytes is associated with MMP-mediated occludin disappearance in brain endothelial cells. *The FASEB Journal* **20**, 2550-2552 (2006).

95. Rosell, A., Ortega-Aznar, A., Alvarez-Sabín, J., Fernández-Cadenas, I., Ribó, M., Molina, C. A., Lo, E. H. & Montaner, J. Increased brain expression of matrix metalloproteinase-9 after ischemic and hemorrhagic human stroke. *Stroke* **37**, 1399-1406 (2006).

96. Chandra, N., Sundaramurthy, A. & Gupta, R. K. Validation of Laboratory Animal and Surrogate Human Models in Primary Blast Injury Studies. *Military Medicine* **182**, 105-113, doi:10.7205/milmed-d-16-00144 (2017).

97. Hyde, D. W. CONWEP 2.1.0.8 (software). Conventional Weapons Effects Program. United States Army Corps of Engineers. Vicksburg, MS. (2004).

98. Becker, H. Elastic modulus of mylar sheet. *Journal of Applied Polymer Science* **9**, 911-916, doi:10.1002/app.1965.070090309 (1965).

99. Glass, I. I. A theoretical and experimental study of shock-tube flows. *Journal of the Aeronautical Sciences* **22**, 73-100, doi:10.2514/8.3282 (1955).

100. Chandra, N., Ganpule, S., Kleinschmit, N., Feng, R., Holmberg, A., Sundaramurthy, A., Selvan, V. & Alai, A. Evolution of blast wave profiles in simulated air blasts: experiment and computational modeling. *Shock Waves* **22**, 403-415 (2012).

101. Needham, C. E. *Blast wave propagation*. (Springer, 2010).

102. Emrich, R. & Curtis, C. Attenuation in the shock tube. *Journal of Applied Physics* **24**, 360-363 (1953).

103. Slepička, F. Attenuation in shock tubes. *Physics of Fluids* **9**, 1865-1866 (1966).

104. Burnside, R. & Mackie, A. A problem in shock wave decay. *Journal of the Australian Mathematical Society* **5**, 258-272 (1965).

105. Zel'dovlch, Y. B. & Raizer, Y. P. *Physics of shock waves and high-temperature hydrodynamic phenomena*. Vol. 1 (Dover Publications Inc., 2002).

106. Kabu, S., Jaffer, H., Petro, M., Dudzinski, D., Stewart, D., Courtney, A., Courtney, M. & Labhasetwar, V. Blast-associated shock waves result in increased brain vascular leakage and elevated ROS levels in a rat model of traumatic brain injury. *PloS One* **10**, e0127971 (2015).

107. Sosa, M. A. G., De Gasperi, R., Janssen, P. L., Yuk, F. J., Anazodo, P. C., Pricop, P. E., Paulino, A. J., Wicinski, B., Shaughness, M. C. & Maudlin-Jeronimo, E. Selective vulnerability of the cerebral vasculature to blast injury in a rat model of mild traumatic brain injury. *Acta Neuropathologica Communications* **2**, 67 (2014).

108. Sosa, M. A. G., De Gasperi, R., Paulino, A. J., Pricop, P. E., Shaughness, M. C., Maudlin-Jeronimo, E., Hall, A. A., Janssen, W. G., Yuk, F. J. & Dorr, N. P. Blast overpressure induces shear-related injuries in the brain of rats exposed to a mild traumatic brain injury. *Acta Neuropathologica Communications* **1**, 51 (2013).

109. Stokum, J. A., Keledjian, K., Hayman, E., Karimy, J. K., Pampori, A., Imran, Z., Woo, S. K., Gerzanich, V. & Simard, J. M. Glibenclamide pretreatment protects against chronic memory dysfunction and glial activation in rat cranial blast traumatic brain injury. *Behavioural Brain Research* **333**, 43-53 (2017).

110. Chandra, N., Holmberg, A. & Feng, R. Controlling the shape of the shock wave profile in a blast facility. *US Provisional patent application* **61542354** (2011).

111. Kuriakose, M., Skotak, M., Misistia, A., Kahali, S., Sundaramurthy, A. & Chandra, N. Tailoring the blast exposure conditions in the shock tube for generating pure, primary shock waves: The end plate facilitates elimination of secondary loading of the specimen. *PloS One* **11**, e0161597 (2016).

112. Yen, L. F., Wei, V. C., Kuo, E. Y. & Lai, T. W. Distinct patterns of cerebral extravasation by Evans blue and sodium fluorescein in rats. *PloS One* **8**, e68595 (2013).

113. Kaya, M. & Ahishali, B. in *Permeability Barrier* 369-382 (Springer, 2011).

114. Sandel, W. R., Hubbard, R. W. & Schehl-Geiger, D. Indocyanine Green (ICG) and Evans Blue: Comparative Study of Plasma Volume Measurement. (ARMY RESEARCH INST OF ENVIRONMENTAL MEDICINE NATICK MA, 1982).

115. Wolman, M., Klatzo, I., Chui, E., Wilmes, F., Nishimoto, K., Fujiwara, K. & Spatz, M. Evaluation of the dye-protein tracers in pathophysiology of the blood-brain barrier. *Acta Neuropathologica* **54**, 55-61 (1981).

116. Chandra, N., Ganpule, S., Kleinschmit, N. N., Feng, R., Holmberg, A. D., Sundaramurthy, A., Selvan, V. & Alai, A. Evolution of blast wave profiles in simulated air blasts: experiment and computational modeling. *Shock Waves* **22**, 403-415, doi:10.1007/s00193-012-0399-2 (2012).

117. Skotak, M., Wang, F., Alai, A., Holmberg, A., Harris, S., Switzer, R. C. & Chandra, N. Rat injury model under controlled field-relevant primary blast conditions: acute response to a wide range of peak overpressures. *Journal of Neurotrauma* **30**, 1147-1160, doi:10.1089/neu.2012.2652 (2013).

118. Garman, R. H., Jenkins, L. W., Switzer III, R. C., Bauman, R. A., Tong, L. C., Swauger, P. V., Parks, S. A., Ritzel, D. V., Dixon, C. E. & Clark, R. S. Blast exposure in rats with body shielding is characterized primarily by diffuse axonal injury. *Journal of Neurotrauma* **28**, 947-959 (2011).

119. Li, W., Long, J. A., Watts, L. T., Jiang, Z., Shen, Q., Li, Y. & Duong, T. Q. A quantitative MRI method for imaging blood-brain barrier leakage in experimental traumatic brain injury. *PloS One* **9**, e114173 (2014).

120. Su, E. J., Fredriksson, L., Kanzawa, M., Moore, S., Folestad, E., Stevenson, T. K., Nilsson, I., Sashindranath, M., Schielke, G. P. & Warnock, M. Imatinib treatment reduces brain injury in a murine model of traumatic brain injury. *Frontiers in Cellular Neuroscience* **9** (2015).

121. Tanno, H., Nockels, R. P., Pitts, L. H. & Noble, L. Breakdown of the blood–brain barrier after fluid percussive brain injury in the rat. Part 1: distribution and time course of protein extravasation. *Journal of Neurotrauma* **9**, 21-32 (1992).

122. Candelario-Jalil, E., Yang, Y. & Rosenberg, G. Diverse roles of matrix metalloproteinases and tissue inhibitors of metalloproteinases in neuroinflammation and cerebral ischemia. *Neuroscience* **158**, 983-994 (2009).

123. Armulik, A., Abramsson, A. & Betsholtz, C. Endothelial/pericyte interactions. *Circulation Research* **97**, 512-523, doi:10.1161/01.RES.0000182903.16652.d7 (2005).

124. Armulik, A., Genove, G., Mae, M., Nisancioglu, M. H., Wallgard, E., Niaudet, C., He, L., Norlin, J., Lindblom, P., Strittmatter, K., Johansson, B. R. & Betsholtz, C. Pericytes regulate the blood-brain barrier. *Nature* **468**, 557-561, doi:10.1038/nature09522 (2010).

125. Nishioku, T., Dohgu, S., Takata, F., Eto, T., Ishikawa, N., Kodama, K. B., Nakagawa, S., Yamauchi, A. & Kataoka, Y. Detachment of brain pericytes from the basal lamina is involved in disruption of the blood–brain barrier caused by lipopolysaccharide-induced sepsis in mice. *Cellular and Molecular Neurobiology* **29**, 309-316 (2009).

126. Abbott, N. J. Astrocyte–endothelial interactions and blood–brain barrier permeability. *Journal of Anatomy* **200**, 523-534 (2002).

127. Abbott, N. J., Rönnbäck, L. & Hansson, E. Astrocyte-endothelial interactions at the blood-brain barrier. *Nature Reviews Neuroscience* **7**, 41 (2006).

128. Benarroch, E. E. in *Mayo Clinic Proceedings.* 1326-1338 (Elsevier, 2005).

129. Polavarapu, R., Gongora, M. C., Yi, H., Ranganthan, S., Lawrence, D. A., Strickland, D. & Yepes, M. Tissue-type plasminogen activator–mediated shedding of astrocytic low-density lipoprotein receptor–related protein increases the permeability of the neurovascular unit. *Blood* **109**, 3270-3278 (2007).

130. Banks, W. A. From blood-brain barrier to blood-brain interface: new opportunities for CNS drug delivery. *Nature Reviews Drug Discovery* (2016).

131. Hue, C. D., Cao, S., Haider, S. F., Vo, K. V., Effgen, G. B., Vogel III, E., Panzer, M. B., Bass, C. R. D., Meaney, D. F. & Morrison III, B. Blood-brain barrier dysfunction after primary blast injury in vitro. *Journal of Neurotrauma* **30**, 1652-1663 (2013).

132. Lucke-Wold, B. P., Logsdon, A. F., Smith, K. E., Turner, R. C., Alkon, D. L., Tan, Z., Naser, Z. J., Knotts, C. M., Huber, J. D. & Rosen, C. L. Bryostatin-1 Restores Blood Brain Barrier Integrity following Blast-Induced Traumatic Brain Injury. *Molecular Neurobiology* **52**, 1119-1134, doi:10.1007/s12035-014-8902-7 (2015).

133. Blyth, B. J., Farhavar, A., Gee, C., Hawthorn, B., He, H., Nayak, A., Stöcklein, V. & Bazarian, J. J. Validation of serum markers for blood-brain barrier disruption in traumatic brain injury. *Journal of Neurotrauma* **26**, 1497-1507 (2009).

134. Burda, J. E., Bernstein, A. M. & Sofroniew, M. V. Astrocyte roles in traumatic brain injury. *Experimental Neurology* **275**, 305-315 (2016).

135. Vajtr, D., Benada, O., Kukacka, J., Prusa, R., Houstava, L., Toupalik, P. & Kizek, R. Correlation of Ultrastructural Changes of Endothelial Cells and Astrocytes Occurring during Blood Brain Barrier Damage after Traumatic Brain Injury with Biochemical Markers of Blood Brain Barrier Leakage and Inflammatory Response. *Physiological Research* **58**, 263-268 (2009).

136. Fernández-López, D. & Vexler, Z. S. in *The Blood Brain Barrier (BBB)* 91-116 (Springer, 2013).

137. Louboutin, J.-P., Chekmasova, A., Marusich, E., Agrawal, L. & Strayer, D. S. Role of CCR5 and its ligands in the control of vascular inflammation and leukocyte recruitment required for acute excitotoxic seizure induction and neural damage. *The FASEB Journal* **25**, 737-753 (2011).

138. Szmydynger-Chodobska, J., Fox, L. M., Lynch, K. M., Zink, B. J. & Chodobski, A. Vasopressin amplifies the production of proinflammatory mediators in traumatic brain injury. *Journal of Neurotrauma* **27**, 1449-1461 (2010).

139. Cavaglia, M., Dombrowski, S. M., Drazba, J., Vasanji, A., Bokesch, P. M. & Janigro, D. Regional variation in brain capillary density and vascular response to ischemia. *Brain Research* **910**, 81-93 (2001).

140. Brown, R. C., Egleton, R. D. & Davis, T. P. Mannitol opening of the blood–brain barrier: regional variation in the permeability of sucrose, but not 86Rb+ or albumin. *Brain Research* **1014**, 221-227, doi:https://doi.org/10.1016/j.brainres.2004.04.034 (2004).

141. Johanson, C. E. Permeability and vascularity of the developing brain: cerebellum vs cerebral cortex. *Brain Research* **190**, 3-16 (1980).

142. LaManna, J. C. & Harik, S. I. Regional studies of blood—brain barrier transport of glucose and leucine in awake and anesthetized rats. *Journal of Cerebral Blood Flow & Metabolism* **6**, 717-723 (1986).

143. Pluta, R., Tomida, S., Ikeda, J., Nowak Jr, T. S. & Klatzo, I. Cerebral vascular volume after repeated ischemic insults in the gerbil: comparison with changes in CBF and brain edema. *Journal of Cerebral Blood Flow & Metabolism* **9**, 163-170 (1989).

144. Holash, J., Sugamori, K. & Stewart, P. The difference in vascular volume between cerebrum and cerebellum is in the pia mater. *Journal of Cerebral Blood Flow & Metabolism* **10**, 432-434 (1990).

145. Allt, G. & Lawrenson, J. G. Is the pial microvessel a good model for blood-brain barrier studies? *Brain Research Reviews* **24**, 67-76, doi:https://doi.org/10.1016/S0165-0173(97)00011-8 (1997).

146. Huber, B. R., Meabon, J. S., Hoffer, Z. S., Zhang, J., Hoekstra, J. G., Pagulayan, K. F., McMillan, P. J., Mayer, C. L., Banks, W. A., Kraemer, B. C., Raskind, M. A., McGavern, D. B., Peskind, E. R. & Cook, D. G. Blast exposure causes dynamic microglial/macrophage responses and microdomains if brain microvessel dysfunction. *Neuroscience* **319**, 206-220, doi:10.1016/j.neuroscience.2016.01.022 (2016).

147. Bochicchio, G. V., Lumpkins, K., O'Connor, J., Simard, M., Schaub, S., Conway, A., Bochicchio, K. & Scalea, T. M. Blast injury in a civilian trauma setting is associated with a delay in diagnosis of traumatic brain injury. *The American Surgeon* **74**, 267-270 (2008).

148. DuBose, J. J., Barmparas, G., Inaba, K., Stein, D. M., Scalea, T., Cancio, L. C., Cole, J., Eastridge, B. & Blackbourne, L. Isolated severe traumatic brain injuries sustained during combat operations: demographics, mortality outcomes, and lessons to be learned from contrasts to civilian counterparts. *Journal of Trauma* **70**, 11-16; discussion 16-18, doi:10.1097/TA.0b013e318207c563 (2011).

149. Reid, M. W. & Velez, C. S. Discriminating military and civilian traumatic brain injuries. *Molecular and Cellular Neuroscience* **66**, 123-128, doi:10.1016/j.mcn.2015.03.014 (2015).

150. Singleton, J. A., Gibb, I. E., Hunt, N. C., Bull, A. M. & Clasper, J. C. Identifying future 'unexpected' survivors: a retrospective cohort study of fatal injury patterns in victims of improvised explosive devices. *BMJ Open* **3**, doi:10.1136/bmjopen-2013-003130 (2013).

151. Wallace, D. Improvised explosive devices and traumatic brain injury: the military experience in Iraq and Afghanistan. *Australasian Psychiatry* **17**, 218-224, doi:10.1080/10398560902878679 (2009).

152. Carbone, F., Teixeira, P. C., Braunersreuther, V., Mach, F., Vuilleumier, N. & Montecucco, F. Pathophysiology and Treatments of Oxidative Injury in Ischemic Stroke: Focus on the Phagocytic NADPH Oxidase 2. *Antioxidants & Redox Signaling* **23**, 460-489, doi:10.1089/ars.2013.5778 (2015).

153. Cooney, S. J., Bermudez-Sabogal, S. L. & Byrnes, K. R. Cellular and temporal expression of NADPH oxidase (NOX) isotypes after brain injury. *Journal of Neuroinflammation* **10**, 155, doi:10.1186/1742-2094-10-155 (2013).

154. Infanger, D. W., Sharma, R. V. & Davisson, R. L. NADPH oxidases of the brain: distribution, regulation, and function. *Antioxidant & Redox Signaling* **8**, 1583-1596, doi:10.1089/ars.2006.8.1583 (2006).

155. Choi, B. Y., Jang, B. G., Kim, J. H., Lee, B. E., Sohn, M., Song, H. K. & Suh, S. W. Prevention of traumatic brain injury-induced neuronal death by inhibition of NADPH oxidase activation. *Brain Research* **1481**, 49-58, doi:10.1016/j.brainres.2012.08.032 (2012).

156. Ferreira, A. P., Rodrigues, F. S., Della-Pace, I. D., Mota, B. C., Oliveira, S. M., de Campos Velho Gewehr, C., Bobinski, F., de Oliveira, C. V., Brum, J. S., Oliveira, M. S., Furian, A. F., de Barros, C. S., dos Santos, A. R., Ferreira, J., Fighera, M. R. & Royes, L. F. HOE-140, an antagonist of B2 receptor, protects against memory deficits and brain damage induced by moderate lateral fluid percussion injury in mice. *Psychopharmacology* **231**, 1935-1948, doi:10.1007/s00213-013-3336-x (2014).

157. Song, S. X., Gao, J. L., Wang, K. J., Li, R., Tian, Y. X., Wei, J. Q. & Cui, J. Z. Attenuation of brain edema and spatial learning deficits by the inhibition of NADPH oxidase activity using apocynin following diffuse traumatic brain injury in rats. *Molecular Medicine Reports* **7**, 327-331, doi:10.3892/mmr.2012.1147 (2013).

158. Kuriakose, M., Kakulavarapu, V., Younger, D. & Chandra, N. Temporal and spatial effects of blast overpressure on blood-brain barrier permeability in traumatic brain injury. *Scientific Reports* **8** (2018).

159. Kim, J. H., Jang, B. G., Choi, B. Y., Kim, H. S., Sohn, M., Chung, T. N., Choi, H. C., Song, H. K. & Suh, S. W. Post-treatment of an NADPH oxidase inhibitor prevents seizure-induced neuronal death. *Brain Research* **1499**, 163-172, doi:10.1016/j.brainres.2013.01.007 (2013).

160. Fu, Y., Rusznak, Z., Herculano-Houzel, S., Watson, C. & Paxinos, G. Cellular composition characterizing postnatal development and maturation of the mouse brain and spinal cord. *Brain Structure and Function* **218**, 1337-1354, doi:10.1007/s00429-012-0462-x (2013).

161. Herculano-Houzel, S., Ribeiro, P., Campos, L., Valotta da Silva, A., Torres, L. B., Catania, K. C. & Kaas, J. H. Updated neuronal scaling rules for the brains of Glires (rodents/lagomorphs). *Brain, Behavior and Evolution* **78**, 302-314, doi:10.1159/000330825 (2011).

162. Fernandez, V., Barrientos, X., Kipreos, K., Valenzuela, A. & Videla, L. A. Superoxide radical generation, NADPH oxidase activity, and cytochrome P-450 content of rat liver microsomal fractions in an experimental hyperthyroid state: relation to lipid peroxidation. *Endocrinology* **117**, 496-501, doi:10.1210/endo-117-2-496 (1985).

163. Rodriguez-Rodriguez, A., Egea-Guerrero, J. J., Murillo-Cabezas, F. & Carrillo-Vico, A. Oxidative stress in traumatic brain injury. *Current Medicinal Chemistry* **21**, 1201-1211 (2014).

164. Angeloni, C., Prata, C., Dalla Sega, F. V., Piperno, R. & Hrelia, S. Traumatic brain injury and NADPH oxidase: a deep relationship. *Oxidative Medicine and Cellular Longevity* **2015**, 370312, doi:10.1155/2015/370312 (2015).

165. Lu, X. Y., Wang, H. D., Xu, J. G., Ding, K. & Li, T. NADPH oxidase inhibition improves neurological outcome in experimental traumatic brain injury. *Neurochemistry International* **69**, 14-19, doi:10.1016/j.neuint.2014.02.006 (2014).

166. Ma, M. W., Wang, J., Zhang, Q., Wang, R., Dhandapani, K. M., Vadlamudi, R. K. & Brann, D. W. NADPH oxidase in brain injury and neurodegenerative disorders. *Molecular Neurodegeneration* **12**, 7, doi:10.1186/s13024-017-0150-7 (2017).

167. Muir, J. K., Tynan, M., Caldwell, R. & Ellis, E. F. Superoxide dismutase improves posttraumatic cortical blood flow in rats. *Journal of Neurotrauma* **12**, 179-188, doi:10.1089/neu.1995.12.179 (1995).

168. Cristofori, L., Tavazzi, B., Gambin, R., Vagnozzi, R., Vivenza, C., Amorini, A. M., Di Pierro, D., Fazzina, G. & Lazzarino, G. Early onset of lipid peroxidation after human traumatic brain injury: a fatal limitation for the free radical scavenger pharmacological therapy? *Journal of Investigative Medicine* **49**, 450-458, doi:10.2310/6650.2001.33790 (2001).

169. Roof, R. L., Hoffman, S. W. & Stein, D. G. Progesterone protects against lipid peroxidation following traumatic brain injury in rats. *Molecular and Chemical Neuropathology* **31**, 1-11 (1997).

170. Wada, K., Alonso, O. F., Busto, R., Panetta, J., Clemens, J. A., Ginsberg, M. D. & Dietrich, W. D. Early treatment with a novel inhibitor of lipid peroxidation (LY341122) improves histopathological outcome after moderate fluid percussion brain injury in rats. *Neurosurgery* **45**, 601-608 (1999).

171. Arlt, S., Beisiegel, U. & Kontush, A. Lipid peroxidation in neurodegeneration: new insights into Alzheimer's disease. *Current Opinion in Lipidology* **13**, 289-294 (2002).

172. Banakou, E. & Dailianis, S. Involvement of Na+/H+ exchanger and respiratory burst enzymes NADPH oxidase and NO synthase, in Cd-induced lipid peroxidation and DNA damage in haemocytes of mussels. *Comparative Biochemistry and Physiology Part C: Toxicology and Pharmacology* **152**, 346-352, doi:10.1016/j.cbpc.2010.06.001 (2010).

173. Stanger, O., Renner, W., Khoschsorur, G., Rigler, B. & Wascher, T. C. NADH/NADPH oxidase p22 phox C242T polymorphism and lipid peroxidation in coronary artery disease. *Clinical Physiology* **21**, 718-722 (2001).

174. Bandak, F. A., Ling, G., Bandak, A. & De Lanerolle, N. C. Injury biomechanics, neuropathology, and simplified physics of explosive blast and impact mild traumatic brain injury. *Handbook of Clinical Neurology* **127**, 89-104, doi:10.1016/B978-0-444-52892-6.00006-4 (2015).

175. Chandra, N. & Sundaramurthy, A. in *Brain Neurotrauma: Molecular, Neuropsychological, and Rehabilitation Aspects Frontiers in Neuroengineering* (ed F. H. Kobeissy) (2015).

176. Courtney, A. & Courtney, M. The Complexity of Biomechanics Causing Primary Blast-Induced Traumatic Brain Injury: A Review of Potential Mechanisms. *Frontiers in Neurology* **6**, 221, doi:10.3389/fneur.2015.00221 (2015).

177. Chong, Z. Z., Li, F. & Maiese, K. Oxidative stress in the brain: novel cellular targets that govern survival during neurodegenerative disease. *Progress in Neurobiology* **75**, 207-246, doi:10.1016/j.pneurobio.2005.02.004 (2005).

178. Dohi, K., Ohtaki, H., Nakamachi, T., Yofu, S., Satoh, K., Miyamoto, K., Song, D., Tsunawaki, S., Shioda, S. & Aruga, T. Gp91phox (NOX2) in classically activated microglia exacerbates traumatic brain injury. *Journal of Neuroinflammation* **7**, 41, doi:10.1186/1742-2094-7-41 (2010).

179. Byrnes, K. R., Loane, D. J., Stoica, B. A., Zhang, J. & Faden, A. I. Delayed mGluR5 activation limits neuroinflammation and neurodegeneration after traumatic brain injury. *Journal of Neuroinflammation* **9**, 43, doi:10.1186/1742-2094-9-43 (2012).

180. Byrnes, K. R., Loane, D. J., Stoica, B. A., Zhang, J. & Faden, A. I. Delayed mGluR5 activation limits neuroinflammation and neurodegeneration after traumatic brain injury. *J Neuroinflammation* **9**, 43, doi:10.1186/1742-2094-9-43 (2012).

181. Ferreira, A. P., Rodrigues, F. S., Della-Pace, I. D., Mota, B. C., Oliveira, S. M., Velho Gewehr Cde, C., Bobinski, F., de Oliveira, C. V., Brum, J. S., Oliveira, M. S., Furian, A. F., de Barros, C. S., Ferreira, J., Santos, A. R., Fighera, M. R. & Royes, L. F. The effect of NADPH-oxidase inhibitor apocynin on cognitive impairment induced by moderate lateral fluid percussion injury: role of inflammatory and oxidative brain damage. *Neurochemistry International* **63**, 583-593, doi:10.1016/j.neuint.2013.09.012 (2013).

182. Luo, T., Wu, J., Kabadi, S. V., Sabirzhanov, B., Guanciale, K., Hanscom, M., Faden, J., Cardiff, K., Bengson, C. J. & Faden, A. I. Propofol limits microglial activation after experimental brain trauma through inhibition of nicotinamide adenine dinucleotide phosphate oxidase. *Anesthesiology* **119**, 1370-1388, doi:10.1097/ALN.0000000000000020 (2013).

183. Cho, H. J., Sajja, V. S., Vandevord, P. J. & Lee, Y. W. Blast induces oxidative stress, inflammation, neuronal loss and subsequent short-term memory impairment in rats. *Neuroscience* **253**, 9-20, doi:10.1016/j.neuroscience.2013.08.037 (2013).

184. Lucke-Wold, B. P., Naser, Z. J., Logsdon, A. F., Turner, R. C., Smith, K. E., Robson, M. J., Bailes, J. E., Lee, J. M., Rosen, C. L. & Huber, J. D. Amelioration of nicotinamide adenine dinucleotide phosphate–oxidase mediated stress reduces cell death after blast-induced traumatic brain injury. *Translational Research* **166**, 509-528. e501 (2015).

185. Sorce, S. & Krause, K. H. NOX enzymes in the central nervous system: from signaling to disease. *Antioxidant & Redox Signaling* **11**, 2481-2504, doi:10.1089/ARS.2009.2578 (2009).

186. Coyoy, A., Olguin-Albuerne, M., Martinez-Briseno, P. & Moran, J. Role of reactive oxygen species and NADPH-oxidase in the development of rat cerebellum. *Neurochemistry International* **62**, 998-1011, doi:10.1016/j.neuint.2013.03.009 (2013).

187. Park, K. W. & Jin, B. K. Thrombin-induced oxidative stress contributes to the death of hippocampal neurons: role of neuronal NADPH oxidase. *Journal of Neuroscience Research* **86**, 1053-1063, doi:10.1002/jnr.21571 (2008).

188. Guilarte, T. R., Loth, M. K. & Guariglia, S. R. TSPO Finds NOX2 in Microglia for Redox Homeostasis. *Trends Pharmacological Science*, doi:10.1016/j.tips.2016.02.008 (2016).

189. Kumar, A., Barrett, J. P., Alvarez-Croda, D. M., Stoica, B. A., Faden, A. I. & Loane, D. J. NOX2 drives M1-like microglial/macrophage activation and neurodegeneration following experimental traumatic brain injury. *Brain, Behavior and Immunity* **58**, 291-309, doi:10.1016/j.bbi.2016.07.158 (2016).

190. Sorce, S., Schiavone, S., Tucci, P., Colaianna, M., Jaquet, V., Cuomo, V., Dubois-Dauphin, M., Trabace, L. & Krause, K. H. The NADPH oxidase NOX2 controls glutamate release: a novel mechanism involved in psychosis-like ketamine responses. *Journal of Neuroscience* **30**, 11317-11325, doi:10.1523/JNEUROSCI.1491-10.2010 (2010).

191. Schiavone, S., Jaquet, V., Sorce, S., Dubois-Dauphin, M., Hultqvist, M., Backdahl, L., Holmdahl, R., Colaianna, M., Cuomo, V., Trabace, L. & Krause, K. H. NADPH oxidase elevations in pyramidal neurons drive psychosocial stress-induced neuropathology. *Translational Psychiatry* **2**, e111, doi:10.1038/tp.2012.36 (2012).

192. Yoshioka, H., Niizuma, K., Katsu, M., Okami, N., Sakata, H., Kim, G. S., Narasimhan, P. & Chan, P. H. NADPH oxidase mediates striatal neuronal injury after transient global cerebral ischemia. *Journal of Cerebral Blood Flow & Metabolism* **31**, 868-880, doi:10.1038/jcbfm.2010.166 (2011).

193. Zhang, Q. G., Raz, L., Wang, R., Han, D., De Sevilla, L., Yang, F., Vadlamudi, R. K. & Brann, D. W. Estrogen attenuates ischemic oxidative damage via an estrogen receptor alpha-mediated inhibition of NADPH oxidase activation. *Journal of Neuroscience* **29**, 13823-13836, doi:10.1523/JNEUROSCI.3574-09.2009 (2009).

194. Evans, P. H. Free radicals in brain metabolism and pathology. *British Medical Bulletin* **49**, 577-587 (1993).

195. Jesberger, J. A. & Richardson, J. S. Oxygen free radicals and brain dysfunction. *International Journal of Neuroscience* **57**, 1-17 (1991).

196. O'Connell, K. M. & Littleton-Kearney, M. T. The role of free radicals in traumatic brain injury. *Biological Research for Nursing* **15**, 253-263, doi:10.1177/1099800411431823 (2013).

197. Siesjo, B. K., Agardh, C. D. & Bengtsson, F. Free radicals and brain damage. *Cerebrovascular and Brain Metabolsim Reviews* **1**, 165-211 (1989).

198. Brown, S. A. & Hall, E. D. Role of oxygen-derived free radicals in the pathogenesis of shock and trauma, with focus on central nervous system injuries. *Journal of American Veterinary Medical Association* **200**, 1849-1859 (1992).

199. Deng-Bryant, Y., Singh, I. N., Carrico, K. M. & Hall, E. D. Neuroprotective effects of tempol, a catalytic scavenger of peroxynitrite-derived free radicals, in a mouse traumatic brain injury model. *Journal of Cerebral Blood Flow & Metabolism* **28**, 1114-1126, doi:10.1038/jcbfm.2008.10 (2008).

200. Mattson, M. P. Calcium and Free Radicals: Mediators of neurotrophic factor and excitatory transmitter-regulated developmental plasticity and cell death. *Perspectives on Developmental Neurobiology* **3**, 79-91 (1996).

201. Willmore, L. J. & Ueda, Y. Posttraumatic epilepsy: hemorrhage, free radicals and the molecular regulation of glutamate. *Neurochemical Research* **34**, 688-697, doi:10.1007/s11064-008-9841-3 (2009).

202. Loane, D. J., Stoica, B. A., Byrnes, K. R., Jeong, W. & Faden, A. I. Activation of mGluR5 and inhibition of NADPH oxidase improves functional recovery after traumatic brain injury. *Journal of Neurotrauma* **30**, 403-412, doi:10.1089/neu.2012.2589 (2013).

203. Zhang, Q. G., Laird, M. D., Han, D., Nguyen, K., Scott, E., Dong, Y., Dhandapani, K. M. & Brann, D. W. Critical role of NADPH oxidase in neuronal oxidative damage and microglia activation following traumatic brain injury. *PLoS One* **7**, e34504, doi:10.1371/journal.pone.0034504 (2012).

204. Schaur, R. J., Siems, W., Bresgen, N. & Eckl, P. M. 4-Hydroxy-nonenal-A Bioactive Lipid Peroxidation Product. *Biomolecules* **5**, 2247-2337, doi:10.3390/biom5042247 (2015).

205. Raghupathi, R. Cell death mechanisms following traumatic brain injury. *Brain Pathology* **14**, 215-222 (2004).

206. Herculano-Houzel, S., Mota, B. & Lent, R. Cellular scaling rules for rodent brains. *Proceedings of the National Academy of Sciences of the United States of America* **103**, 12138-12143, doi:10.1073/pnas.0604911103 (2006).

207. Wang, X. & Michaelis, E. K. Selective neuronal vulnerability to oxidative stress in the brain. *Frontiers in Aging Neuroscience* **2**, 12, doi:10.3389/fnagi.2010.00012 (2010).

208. Wang, X., Pal, R., Chen, X. W., Limpeanchob, N., Kumar, K. N. & Michaelis, E. K. High intrinsic oxidative stress may underlie selective vulnerability of the hippocampal CA1 region. *Molecular Brain Research* **140**, 120-126, doi:10.1016/j.molbrainres.2005.07.018 (2005).

209. Friedman, J. in *Oxidative Stress and Free Radical Damage in Neurology* (eds N. Gadoth & H.H. Göbel) Ch. 2, 19-27 (Human Press, 2011).

210. Tan, X., Przekwas, A. J. & Long, J. B. in *ASME 2013 International Mechanical Engineering Congress and Exposition.* V03AT03A011-V003AT003A011 (American Society of Mechanical Engineers).

211. Rama Rao, K. V., Iring, S., Younger, D., Kuriakose, M., Skotak, M., Alay, E., Gupta, R. K. & Chandra, N. A single primary blast-induced traumatic brain injury in rodent model causes cell-type dependent increase in NADPH oxidase isoforms in vulnerable brain regions. *Journal of Neurotrauma* (2018).

212. Abdul Muneer, P. M., Alikunju, S., Szlachetka, A. M. & Haorah, J. The mechanisms of cerebral vascular dysfunction and neuroinflammation by MMP-mediated degradation of VEGFR-2 in alcohol ingestion. *Arterioscler Thromb Vasc Biol* **32**, 1167-1177, doi:10.1161/ATVBAHA.112.247668 (2012).

213. Jenner, P. Oxidative damage in neurodegenerative disease. *The Lancet* **344**, 796-798 (1994).

214. Uttara, B., Singh, A. V., Zamboni, P. & Mahajan, R. Oxidative stress and neurodegenerative diseases: a review of upstream and downstream antioxidant therapeutic options. *Current Neuropharmacology* **7**, 65-74 (2009).